Reliable experimental setup to test the pressure modulation of Baerveldt Implant tubes for reducing post-operative hypotony

By

Ajay Ramani

Submitted to the graduate degree program in Mechanical Engineering and the Graduate Faculty of the University of Kansas in partial fulfillment of the requirements for the degree of Master of Science.

_____

Co - Chairperson Dr. Ronald L. Dougherty

_____

Co - Chairperson Dr. Sarah L. Kieweg

_____

Dr. Paul Munden

Date Defended: August 28, 2015

The Thesis Committee for Ajay Ramani

certifies that this is the approved version of the following thesis:

RELIABLE EXPERIMENTAL SETUP TO TEST THE PRESSURE MODULATION OF BAERVELDT IMPLANT TUBES FOR REDUCING POST-OPERATIVE HYPOTONY

_____

Co – Chairperson Dr. Ronald L. Dougherty

_____

Co – Chairperson Dr. Sarah L. Kieweg

Date approved: _____

ABSTRACT

Glaucoma encompasses a group of conditions that result in damage to the optic nerve and can cause loss of vision and blindness. The nerve is damaged due to an increase in the eye's internal (intraocular) pressure (IOP) above the nominal range of 15 – 20 mm Hg. There are many treatments available for this group of diseases depending on the complexity and stage of nerve degradation. In extreme cases where drugs or laser surgery do not create better conditions for the patient, ophthalmologists use glaucoma drainage devices to help alleviate the IOP. Many drainage implants have been developed over the years and are in use; but two popular implants are the Baerveldt Glaucoma Implant and the Ahmed Glaucoma Valve Implant. Baerveldt Implants are non-valved and provide low initial resistance to outflow of fluid, resulting in post-operative complications such as hypotony, where the IOP drops below 5 mm of Hg. Ahmed Glaucoma Valve Implants are valved implants which initially restrict the amount of fluid flowing out of the eye. The long term success rates of Baerveldt Implants surpass those of Ahmed Valve Implants because of post-surgical issues; but Baerveldt Implants' initial effectiveness is poor without proper flow restriction. This drives the need to develop new ways to improve the initial effectiveness of Baerveldt Implants. A possible solution proposed by our research team is to place an insert in the Baerveldt Implant tube of inner diameter 305 microns. The insert must be designed to provide flow resistance for the early time frame [e.g., first 30 – 60 post-operative days] until sufficient scar tissue has formed on the implant. After that initial stage with the insert, the scar tissue will provide the necessary flow resistance to maintain the IOP above 5 mm Hg.

The main objective of this project was to develop and validate an experimental apparatus to measure pressure drop across a Baerveldt Implant tube, with and without inserts. This setup will be used in the future to evaluate custom inserts and their effects on the pressure drop over 4

– 6 weeks. The design requirements were: simulate physiological conditions [flow rate between 1.25 and 2.5 μl/min], evaluate small inner diameter tubes [50 and 75 μm] and annuli, and demonstrate reliability and repeatability. The current study was focused on benchmarking the experimental setup for the IOP range of 15 – 20 mm Hg. Repeated experiments have been conducted using distilled water with configurations [diameter of tube, insert diameter, lengths of insert and tube, and flow rate] that produce pressure variations which include the 15 – 20 mm Hg range. Two similar setups were assembled and evaluated for repeatability between the two. Experimental measurements of pressure drop were validated using theoretical calculations. Theory predicted a range of expected values by considering manufacturing and performance tolerances of the apparatus components: tube diameter, insert diameter, and the flow-rate and pressure [controlled by pump].

Benchmarking trials for Poiseuille flow used tubes [without inserts] that have inner diameters of 50 and 75 microns. The experimental data were within the theoretical range of 48.2 – 103.2 mm Hg for 50 μm tubes and 9.2 – 16.8 mm Hg for 75 μm tubes for experiments run at 2.5 μl/min. The two setups differed by about 1 mm Hg for a 15 mm Hg pressure drop [about 6%] in a 75 micron tube. Further benchmarking trials for annular flow were conducted using a standard size wire [diameter 0.270 mm] inserted in a syringe needle [inner diameter of 0.340 mm]. The two pieces of apparatus produced results [with an average of 2.98 ± 0.32 mm Hg] which were within the theoretical pressure range [0.13 to 3.23 mm Hg] and had a difference of about 0.5 – 1 mm Hg in the measured pressures. Trials were also conducted with different types of sutures placed in the implant tubes to form annular flow. The following suture properties were varied: absorbable/non-absorbable, flow rates [1.5 and 2.5 μl/min], lengths [4 and 8 mm] and diameters [0.15, 0.2, and 0.3 mm]. The results from these trials indicated that the pressure profiles of absorbable sutures increase over time [from 3 to 5 mm Hg], probably because the

sutures expand as they become hydrolyzed. However, the pressure profiles for non-absorbable sutures demonstrated a steady pressure [from 0.5 to 1.5 mm Hg]. Hence, the two setups can be used to verify the pressure responses of different types of inserts when they are placed within tubes of dimensions similar to those of Baerveldt Implant tubes. It is recommended that trials be conducted with different needle and wire combinations to generate a good data base to further benchmark the annular flow.

In addition, preliminary experiments evaluated the dissolution of suture samples in a balanced salt solution and in distilled water. The balanced salt solution approximates the eye's aqueous humor properties, and it was expected that the salt and acid would help to hydrolyze sutures much faster than distilled water. Suture samples in a balanced salt solution showed signs of deterioration [flaking] within 23 days, and distilled water samples showed only slight signs of deterioration after about 30 days. These preliminary studies indicate that future dissolution and flow experiments should be conducted using the balanced salt solution. Also, the absorbable sutures showed signs of bulk erosion/deterioration in a balanced salt solution after 14 days, which indicates that they may not be suitable as inserts in the implant tubes because flakes could block the tube entrance. Further long term studies should be performed in order to understand the effects of constant fluid movement over the surfaces of the absorbable sutures, by better means of rocking/shaking test suture samples to simulate flow conditions.

ACKNOWLEDGEMENTS

I would like to begin by expressing my sincere gratitude to **Dr. Ronald L. Dougherty**, my co-advisor and co-committee chair, for his support, motivation and enthusiasm in this research. His guidance helped me all the time and also in writing this thesis. I could not have imagined having a better advisor and mentor. I would also like to thank, **Dr. Sarah L. Kieweg**, my co-advisor and co-committee chair, for her immense support and passion she showed towards this research. I am ever grateful to **Dr. Paul M. Munden**, for his insightful comments, encouragement and hard questions that inspired me to widen my research from various perspectives. I must thank him for sponsoring this project and for relieving me of the financial burden towards my education.

I would like to thank the University of Kansas, specifically the Department of Mechanical Engineering, for giving me the opportunity to pursue my academic dreams.

I would like to express my deepest gratitude to the following people for all the help I received from them:

Dr. Elizabeth A. Friis – Associate Professor, Department of ME

Peggy Keefe – Lab Manager [Dr. Detamore's Lab]

Stephanie Moore – Senior Administrative Associate, Department of ME

Kathryn Maisch – Administrative Associate, Department of ME

Jim Hammen – Accountant, Department of ME

Al Syvongsay & Jason Habiger, Department of ME

Finally, I would like to thank all my friends from KU, and my family who have helped me get to this part of my life.

'Defeat the defeatism'

Dr. A. P. J. Abdul Kalam

11th President of India

"It may be that the gulfs will wash us down;

It may be we shall touch the Happy Isles,

And though we are not now that strength which in old days

Moved earth and heaven, that which we are, we are—

Made weak by time and fate, but strong in will;

To strive, to seek, to find, and not to yield."

Shortened version of Alfred Lord Tennyson's "Ulysses"

This thesis is dedicated to

My parents, for inspiring me to aim high in life.

Hridya and Sahana, for being there for me when I needed someone the most.

Mahesh anna, KGS mama and Divya akka, for your timely help.

Shrini, for all the support and advice you gave when I first came to the US.

Table of Contents

List of figures

List of tables

Appendix J

Appendix L

Nomenclature

A_X	Area of cross-section at Section X of the experimental setup, where X can refer to tube [t], catheter hub [CH], needle hub [NH], or PEEKsil tube [p] [m^2]
C_c	Contraction coefficient
d	Outer diameter of suture/insert [m]
D	Inner diameter of tubing [m]
D_h	Hydraulic diameter or effective diameter for flow through annulus [m]
D_X	Diameter of tubing in Section X of experimental setup, where X can refer to tube [t], catheter hub [CH], needle hub [NH], or PEEKsil tube [p] [m]
e	Eccentricity of insert within tube [m]
f	Friction factor
g	Acceleration due to gravity [m/s^2]
h_fx	Frictional loss in Section X of experimental setup, where X can be A, B, C, or D [m of water]
h_mx	Minor loss due to expansion or contraction in Section X of experimental setup, where X can be A, B, C, or D [m of water]
h_{diff}	Head loss due to elevation [m]
IOP	Intraocular pressure [mm Hg]
k_m	Expansion/Contraction loss coefficient
L	Length of insert [m]
L_X	Length of Section X of the experimental setup, where X can refer to tube [t], catheter hub [CH], needle hub [NH], or PEEKsil tube [p] [m]
P	Pressure [Pa or mm Hg]
Q	Flow rate through tube [µl/min or m^3/s]
r	Coordinate in the radial direction [m]

r_1	Outer radius of the insert [m]
r_2	Inner radius of the tube [m]
R_{flow}	Resistance to flow [mm Hg/(µl/min)]
Re	Reynolds number
t	Time [seconds]
V_x	Velocity of fluid through Section X of experimental setup, where X can refer to tube [t], catheter hub [CH], needle hub [NH], or PEEKsil tube [p] [m/s]
v	Output voltage reading [mV]
Greek	
β	Angle between tube surfaces, at the point of expansion or contraction [º]
ΔL	Overlap length between outer and inner tubes [m]
ΔP	Pressure drop [Pa or mm Hg]
ε	Eccentricity ratio
ρ	Density of fluid [kg/m^3]
µ	Dynamic viscosity of fluid [Pa.s]
ν	Kinematic viscosity of fluid [m^2/s]

Chapter 1: Introduction

1.1 Overview

This chapter reviews the objectives of this thesis. The second chapter introduces the disease glaucoma: different types, the causes, and various treatment procedures available. Then implant selection is covered, and a comparison between the two most commonly used implants is given. The theory behind the flow through tubes and a general overview of the different types of sutures is also discussed. The third chapter goes into the components used to make the setup, benchmarking trials for the setup, residual pressure trials, and the trial matrix. The fourth chapter contains a discussion of the results from the short term flow trials that were conducted. The fifth chapter discusses the results from the long term flow trials, and suture deterioration trials. The sixth chapter goes over the conclusions and recommendations for future study.

Medical terminology for several common medical terms is provided in **Appendix A**. **Appendix B** lists the major components in the experimental setups. **Appendix C** lists the important PneuWave pump specifications. **Appendix D** enumerates the steps that need to be followed when using the PneuWave pump software. **Appendix E** has the basic specifications of the Omega pressure transducer installed in the experimental setup. **Appendix F** shows the process to be followed to log data using Omega data logging software. **Appendix G** gives the general specifications of the Omega data logger. The calibration curve used to convert the millivolt readings from the data logger to pressure readings is given in **Appendix H**. **Appendix I** shows the theoretical pressure calculation for a standard tube, annulus, and annulus with eccentricity. **Appendix J** enumerates the procedure used to calculate the overall theoretical pressure drop for all of the benchmarking trials. **Appendix K** lists the procedure to be followed to conduct experiments. **Appendix L** goes over the flow rate variation due to the pump controller.

1.2 Objectives

Glaucoma is a very common eye disease that is treated with medications or with surgical implantation of tube shunts, such as the Ahmed Glaucoma Valve Implant or the Baerveldt Glaucoma Implant, depending on the amount of damage to the optic nerve in the eye [1-5]. The overall aim of this study is to research how to improve the initial effectiveness of Baerveldt Glaucoma Implants by eliminating hypotony in the early post-operative period. A method for improvement is to increase the flow resistance on a temporary basis [say 30 – 60 days] which could resolve some of the early post-surgical issues associated with the implant. These issues and their implications are explained in detail in Chapter 2. Different methods to increase the flow resistance temporarily are analyzed. These methods are simple modifications performed by doctors during surgery such as internal tube occlusion [stent], external tube occlusion [ligature], and two stage procedures [5]. However, this thesis is focused on determining if inserts of a specific size and type would help to achieve this objective. In order to test the inserts, an experimental flow apparatus was designed in order to collect repeatable and accurate pressure data at low flow rates [1.25 – 10 μl/min]. This thesis covers the initial stage of the research. Keeping this in mind, the main objectives of this research were as follows:

- Develop a reliable experimental apparatus to measure pressures in the range of 0 – 50 mm Hg, in tubes and annuli of less than 300 micron diameter, and at flow rates of 1 – 10 μl/min.
- Benchmark the setup for selected sets of tube and flow configurations.
- Determine the amount of pressure increase in the system when various suture strips are inserted into the Baerveldt Implant tube, and determine when or if the pressure returns to levels similar to there being no sutures in the tube.

- Evaluate the swelling and deterioration rates of absorbable sutures in distilled water and a balanced salt solution.
- Evaluate the increase in pressure when different suture materials [absorbable and non-absorbable] are inserted into the implant tubing. Also evaluate which suture material works best, and what characteristics of the suture [diameter, length, type and composition] impact the pressure increase.

The strategic aim is to be able to develop a method to improve the effectiveness of Baerveldt Glaucoma Implants by eliminating or significantly reducing post-operative hypotony.

Chapter 2: A Brief Introduction to Glaucoma and Treatment, and Fluid Flow Theory

2.1 What is Glaucoma?

Glaucoma is a term inclusive of many different conditions that have a common result of optic nerve damage related to elevated intraocular pressures [IOP] [3, 6]. If left untreated, the pressure-related optic nerve damage can be progressive and result in partial or complete loss of vision. Normally, the IOP is between 8 – 21 mm of Hg [7]. In a study conducted in 1958, Leydhecker [7] measured the eye pressures of 10,000 people with no known eye disease; the resulting distribution of IOP resembled a Gaussian curve centered at 15 mm of Hg [± 2.5 mm Hg]. A healthy IOP is a result of the equilibrium between the amount of aqueous humor being produced within the eye and the physiologic outflow of the fluid from the eye [8]. Aqueous humor is a fluid produced in the eye, rich in nutrients and electrolytes, to nourish all the parts of the eye. In most cases, aqueous humor production rates are constant, within a range of 1.5 – 2.5 μl/min, which implies that elevated IOPs are a result of increased resistance to the outflow of fluid [9, 10]. For elevated IOPs, the flow rate can drop to about 1 μl/min, but the aqueous humor production does not stop permanently [10]. Refer to **Appendix A** for a glossary of medical terms used in this thesis.

2.2 Types of Glaucoma

There are many types of glaucoma, such as neovascular, traumatic and pseudoexfoliative [3], some of which are very rare as compared to the following types.

2.2.1 Open-angle glaucoma [wide-angle glaucoma]

The most common type of glaucoma is open-angle glaucoma or wide-angle glaucoma [1]. The configuration of a normal eye does not have any obstructions to the ‘angle’ [Fig.1]. For

an eye with open-angle glaucoma, the trabecular meshwork gets “clogged”, due to various factors, and the angle between the iris and posterior surface of the eye remains unchanged.

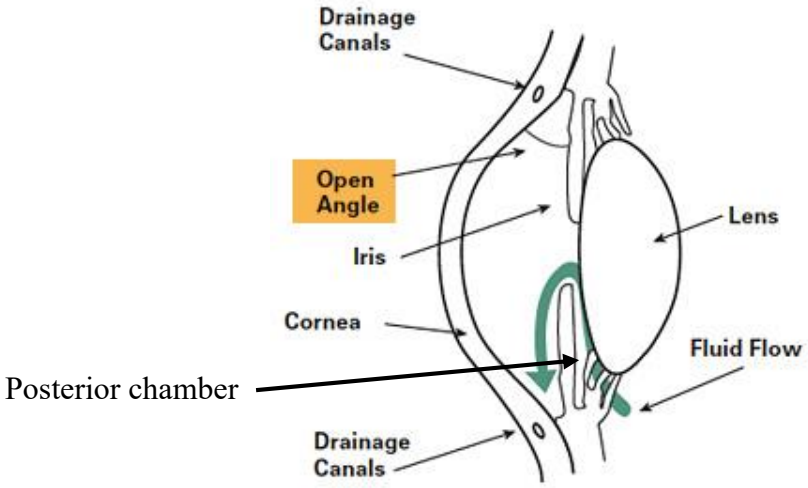

Figure 1: Open-angle glaucoma [reproduced from Ref. 1]

2.2.2 Angle-closure glaucoma

Another type is acute or chronic angle-closure or narrow-angle glaucoma. This is less common than open-angle glaucoma but is usually characterized by an acute increase in the IOP [1]. The angle between the iris and the posterior chamber of the eye is narrowed by the configuration of the internal eye anatomy [Fig. 2]. The drainage channels become occluded by the iris and the surrounding structures, resulting in a sudden and sharp increase in IOP.

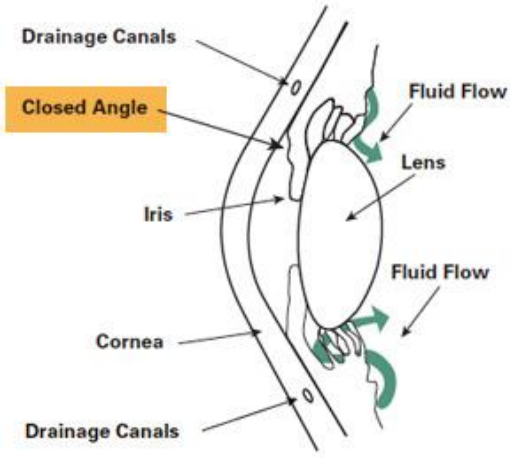

Figure 2: Angle-closure glaucoma [reproduced from Ref. 1]

2.2.3 Normal-tension glaucoma

Normal-tension glaucoma is also called low-tension or normal pressure glaucoma. In this condition, the angle between the iris and posterior chamber is normal, and the IOP is in the normal range [1]. However, there is damage to the optic nerve that has the characteristics typical of an eye affected with open-angle glaucoma but without the elevated IOP. The reason is thought to be related to some internal weakness or dysfunction in the optic nerve [1].

2.2.4 Congenital glaucoma

This type of glaucoma usually occurs in newborns in conjunction with incomplete development of the eye's drainage canal during the prenatal period. This is a very rare condition that occurs in 1 out of every 10,000 births. This is a common term used for glaucoma diagnosed in infancy or early childhood [1, 3].

2.2.5 Other types of glaucoma

Other variants of open-angle and angle-closure glaucoma include [1]:

- Secondary glaucoma
- Pigmentary glaucoma
- Pseudoexfoliative glaucoma
- Traumatic glaucoma
- Neovascular glaucoma
- Irido Corneal Endothelial Syndrome (ICE)

These types are variations of open-angle or angle-closure glaucoma which can be caused due to small inflammation or injury of the eye. They can occur in either one eye or both eyes. These are very rare, and less than 10% of Americans [approximately] with glaucoma have one of these types [4].

2.3 Causes

IOP is a result of the equilibrium between the production of aqueous humor in the eye and subsequent outflow from the eye through drainage canals. The aqueous humor is produced in the ciliary body of the eye at a nominal rate of about 2.5 μl/min [though the flow rate ranges between 1.5 – 2.5 μl/min for the average person, depending on various factors] and circulates around structures in the anterior part of the eye in order to provide nutrition and oxygenation to clear structures which lack blood vessels [2, 4]. The aqueous humor then exits the eye through the drainage canals to be recycled within the blood stream [4]. The normal production of aqueous humor is relatively constant. As a result, the IOP becomes a function of resistance to outflow through the drainage canals. Improper circulation/drainage of aqueous humor can result in increased IOP. This fluid flows out of the eye through a mesh-like channel, called the trabecular meshwork, into Schlemm's canal [refer to Fig. 3] [11]. If the canal becomes blocked, for reasons unknown at this time, fluid builds up in the eye and cannot filter out at the usual rate, resulting in an increased IOP. This condition has been observed to be hereditary and limited to certain ethnic groups of a particular age group [5]. Glaucoma can occur in both eyes, but the extent of damage in each eye may not be the same [12].

In the case of open-angle glaucoma, the angle formed between the iris and the cornea is wide; but since Schlemm's canal is partially blocked, it causes the outflow rate of the aqueous humor from within the eye to drop. This in turn results in an increase in IOP [3]. The damage caused by the increase in IOP does not induce significant pain or show any symptoms until much later, say a few months [2]. The damage to the optic nerve occurs slowly; but one may lose an extensive amount of vision before this problem has been detected [5].

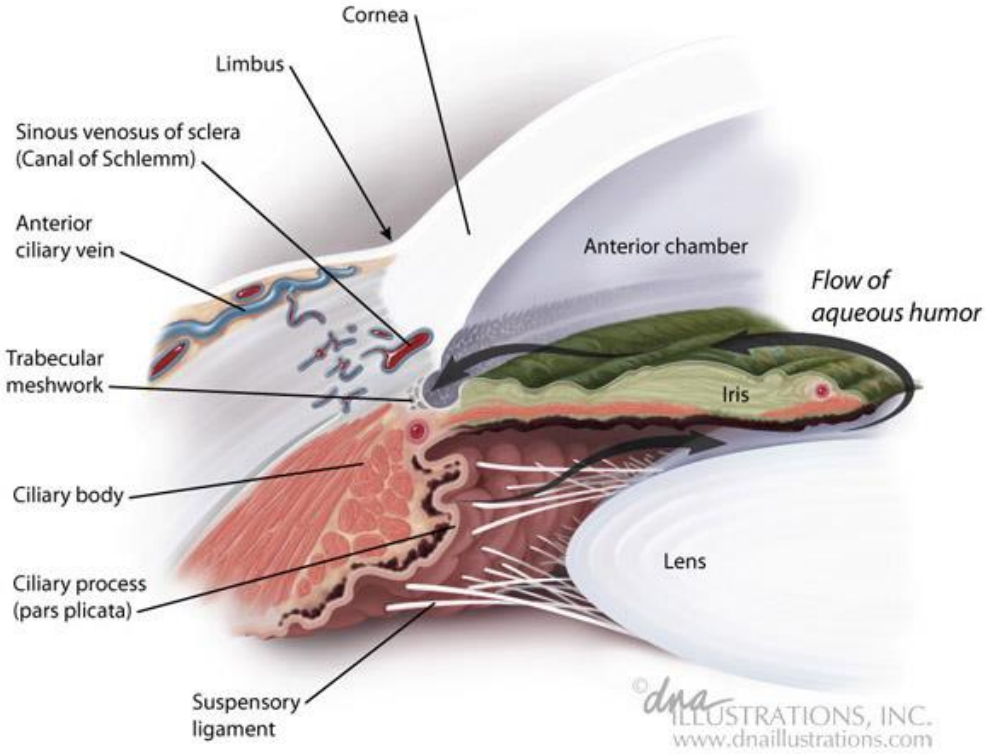

Figure 3: Flow path of aqueous humor [reproduced from Ref. 11]

Angle-closure glaucoma occurs when the IOP increases. The iris bulges out causing the angle between the iris and the cornea to narrow. As a result, the aqueous humor will not be able to drain out, causing the IOP to increase even more [1]. Angle-closure glaucoma usually occurs abruptly but can also occur gradually. If one has a narrow drainage angle, sudden dilation of the pupils can trigger acute angle-closure glaucoma [1].

2.4 Treatment

Although glaucoma cannot be completely cured and any optic nerve damage is irreversible, the main goal of treatment procedures adopted by doctors is to help reduce the IOP. The treatment is concentrated on curbing further damage to the optic nerve [5]. There are many treatments administered to patients depending upon the stage of the disease. Initial therapy usually consists of administration of eye drops, and/or oral medication. These medications help

lower the IOP by decreasing the amount of aqueous humor produced [1]. If the administration of medications is insufficient to lower the IOP to a safe level for the optic nerve, then treatment progresses to laser or surgical therapy. Laser treatment, filtering surgery and/or drainage implants are proposed based on the complexity of the disease or extent of damage; and the potential responsiveness of the patient to the treatment [most patients fall in the age group of 60 years and above]. Laser treatment is performed to clear the blockage in the drainage canal [4]. Initially the IOP is well within the normal range; but as time progresses, the IOP tends to increase again. Drainage implants are used only when the patient is at an advanced stage of glaucoma or has secondary glaucoma [3, 9]. In surgical therapy, alternate outflow pathways for the aqueous humor are established either by creating a fistula [or hole] from inside the eye to the exterior or by implanting a tube shunt, such as a Baerveldt Glaucoma Implant or Ahmed Glaucoma Valve Implant, to drain the aqueous humor from the anterior chamber to the exterior of the eye ball [5].

The drainage devices [or aqueous shunts] are designed to create an alternate path for the aqueous humor to flow as needed from the anterior chamber of the eye to the exterior of the eye. All implants are designed to reduce the IOP by restoring the outflow of the aqueous humor to the normal flow rate, regardless of the implant type [3, 5]. These drainage devices have good success in controlling the IOP as compared to other surgical methods. The first implant to be tested was the Molteno Implant in 1969 [1, 5, 8] shown in Fig. 4. There have been significant developments in the basic design over the past 40 years; and this has led to lower post-surgery complications. Some drainage devices have been developed that offer special features to improve IOP, reduce acute postoperative hypotony, and facilitate implantation [5].

Drainage devices come in different configurations, materials, etc., some with regulating valves [Molteno, Fig. 4; Ahmed Glaucoma Valve, Fig. 5; Shocket, and Eagle vision implants] or

without [Baerveldt [13] [14], Fig. 6]. The regulating valves are used to restrict the flow and to allow unidirectional flow of aqueous humor from the anterior chamber to the exterior channels. The valves are used until the scar tissue grows over the implant, increasing the flow resistance. These implants are reserved for patients with very severe uncontrolled glaucoma and for those who have failed to respond to other techniques/surgeries [12].

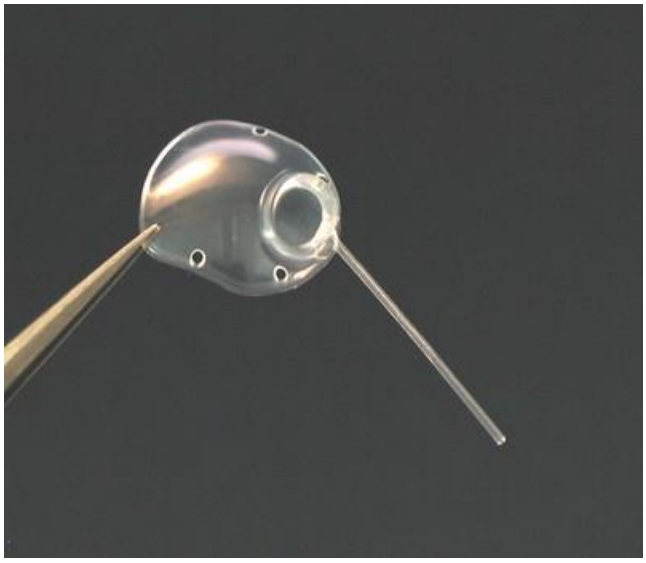

Figure 4: Molteno Implant [reproduced from Ref. 5]

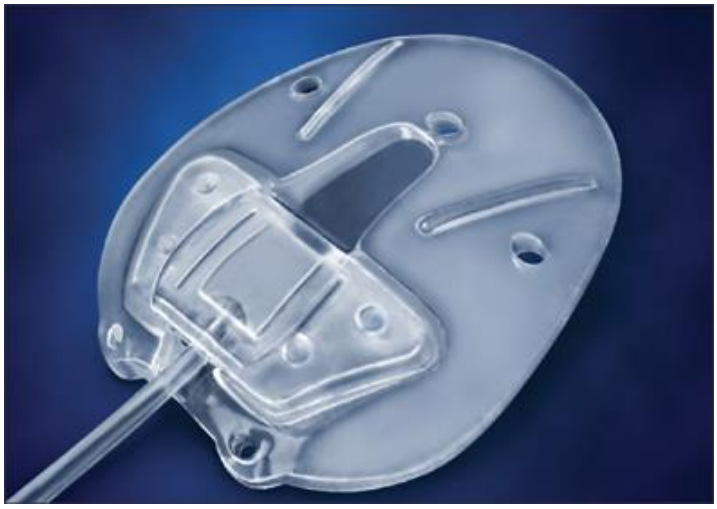

Figure 5: Ahmed Glaucoma Valve Implant [reproduced from Ref. 5]

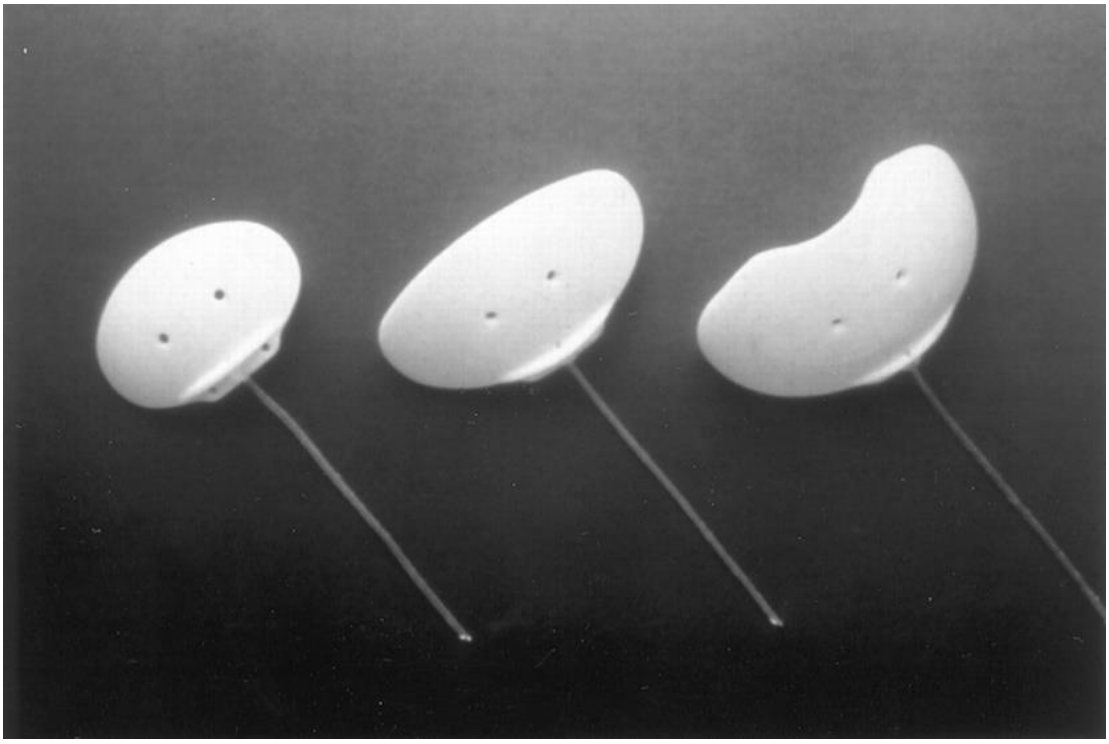

Figure 6: Baerveldt Glaucoma Implant [reproduced from Ref. 14]

2.5 Selection of the Appropriate Implant

There are many factors that influence the decision of the surgeon when selecting the type of implant for the patient.

One of the factors is IOP control. It is easy to control the IOP in the early postoperative stage when devices such as the Ahmed Glaucoma Valve or Molteno Implant are used because of the flow restriction that the valves produce. Such implants are always preferred for patients with poor compliance to the medication and hence requires very few follow-up visits post-surgery [5].

Another factor that influences the decision is the growth rate of scar tissue on the implant. The rate of growth helps determine the type and size of implant [Fig. 7]. However, the most important factor would be the IOP range targeted by the surgeon post-surgery [5].

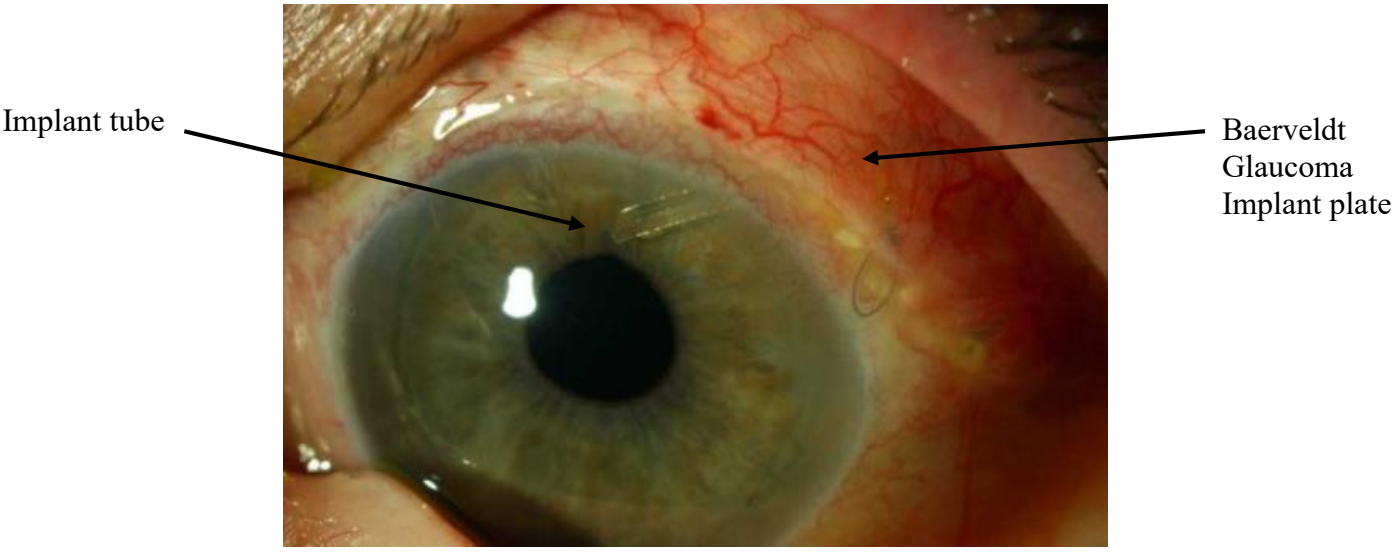

Figure 7: Baerveldt Glaucoma Implant in the eye [reproduced from Ref. 4]

Early post-surgery IOPs are controlled by the resistance to flow offered by valved or non-valved implants. Because of the increased resistance to flow, valved implants offer more chances to control IOP and have lower probability of causing hypotony. As a defense mechanism against any foreign material implanted in the body, scar tissue begins to cover the implant and forms a permeable casing over the implant. The scar tissue growth depends on the patient's age and metabolism, but typically occurs within 30 – 60 days [4].

For the non-valved devices, doctors usually tie down/sew the tubes partially closed to offer some resistance until the scar tissue grows sufficiently. This method adopted by doctors is one of the reasons why the postoperative IOP can be controlled for non-valved implants [5]. Studies have shown that the surface area of the implant and thickness of the scar tissue growth on the implant play an important role in having better control of IOP in the long run. The growth of the scar tissue in turn controls the percolation of the aqueous humor [15].

2.6 Possible Post-Surgical Complications

Usually, some form of flow restriction [e.g., tying sutures] is implemented so that aqueous humor does not flow out of the anterior chamber uncontrollably, which would cause a drastic drop in IOP in the eye. This is the main reason why Baerveldt Implants might not be preferred, though their long term performance is much better than valved implants [covered in Section 2.7] like Ahmed Valve Implants [5, 16]. In the long run, when the scar tissue develops over the implant, the resistance to flow increases, and there is no need for valves or any other form of flow restriction to maintain the IOP above 5 mm of Hg.

2.7 Ahmed Glaucoma Valve Implant vs. Baerveldt Glaucoma Implant – A Comparison

Drainage devices with open tubes are more likely to cause complications such as early postoperative hypotony, and hence the tubes should be temporarily closed using stents or ligatures [1]. The research interest of this thesis is focused on Baerveldt Glaucoma Implants because they have shown better success rates than Ahmed Implants in the long run [17]. The central idea of this work is to develop a technique by which the existing Baerveldt Implants could be modified easily and in a safe manner to avoid early postoperative hypotony.

Based on five year treatment outcomes in an Ahmed and Baerveldt comparison study [17], it was determined that there are similar rates of long-term surgical success for both implants. However, the Baerveldt Glaucoma Implant showed a greater reduction in the IOP [12.7 ± 4.5 mm Hg for the Baerveldt Glaucoma Implant against 14.7 ± 4.4 mm Hg for the Ahmed Glaucoma Valve] and a lower rate of reoperation than that of the Ahmed Glaucoma Valve Implant, although the Baerveldt Glaucoma Implant showed twice as many failures because of safety issues like hypotony, implant ex-plantation [removal of implants after surgery] and loss of light perception [low vision/blindness]. The reasons for treatment failure were different for the

Ahmed Glaucoma Valve Implant: a higher IOP range, even though the Ahmed Glaucoma Valve controlled IOP to a greater extent in the early postoperative period as compared with the Baerveldt Glaucoma Implant. The point that a Baerveldt Glaucoma Implant yields two mm of Hg lower IOP than the Ahmed Valve [17] must be weighed against the larger number of safety end points [higher rate of hypotony] in the Baerveldt Implant study group when compared with the Ahmed Glaucoma Valve.

From a comparison study of the design, baseline patient characteristics and intraoperative complications [18], it was noted that both devices had similar baseline characteristics; and there were a similar number of intraoperative complications for both devices.

On long term follow-ups in which 'success' was defined as a low-end cutoff of about 5 – 6 mm of Hg and a high end of 21 – 22 mm of Hg with or without medication, Baerveldt Glaucoma Implants shared a success rate of about 93% and 88% for 350-mm^2 and 500-mm^2 implants, respectively, after 18 months [19].

2.8 Theory

In order to be able to validate the experimental setup, some basic flow concepts are needed to predict the pressure created by a set of flow parameters. The following theoretical concepts were used to model the pressure drop for normal flow and annular flow through a tube having a concentric annulus.

2.8.1 Flow through tube – Poiseuille's flow

The concept of Poiseuille's flow [20] was used to model pressure drop for flow through small diameter tubes, in order to benchmark the setup. The operating flow rate range for this application is in microliters per min [1.5 – 2.5 μl/min]. Steady, fully-developed, axisymmetric, laminar flow of an incompressible, Newtonian fluid allows the use of Poiseuille's law [20, 21].

$$\Delta P = \frac{8\,\mu L_t Q}{\pi r_2^4} \quad (1)$$

where,

ΔP Pressure drop [mm Hg or Pa]

μ Dynamic viscosity of fluid [Newtonian fluid] [Pa.s]

L_t Length of tube [m]

Q Flow rate of fluid [m^3/s]

r_2 Inner radius of the tube [m]

The boundary conditions used for deriving this equation are: no-slip at the tube surface [$r=r_2$], and an axisymmetric flow profile which sets the rate of change of the velocity at the center of the tube [r=0] to zero.

2.8.2 Flow through annulus – Poiseuille's flow

A modified version of Poiseuille's equation [22], considering flow through an annulus, was used to develop a better understanding of the flow profile when there is flow between concentric tubes. As seen in Fig. 8, frictional effects occur on both surfaces: the inside of the outer tube and the outside of the inner tube.

The equation for such a situation can be derived with the same assumptions as used for Eq. (1), but with different boundary conditions: no-slip conditions on the outer surface of the inner tube and inner surface of the outer tube [23, 24]:

$$Q = \frac{\pi}{8\mu}\frac{\Delta P}{L_t}\left[r_2^4 - r_1^4 - \frac{\left(r_2^2 - r_1^2\right)^2}{\ln r_2 / r_1}\right] \quad (2)$$

where,

Q Flow rate of fluid [m^3/s]

ΔP Pressure drop [Pa or mm Hg]

μ Dynamic viscosity of fluid [Pa.s]

L_t Length of tube [m]

r_1 Outer radius of inner tube/insert [m]

r_2 Inner radius of outer tube [m]

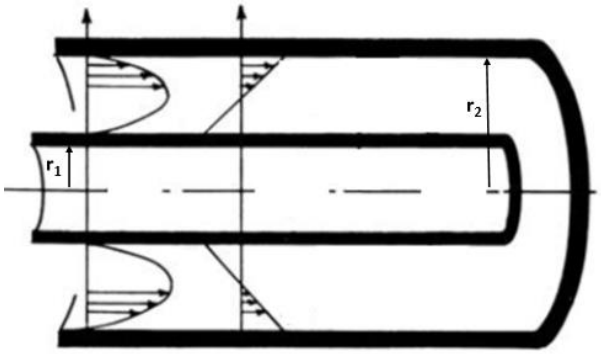

Figure 8: Flow between two concentric tubes [reproduced from Ref. 22]

Note that, as $r_1 \rightarrow 0$, Eq. (2) goes to Eq. (1).

2.9 Sutures – Types and Background

There are basically two types of surgical sutures [25, 26]: absorbable/degradable and non-absorbable/non-degradable. As the names suggest, the first type dissolves over time when exposed to liquid such as water or saline solution, and the latter does not dissolve. For example, in the case of a monofilament [Monocryl] suture in surgical settings, the dissolution takes approximately two weeks to begin [27]. At that time, the tensile strength of the suture starts to deteriorate [27]. Absorption rates vary and can be affected by patient health. For instance, having a fever, infection, or protein deficiency can increase the absorption rates [25]. There are different materials which are used to make absorbable and non-absorbable types of sutures. Some materials used to make absorbable sutures are polyglactin 910, poliglecaprone 25 and polydioxanone [26]. Materials such as polyester, nylon, silk, polypropelene and sometimes 316L stainless steel, are used to make non-absorbable sutures [27]. In addition, it is thought that non-braided sutures cause less reactivity in the body and are not as prone to becoming infected

because they lack the grooves and rough surfaces to which molecules/bacteria may adhere [25]. Plain catgut and chromic catgut are variations of absorbable sutures that have very low tensile strength and deteriorate much faster [within 7 – 10 days of surgery] than the other absorbable sutures [26]. However non-braided sutures may have a greater tendency to loosen at the surgical knot due to there being less 'grip' [26]. Figure 9 shows examples of some of the different types of sutures.

The absorbable sutures are of interest because, when they are inserted in BGI tubing and begin to deteriorate over time, they could provide the much needed initial flow resistance. Then, later, these sutures would disappear; and the flow resistance would be due to scar tissue on the plate of the BGI. Hence, a part of the study analyzed the different sutures and how they deteriorated, and checked to see if the 'resistance to flow' initially increased in order to maintain clinically relevant pressures [around 15 mm Hg]. The results from these trials are discussed in detail in Chapter 5.

Figure 9: Different types of sutures [reproduced from Ref. 25]

Chapter 3: Development and Validation of the Experimental Apparatus

3.1 Overview of Apparatus

The experimental setup was developed based on a preliminary concept provided by Dr. Paul Munden, ophthalmologist at the KU Eye Clinic. The setup must be able to pump fluid at a constant rate of 1 – 10 µl/min, with 2.5 µl/min being preferred, the typical flow rate of aqueous humor in a normal human eye; measure the differential pressure in the system when an insert is placed in the BGI tube; and record the flow and pressure trends over a set period of time. The term "system" refers to the setup, and the term "tube" refers to the BGI tubing that is attached to the setup. The flow rate for these experiments was very low; hence a peristaltic or syringe pump was envisioned. But since these experiments ran over long periods of time, between 24 hours and approximately 20 days, a PneuWave pump [28] was purchased. The PneuWave pump comes with a flow sensor that measures the low flow rate precisely [1 – 50 µl/min, ±5% of set point value]. Also, the pump has the capability to accommodate a bigger reservoir, say 500 ml, than most pumps that handle such low flow rates, in order to enable smooth long term trials without the need to refill/replace the fluid in the reservoir.

A schematic of the overall experimental setup is shown in Fig. 10. The setup consists of a 500 ml bottle, the PneuWave pump, and a pressure transducer and data logger [Omega] that are connected to a computer in order to record and retrieve data. A trough is placed at the outlet in order to collect the fluid exiting the setup. All of these items are explained in detail in Section 3.2.

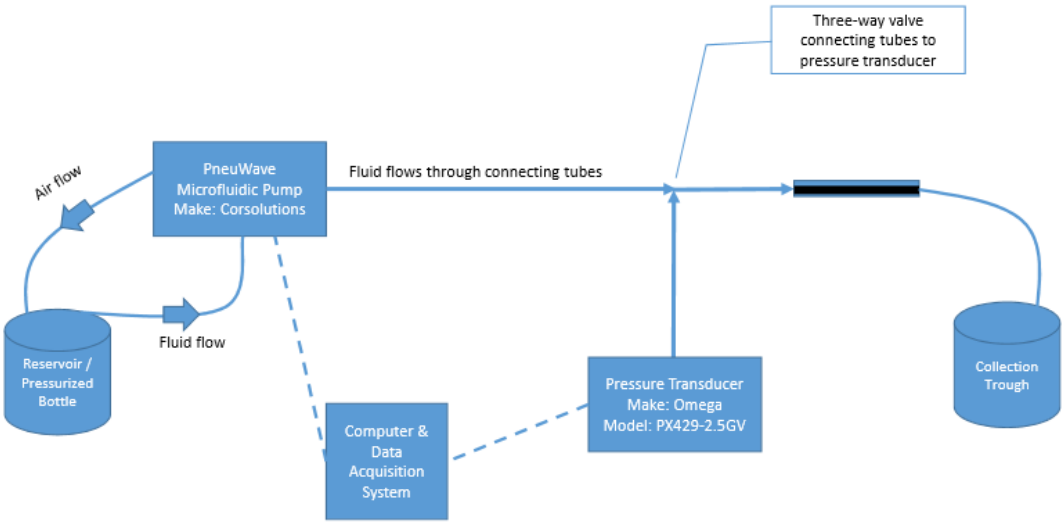

Figure 10: Schematic of experimental setup showing all major components

Figures 11 and 12 show the actual setups as assembled in LEA 3127 of Learned Hall, Mechanical Engineering. Two nearly identical setups were used, which helped to perform twice the number of trials for speedier data collection. For the same input parameters, the results and operation of both the setups were compared. **Appendix B** details the pieces of equipment in both setups.

Figure 11: Benchtop experimental setups

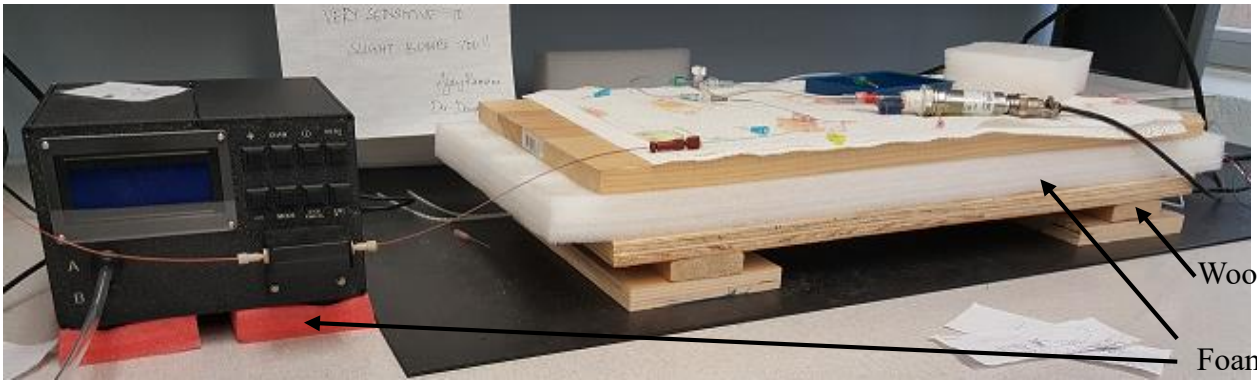

Figure 12: Assembled experimental Setup #2

3.2 Components in the Setup

3.2.1 Pump

The PneuWave pump [28] is a high-precision [within ±5% of set point flow rate], closed loop, programmable, pulse-free pump that best fits this microfluidic application as outlined in the following discussion. A block diagram of the PneuWave pump is shown in Fig. 13. Refer to **Appendix C** for the pump's specifications. **Appendix D** enumerates the steps followed in order to operate the pump using the 'PneuWave' software tool.

The pump consists of a pressure regulation system and a flow sensor which are in constant communication with a microprocessor. The pump pressurizes an easy-to-access fluid vessel which can range in volume from a few microliters to greater than a liter. The vessel is pressurized with a quiet, integrated, miniature pressure regulation system [28]. Once the vessel is pressurized, fluid moves through the tubing. An in-line flow sensor measures the actual displacement or flow rate. When operated in flow-control mode, both the flow sensor and the compressor regulation system are in continuous communication with the microprocessor. Based on the flow sensor readings, the microprocessor sends commands to the compressor regulation system, allowing for highly precise [within ±5% of set point value] flow control with micro-liter resolution [about ± 0.01 µl/min] [28]. In this manner, programmable flow profiles can be

achieved. Alternatively the PneuWave pump can be operated in pressure-control mode where the compressor regulation system is set at a user-defined pressure value [0 – 12 psi or 0 – 620.4 mm Hg], and adjustments based on flow sensor readings are not made.

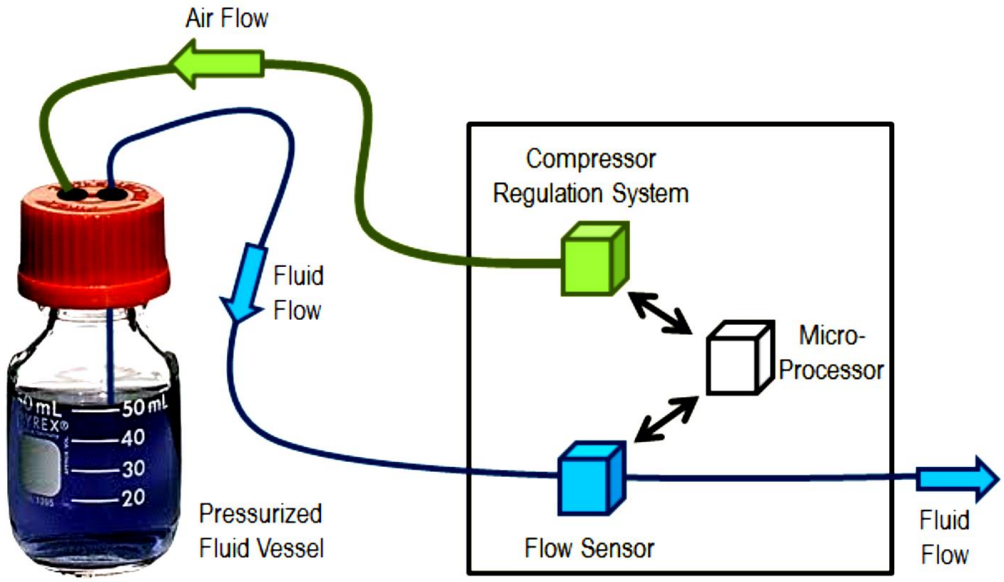

Figure 13: Block diagram of PneuWave pump, including a fluid reservoir bottle [reproduced from Ref. 25]

The flow rate is measured using a thermal propagation wave that is detected by RTDs placed around the tubing. A heater filament emits a thermal signal, depending on the set point/target value, and the RTDs measure the temperature on both sides of the tube and compare these temperatures [28]. If the temperature measured on one side is lower or higher than the filament's temperature, the micro-regulator in the pump activates or deactivates the air pressure control (air compressor). This method of flow rate measurement eliminates physical contact of any mechanical/moving parts with the fluid. The pump was specifically designed by the vendor for this application wherein a 500 ml bottle can be used to run long term trials [up to 60 days] without the need to refill the bottle or disturb the setup. A custom program was developed by the vendor to allow control of the data capture rate [0.1 – 10 second intervals], the length of each

trial [whatever duration is required from a few minutes to 60 days] and the mode used [either flow-control or pressure-control].

3.2.2 Pressure transducer and data logger

The Omega pressure transducer chosen for this application has a 0 – 2.5 ± 0.2 psi range [0 – 130 ± 10.5 mm Hg; see **Appendix E**] [29]. The piezo-resistive process uses strain gages molecularly embedded into a highly stable silicon wafer. The silicon wafer is divided into individual dies, each of which contains a full strain gage bridge. Each die is mounted in a sealed chamber protected from the environment by glass-to-metal seals and a stainless steel diaphragm. A small volume of silicone oil transfers the pressure from the diaphragm to the strain gage bridge. The construction provides an accuracy of ± 0.08% of best fit straight line and stability, and minimal thermal effects [refer to **Appendix E** for the specifications and to **Appendix F** for the operating procedure]. This design provides secondary fluid containment in the event of a diaphragm rupture.

The Omega transducer is connected to an independent data logging device [refer to **Appendix G** for specifications] [30], which can be accessed using OMEGA software to start/stop data logging and download data from the logger. A constant DC power source [5 – 10 V, see **Appendix B**] supplies power to the transducer. The output from the transducer is in millivolts and can be converted to psi using the calibration curve/equation provided with the transducer [refer to **Appendix H** for the calibration data]. The end of the transducer that measures the pressure is connected to the setup using a simple rubber-tube connector. There were leaks when the rubber-tube connector was used. Hence, in order to stop the leaks, the connection was completely covered with caulk and super glue [refer to Fig. 14]. After letting the caulk and super glue dry, repeated trials were conducted, at high pump pressures [10 – 12 psi], to ensure that the seal held. This was verified by checking for leaks when trials were conducted at

these high pump pressures, by temporarily closing the three-way valve causing the pressure at the transducer to build up to about 100 mm Hg. Once the pressure reached 100 mm Hg at the transducer, and no leaks could be detected on the seal, it was confirmed that there were no leaks in the setup.

3.2.3 Connectors and other items

The air-pressurized bottle [refer to **Appendix B**] was filled to its maximum level [500 ml mark on the bottle] with distilled water, leaving space for pressurizing the air. The pump was placed on foam pads [refer to Fig. 12] so that vibration from its air compressor did not affect the experimental setup. The rest of the setup was placed on a wooden board [refer to Fig. 12], elevated to about five inches above the water level at the pump outlet. The setup was initially placed lower than the pump outlet, and problems were experienced because of backflow and/or no outflow of fluid [refer to Fig. 12]. For this reason, the wooden boards were used to raise the setup to a height of about five inches above pump outlet. The wooden boards and foam pads were used to make a sturdy base for the setup, not affected by vibration which might be transmitted through the table on which the setup was placed.

Medical grade tubes were used to form a simple connection between the pump and the 20 gauge cannula. The pump was connected to the rest of the setup using a PTFE [polytetrafluoroethylene] connection tube, provided by the pump vendor. The PTFE tubes provided for the two setups were different lengths. The tubes were connected in a way so that one setup had the longer tube and the other had the shorter tube. A three-way valve [refer to Fig. 14] was used to connect the pressure transducer's tubing to the rest of the setup. The remaining portion of the setup had a 20 gauge cannula with a BGI tube [ID 0.305 mm] inserted in the cannula. The implant tube was glued in place using cyanoacrylate [discussed in Section 3.3]. A small trough was used to collect the water exiting the setup. The trough had 10 sub-troughs, most

of which were not filled with water. This was done to allow the excess water collecting in the sub-trough, with the outlet in it, to spill over to the neighboring sub-troughs, thereby avoiding disturbances in the readings by maintaining the water level above the outlet.

The 500 ml glass bottle was autoclaved before starting the trials in order to ensure that no bacteria were present. For about a month, the trials were run with a balanced salt solution [98.5% distilled water + 1.5% salt]; but over time, it was discovered that the salt solution became a breeding ground for bacteria and fungi. This finding led to the replacement of the salt solution with distilled water [from October of 2014] so as to ensure clean trials. The bottle was autoclaved again before using distilled water.

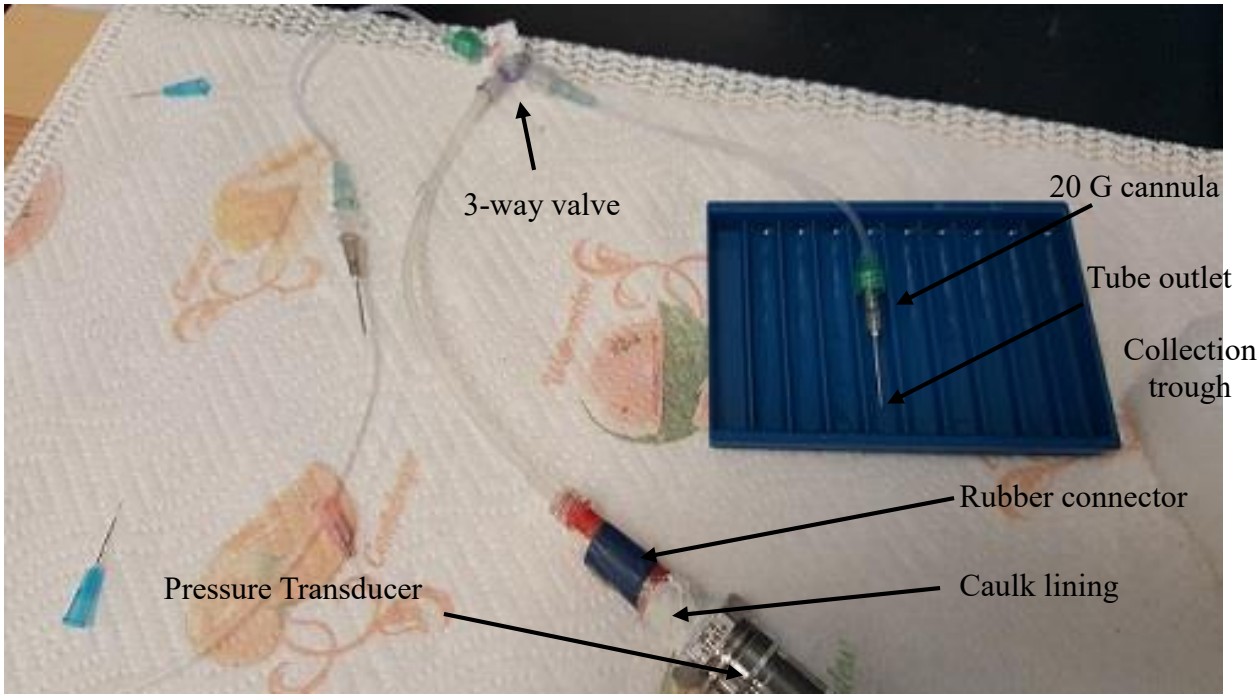

Figure 14: Connectors and other items in the setup

Repeated baseline trials were run until repeatable pressure profiles were recorded. This was done in order to determine the residual pressure drop in the system. Details on the residual pressure trials are provided in Section 3.4. Poiseuille's equation [Eq. (1), Section 2.8] was used to predict the theoretical pressure reading at the transducer by determining the losses across the

various components [e.g., connectors and tubing] in the setup. Sample calculations are shown in **Appendices I & J.** Table 1 shows the changes made to the experimental setup over the one year period of this project.

Table 1: Changes made to the setup over one year period of this project

Month	Changes made	Reason
November 2014	Collection trough [Fig.12] installed	Drop formation at the outlet created fluctuations in pressures measured by transducer.
February 2015	New data logger installed in Setup #1	Data logger sent to OMEGA for repair in December 2014 [but never returned]. New data logger was bought and installed because of the delay.
March 2015 [4th week]	Second setup [Setup #2] installed	To make twice as many runs, but they cannot be run separately because a single software interface and computer are used to run the pump.
June 2015 [3rd week]	Needle connector used instead of cannula for Setup #2	Continuous leak from cannula connection.
July 2015 [3rd week]	Caulk lining and super glue coating on transducer connector for Setup #2	Caulk lining of Setup #2 pressure transducer failed.
August 2015 [1st week]	Pump, PTFE tubes and reservoir exchanged between Setups #1 & #2	Process of assessing differences between the two setups. Longer tubes in Setup #2 and shorter tubes in Setup #1.
August 2015 [2nd week]	Needle connector used instead of cannula for Setup #1	To ensure that both setups were similar.

3.3 Experimental Setup Validation

In order to validate the experimental setups, experiments were conducted to see if the setups were able to produce pressures close to the clinically relevant range of 15 – 20 mm of Hg. One of the objectives of this research was to be able to run experiments simulating flow through an annulus. However, since it was difficult to know the amount [and eliminate the effects] of annulus eccentricity, the benchmarking was first done using some experiments with flow through a circular flow passage [tube] of set diameter and length that would yield nominal pressures close to physiologic IOP [around 15 mm Hg]. Since the differential pressure measured at the transducer would be affected by flow through the connections and tubing downstream, theoretical calculations were performed in order to determine the losses in the tubing between the three-way valve and the outlet immersed in the trough [Fig. 14]. The calculations showed that, if fluid flows at 2.5 µl/min through an 8 mm long BGI-like tube of internal diameter 50 microns, the observed pressure would be around 15 mm Hg. However, due to restrictions in the experimental setup, the trials had to be conducted using a 35 mm long tube instead of 8 mm, reasons for which are explained in detail later in this section [refer to **Appendix I** for theoretical calculations for 35 mm long tube].

It was difficult to find a tube with small inner diameter [50 microns] from conventional tubing manufacturers. However, gas chromatography tubing manufacturers suggested the use of PEEKsil tubes [31]. PEEKsil tubes [Figs. 15 and 16] are polymer-sheathed fused silica tubing, where the polymer is polyether ether ketone [PEEK]. These tubes are robust, inert to the fluid flowing through the tubes, and have smooth wall surfaces with precise inner diameters [± 5 microns].

The PEEKsil tubes had to be cut using a special ceramic column cutter [32] [Fig. 17]. The resulting cut could be rough, and it was crucial that the ends be checked for burrs and loose

silica fragments using a microscope [Figs. 15 and 16]. Care was taken to make sure that the inner linings of the tubes were not damaged in the process. For each test run, a tube was connected to a 25 G syringe needle using super glue as shown in Fig. 18. However, there were problems because of the glue flowing into the needle and blocking the entrance to the tube. This problem occurred due to capillary effects between the tube and needle. This drawback led to inserting a longer tube [about 33 – 35 mm] into the needle so that there was no glue blockage at the entrance of the tube [refer to Table I.1.1 in **Appendix I**]. Since the length was more than the length of the needle, the super glue did not reach the entrance of the tube.

The use of a 35 mm long tube resulted in a higher theoretical pressure of about 67 mm Hg [~ 4 times that of an 8 mm long tube]. This calculation did not consider tolerance factors for the inner diameter of the tube or pump flow rate. The tubes have an inner diameter of 50 ± 4 microns. But even a one micron change in inner diameter would result in a huge change [about 5 – 10 mm Hg, depending on the tube size] in the pressure calculation [see **Appendix J**]. Table 2 lists the theoretical pressure range and the time-averaged pressures for each of the tube flow trials performed to validate both of the setups. For each trial, an average pressure was computed using the data points between a specific time frame when the pressure stabilized, say $3000 < t < 7500$ seconds, and the average of these time-averaged means is listed in Table 2.

Table 2: Theoretical and experimental data for tube flow validation trials

# of trials	Flow rate with tolerance (µl/min)	Tube internal diameter (microns)	Sample length (mm)	Mean of time-averaged pressure ± std. dev. (mm Hg)	Theoretical pressure range (mm Hg)
7	2.5 ± 0.125	50 ± 4	35	101.5 ± 3.2	48.2 – 103.2
5	2.5 ± 0.125	75 ± 4	35	15.0 ± 0.4	9.2 – 16.8
5	1.25 ± 0.0625	75 ± 4	35	8.4 ± 0.2	3.7 – 7.6

Figure 15: 50 µm ID PEEKsil tube under the microscope [40X Magnification]

Figure 16: Cross-sectional view of 50 µm ID PEEKsil tube [40X Magnification]

Figure 17: Ceramic column cutter [reproduced from Ref. 29]

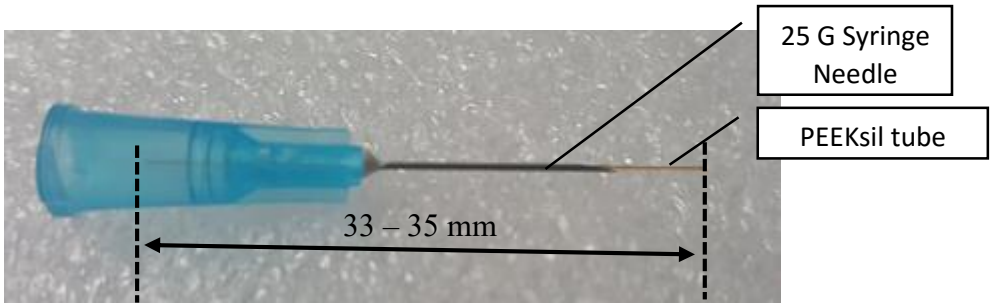

Figure 18: 25 Gauge needle with PEEKsil tube of inner diameter 50 microns

The pump flow rate has a tolerance of ±5% of the set point. This amounts to a variation of ±0.125 µl/min if the set point were 2.5 µl/min, and a variation of ±0.0625 µl/min if the set point were 1.25 µl/min. The theoretical calculations were done accounting for both of these variations. The resulting expected [theoretical] pressure range was 48 – 103 mm Hg. Table 3

shows how the individual components contributed to produce this pressure range. One can note that the possible variation of measured height, of about ±0.5 mm of water, has also been incorporated. Figure 19 shows a schematic representation of the different sections in the setup and the head loss in each section. As can be seen, only two loss sources, friction in the PEEKsil tubing and elevation change, are critical. The other sources are less than 0.01% of these two sources.

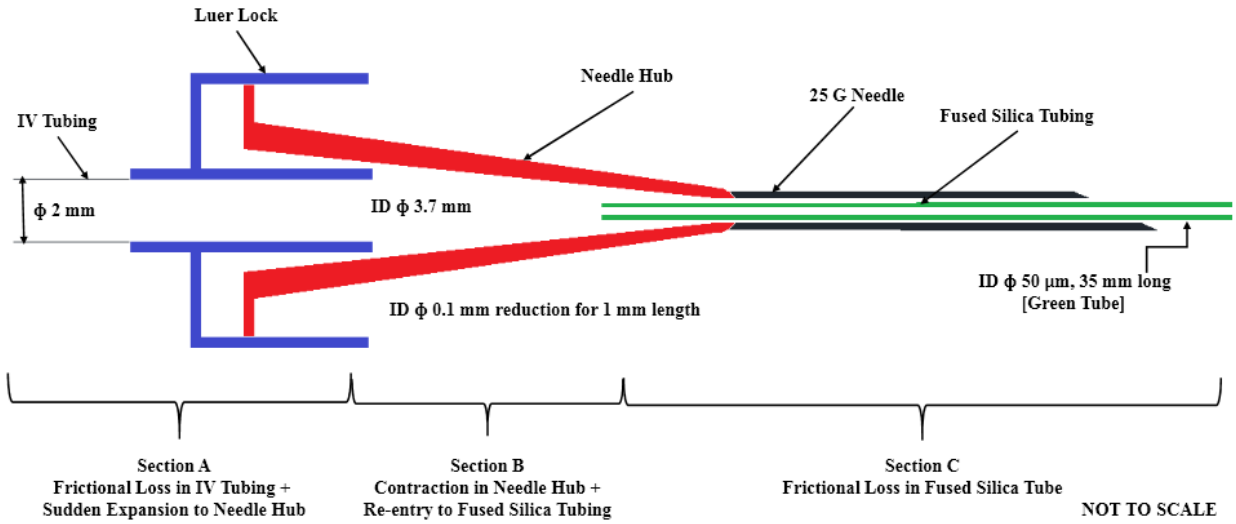

Figure 19: Schematic representation of the connections and losses for flow through the critical parts of the setup for tubular flow

The experiments were conducted with a 35 mm long tube [outer diameter = 0.22 mm, inner diameter = 0.05 mm] inserted in a 25 gauge syringe needle [inner diameter = 0.26 mm]. Figures 20 and 21 show the results from these experiments, and it can be seen that the pressures level off between 95 – 110 mm Hg. The experimental setup yielded results close to the maximum of the range of predicted theoretical pressures, and the time averages varied by about ± 3.2 mm Hg between different trials showing reproducibility.

It can also be seen in Fig. 20 that the pressures start off higher or lower and stabilize over time. The reason for the higher starting pressures in the data plot is because the setup was run at a higher flow rate [about 55 µl/min for 15 to 20 minutes] to remove any air bubbles in the setup

before actual data was recorded [Fig. 20]. Figure 21 shows a magnified portion of Fig. 20 when the pressures have settled down. Some trials were performed immediately after a previous trial without having the need to stop the pump; hence there was no need to run the setup at a higher flow rate to prime the setup and/or remove air bubbles. Therefore, when the needle–tube sample was replaced without shutting down the pump, the pressures initially dropped and gradually increased over time. This is the reason that some of the plot lines in Fig. 20 start at lower pressures.

Table 3: Theoretical pressure range for 50 micron inner diameter tubing, flow rate of 2.5 µl/min [from Appendix I]

Section of the tube connection	**Theoretical Pressure Change (mm Hg)**	
	Lower limit	**Upper Limit**
Frictional loss in tube connecting three-way valve and needle hub [Section A of Fig. 19]	1.16×10^{-4}	1.28×10^{-4}
Sudden expansion in needle hub [Section B of Fig. 19]	4.56×10^{-11}	5.57×10^{-11}
Frictional loss in conical needle hub [Section B of Fig. 19]	3.64×10^{-7}	4.02×10^{-7}
Contraction loss in needle hub [Section B of Fig. 19]	1.27×10^{-12}	1.55×10^{-12}
Contraction loss – Re-entry to needle [Section B of Fig.19]	1.12×10^{-3}	2.59×10^{-3}
Frictional loss in silica tubes [Section C of Fig. 19]	49.96	104.87
Change in elevation [from Sections A to C, exit of Fig. 19]	- 1.73	- 1.65
Total	**48.23**	**103.22**

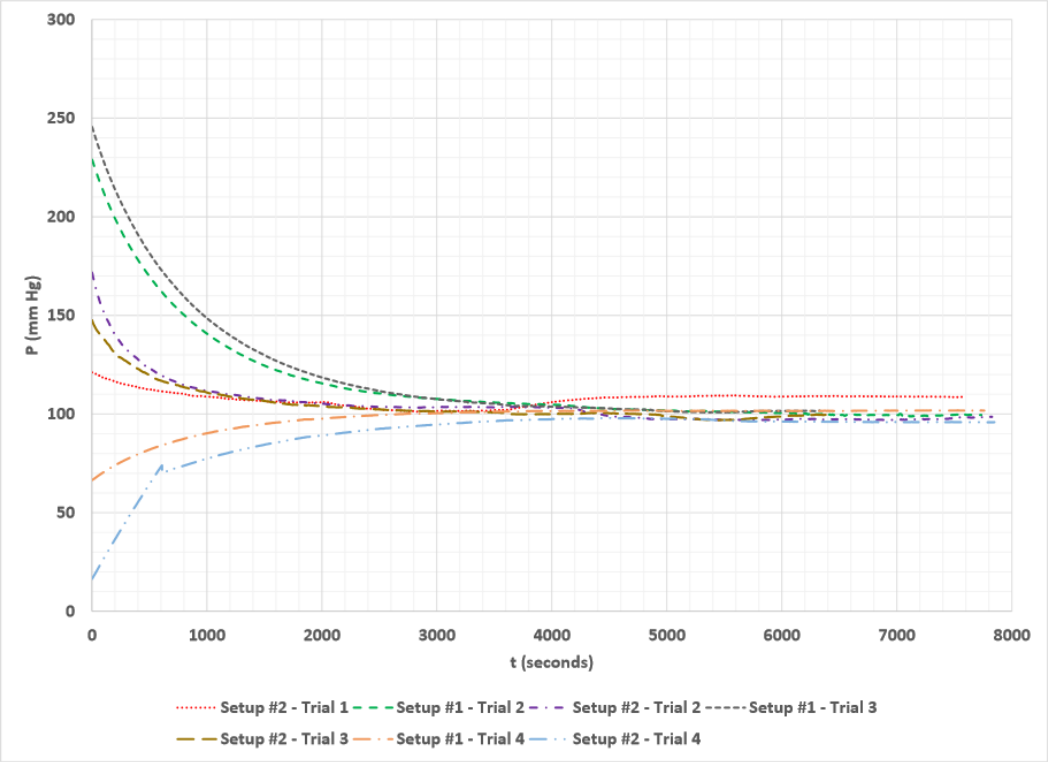

Figure 20: Pressure variations for trials with 50 micron inner diameter tubing at a flow rate of 2.5 µl/min [Dates run: July 29 – 30, 2015]

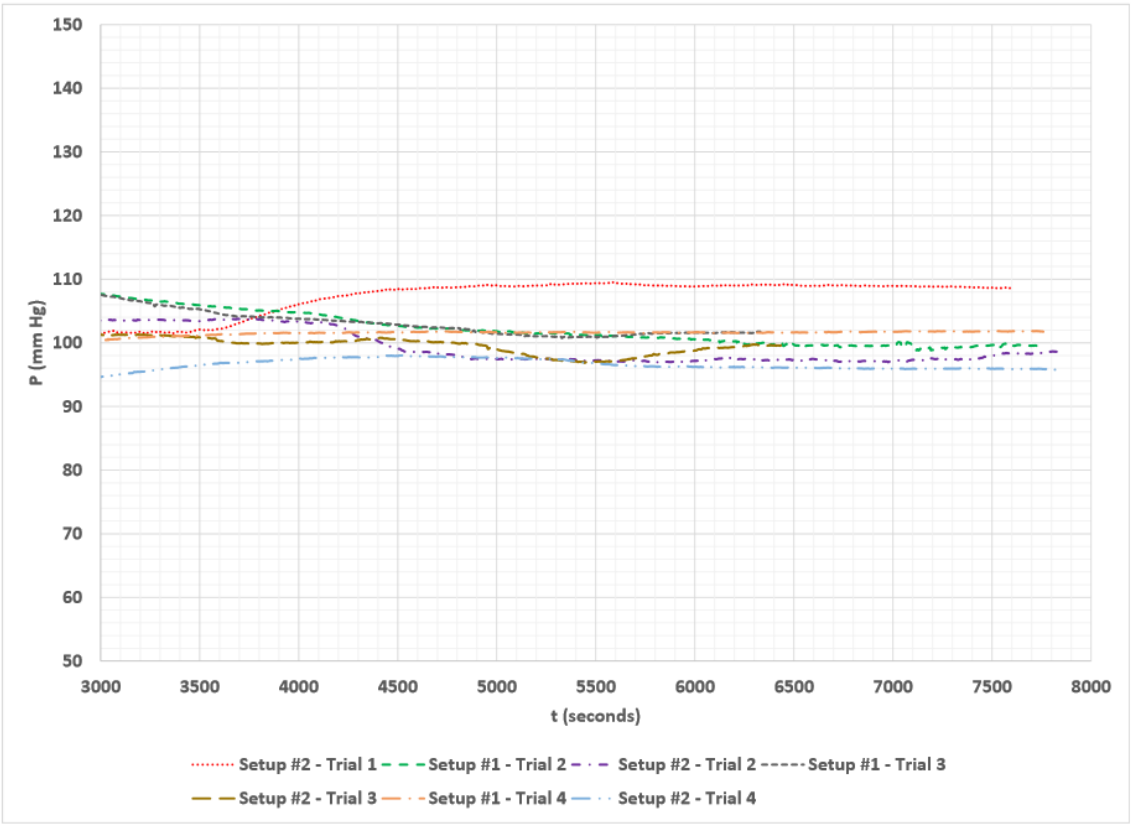

Figure 21: Magnified section of Figure 20 for time ≥ 3000 s

However, since the pressures observed in this range were not near the clinical range of 15 – 20 mm Hg, another set of trials was run with tubing having a bigger inner diameter of 75 microns [Fig. 22]. The same approach was used to determine the theoretical pressure range, considering the tolerance of the tubing diameter [±4 microns] and flow sensor [±5% of set point]. The resulting theoretical pressure range for a 35 mm long tube with inner diameter of 75 microns was 9 – 17 mm Hg [refer to Table 4 for pressure drop break down]. Again, only the frictional and elevation losses contributed significantly to the theoretical results. Experiments were run with the above configuration, and Fig. 22 shows the pressure variation for these trials. All data points beyond a time stamp of 1000 seconds were within a pressure range of 14 – 15 mm Hg with an average of 15 ± 0.4 mm Hg. The trials were conducted at 2.5 µl/min for a period of two hours using different tube samples. All samples were cut from a two meter long tube, and the cut edges were checked under the microscope to make sure that the edges were smooth [as seen in Figs. 15 and 16]. This was done to ensure repeatability of the trials [refer to Fig. 22]. Figure 23 shows a magnified section of Fig. 22.

Table 4: Theoretical pressure range for 75 micron inner diameter tubing, flow rate of 2.5 µl/min [from Appendix I]

Section of the tube connection	**Theoretical Pressure Change (mm Hg)**	
	Lower limit	**Upper Limit**
Frictional loss in tube connecting three-way valve and needle hub [Section A of Fig. 19]	1.16×10^{-4}	1.28×10^{-4}
Sudden expansion in needle hub [Section B of Fig. 19]	4.56×10^{-11}	5.57×10^{-11}
Frictional loss in conical needle hub [Section B of Fig. 19]	3.64×10^{-7}	4.02×10^{-7}
Contraction loss in needle hub [Section B of Fig. 19]	1.27×10^{-12}	1.55×10^{-12}
Contraction loss – Re-entry to needle [Section B of Fig.19]	2.44×10^{-4}	4.56×10^{-4}
Frictional loss in silica tubes [Section C of Fig. 19]	10.91	18.48
Change in elevation [from Sections A to C, exit of Fig. 19]	- 1.73	- 1.65
Total	**9.18**	**16.83**

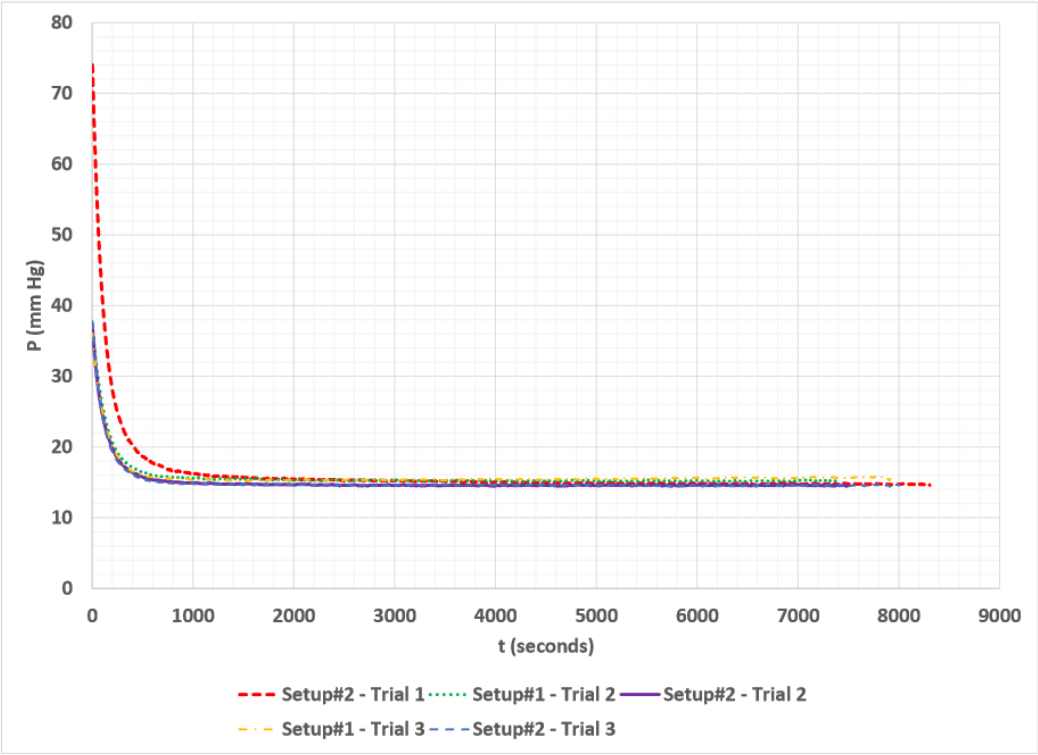

Figure 22: Pressure variations for trials with 75 micron inner diameter tubing and flow rate of 2.5 µl/min [Dates run: July 30 – 31, 2015]

Figure 23: Magnified section of Figure 22 for time ≥ 1000 s

The data collected from both setups were compared for the 75 micron tube trials. The time-averaged data from Setup #1 [15.4 ± 0.1 mm Hg] was higher than that for Setup #2 [14.8 ± 0.2 mm Hg]. The difference in the averages is around 0.8 mm of Hg [or 4%] and indicates that the setups produce different pressure data. The difference between the setups could be deemed negligible considering the clinical application that these setups will be used to simulate. This minor gap in average pressure could be because of the differences in the arrangement of the setups. For example, Setup #2 has longer connecting tubes than Setup #1, which could explain the higher observed pressures in Setup #1 than in Setup #2. However, further work needs to be done to make both the setups identical [same length tubes, better connectors, etc.,] thereby eliminating the difference in pressure measurement between the setups.

The results from the 75 micron tubing trials match the clinical pressure range of interest. In order to check if the observed pressure would reduce by half if the flow rate were halved, more trials were run at 1.25 µl/min with the rest of the configuration remaining the same [75 µm diameter tubes]. Theoretical calculations predicted that the observed pressures would be in the range of 3.72 – 7.59 mm Hg [refer to Table 5 for pressure drop break down]. Figure 24 shows the pressure curves from the different trials run at 1.25 µl/min. Figure 25 shows a magnified section of Fig. 24. From Table 5, it can be seen that the elevation and frictional losses are the major contributors.

From the pressure curves of Figs. 24 and 25, it can be noted that the observed stabilized pressures had an average of 8.4 ± 0.4 mm Hg, higher than the predicted theoretical range. The reason that the observed pressure readings were higher than the predicted theoretical range may be because the difference in elevation between the center of the transducer and the outlet was not accurately measured and had an error of about ± 0.5 mm of water. This translates to about ± 0.07 mm Hg. Also, the transducer's measurement could vary by ± 0.1 mm Hg.

Table 5: Theoretical pressure range for 75 micron inner diameter tubing, flow rate of 1.25 µl/min

Section of the tube connection	Theoretical Pressure Change (mm Hg)	
	Lower limit	**Upper Limit**
Frictional loss in tube connecting three-way valve and needle hub [Section A of Fig. 19]	5.78×10^{-5}	6.39×10^{-5}
Sudden expansion in needle hub [Section B of Fig. 19]	1.14×10^{-11}	1.39×10^{-11}
Frictional loss in conical needle hub [Section B of Fig. 19]	1.82×10^{-7}	2.01×10^{-7}
Contraction loss in needle hub [Section B of Fig. 19]	3.16×10^{-13}	3.86×10^{-13}
Contraction loss – Re-entry to needle [Section B of Fig.19]	6.09×10^{-5}	1.14×10^{-4}
Frictional loss in silica tubes [Section C of Fig. 19]	5.45	9.24
Change in elevation [from Sections A to C, exit of Fig. 19]	- 1.73	- 1.65
Total	**3.72**	**7.59**

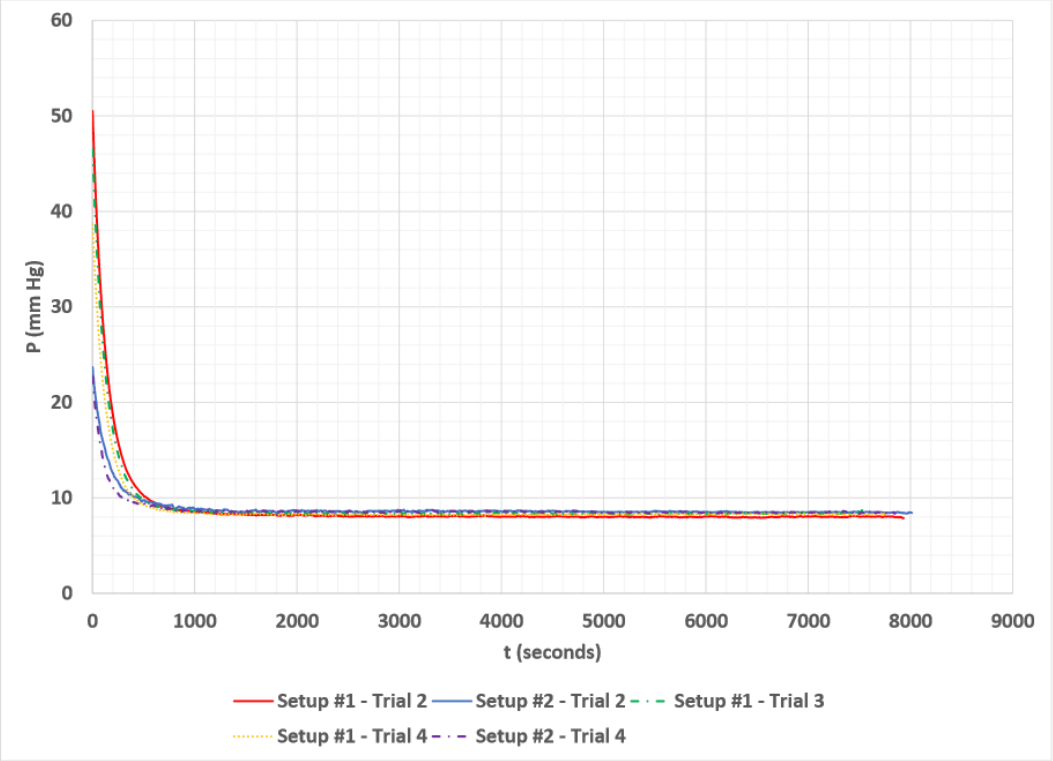

Figure 24: Pressure variations for trials with 75 micron inner diameter tubing at a flow rate of 1.25 µl/min [Dates run: July 31 – August 1, 2015]

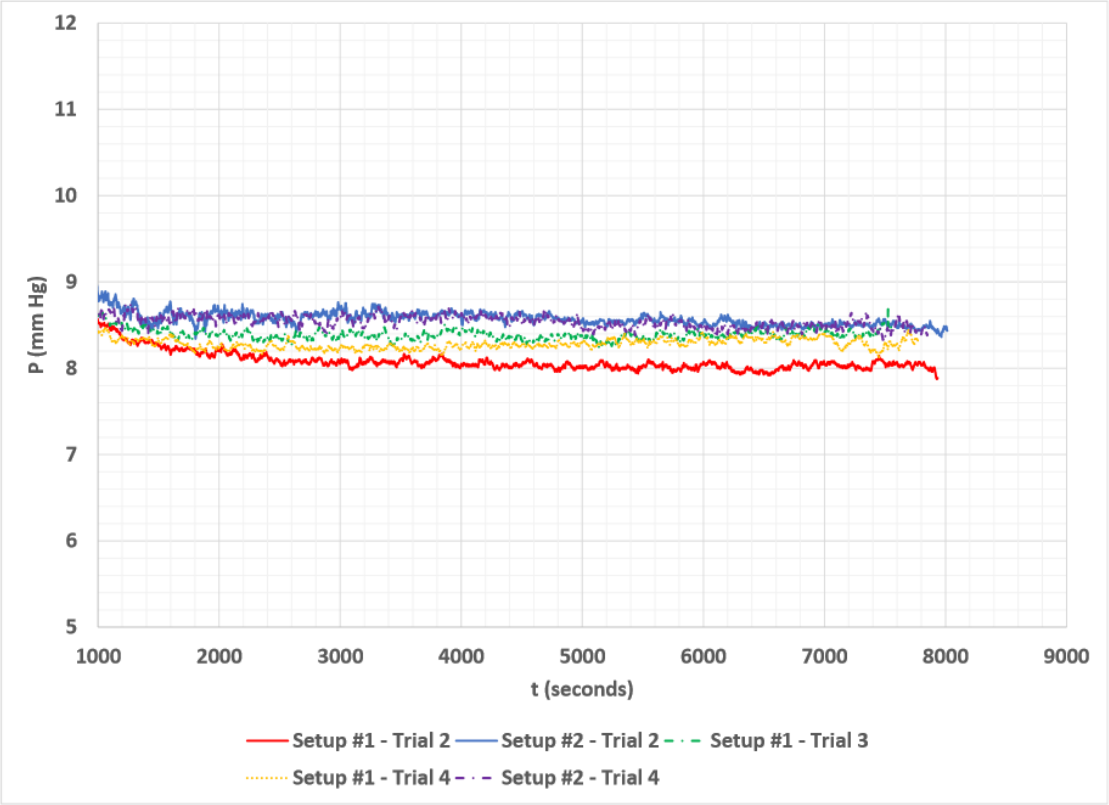

Figure 25: Magnified section of Figure 24 for time ≥ 1000s

The next phase of benchmarking was to run trials with inserts inside the tubes in order to determine the level of consistency [experimental data matching predicted theoretical range] for annular flow readings. A 15 mm long piece of 29 gauge steel wire [average diameter of 0.270 ± 0.005 mm] was inserted in a 23 gauge syringe needle [inner diameter of 0.340 ± 0.005 mm]. The outer diameter of the 29 gauge wire and inner diameter of the 23 gauge syringe needle were measured using a stage micrometer under a 40X magnification microscope [Fig. 26]. If the flow rate were set at 10 µl/min, the annulus effect should produce a theoretical pressure range of 0.13 – 3.23 mm Hg. This range was calculated based on the tolerances in the diameters of both the wire and needle, and elevation. The lower limit [0.13 mm Hg] of the resulting range was calculated using the biggest needle diameter [0.345 mm], smallest wire diameter [0.265 mm] and lowest flow rate [9.5 µl/min]; and vice versa [0.335 mm, 0.275 mm, 10.5 µl/min] for the upper limit [refer to Table 6 for pressure drop break down].

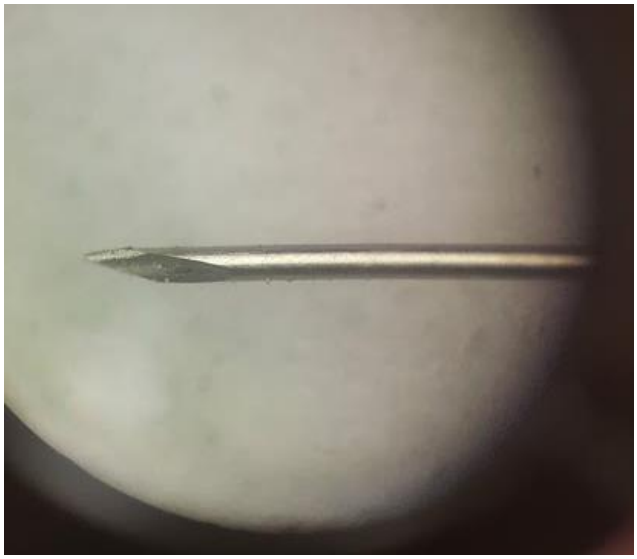

Figure 26: Magnified view of 23 gauge syringe needle

As in the previous calculations, only friction and elevation were significant. Figure 27 shows a schematic of the connections and the possible losses in each section. Experiments were conducted with this configuration, and Fig. 28 shows the measured pressure variations. One can see that there are no high pressures at early times and throughout the period of the trial as shown in Fig. 28 as were seen in Figs. 20, 22 and 24. This is because the effective cross-sectional area for flow was higher for annular flow validation trials as compared with those of the 50 and 75 micron diameter tubing trials. The flow rate at which Fig. 28's experiments were conducted [10 µl/min] was a much higher rate than the nominal physiological flow rate of 2.5 µl/min. The experiments were performed at a higher flow rate because the theoretical calculations predicted an even lower pressure range for 2.5 µl/min [-1.27 to -0.47 mm Hg].

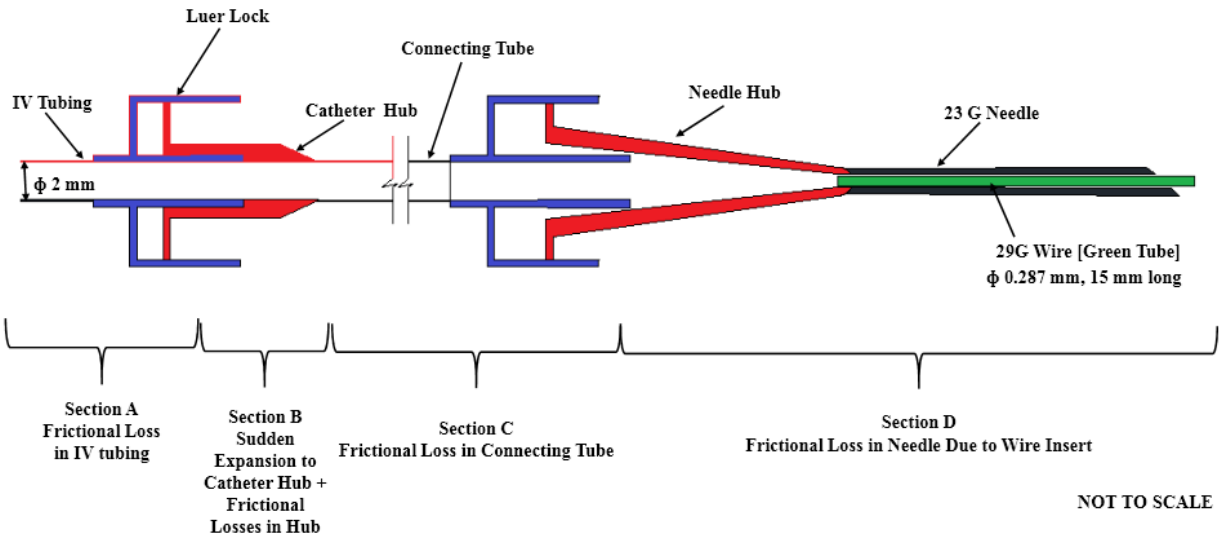

Figure 27: Schematic representation of the connections and losses for flow through the critical parts of the setup for annular flow

Table 6: Theoretical pressure range for flow through annulus, flow rate of 10 µl/min

Section of the tube connection	**Theoretical Pressure Change (mm Hg)**	
	Lower limit	**Upper Limit**
Frictional loss in tube connecting three-way valve and catheter hub [Section A of Fig. 27]	4.62×10^{-4}	5.11×10^{-4}
Sudden expansion in catheter hub [Section B of Fig. 27]	5.4×10^{-10}	6.59×10^{-10}
Frictional loss in conical hub [Section B of Fig. 27]	1.3×10^{-6}	1.43×10^{-6}
Contraction loss in conical hub [Section B of Fig. 27]	1.62×10^{-11}	1.98×10^{-11}
Frictional loss in connecting tubes [Section C of Fig. 27]	1.06×10^{-4}	1.17×10^{-4}
Frictional loss in needle due to wire insert [Section D of Fig. 27]	1.86	4.88
Change in elevation [from Sections A to C, exit of Fig. 27]	- 1.73	- 1.65
Total	**0.13**	**3.23**

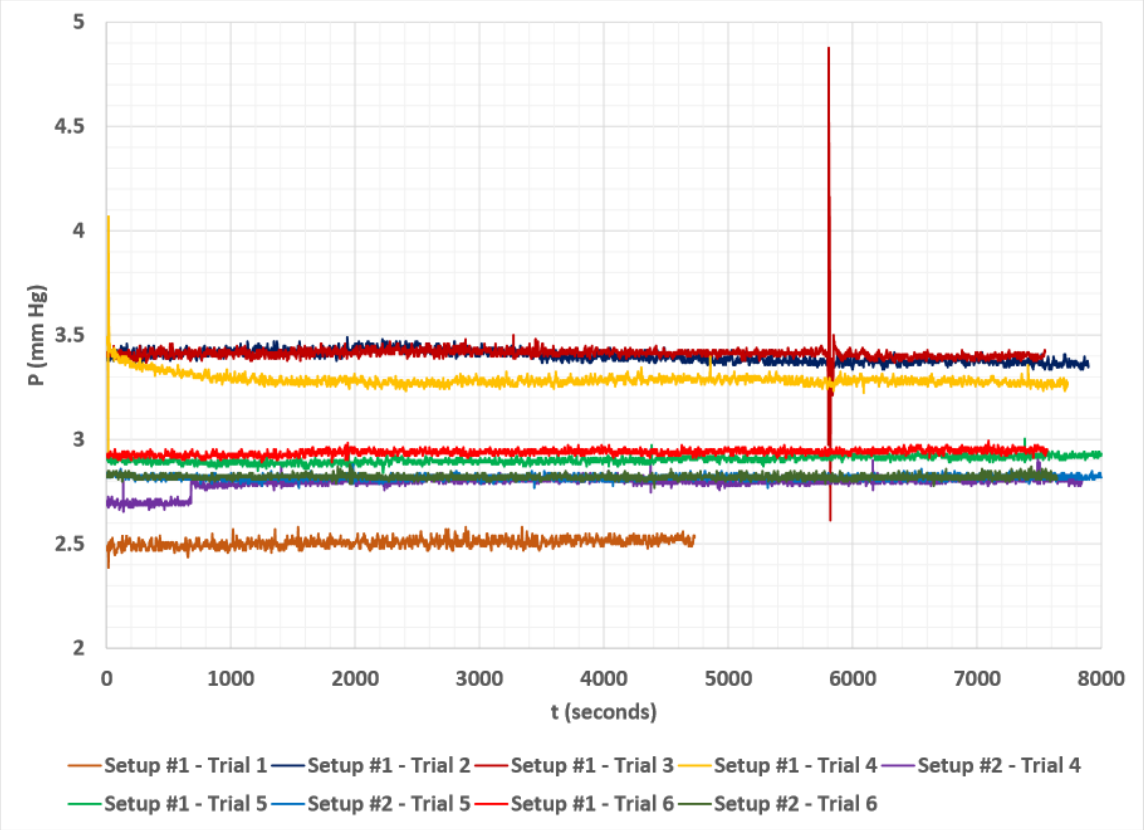

Figure 28: Pressure variation for trials with 29 gauge wire in 23 gauge needle at a flow rate of 10 µl/min [Dates run: August 12 – 13, 2015]

3.4 Residual Pressure in Baerveldt Tubing

It is very important to be able to produce repeatable results for a set of similar flow conditions. This repeatability helps to guarantee the setups' reliability; and it helps to know that, when changes are made in the original setup, these changes cause the measured pressures. A formal baseline for flow through a Baerveldt tube without an insert had to be defined for the setups and repeated at least twice in order to ensure repeatability. The baseline trials were performed at two flow rates: 1.5 and 2.5 µl/min with no insert in the BGI tube. These trials were run for a period of 24 hours. Pressure data from the transducer and flow data from the pump were recorded and reviewed. Figures 29 and 30 show the pressure at the three-way valve for repeated baseline trials conducted at 1.5 and 2.5 µl/min, respectively. Setups 1 and 2 refer to the

two experimental setups, which are identical in terms of components and heights but have slightly different lengths of connecting tubes. The length of the PEEK tube connecting the reservoir to the pump and pump to the rest of the setup, was different for each setup. Refer to **Appendix K** for the experimental procedure followed to conduct all trials. Table 7 lists the theoretical pressures predicted for one of the residual pressure trials. It must be noted that the negative values for the upper and lower limit are due to the elevation difference between the outlet and transducer. It is not clear why the theoretical calculations would yield a negative pressure range when experimental data are all positive. The reason for the ambiguity is unclear: however, further study of the theoretical calculations might shed some light on the negative theoretical pressure range.

Table 7: Theoretical pressure range for residual pressure trials, flow rate of 2.5 µl/min

Section of the tube connection	**Theoretical Pressure Change (mm Hg)**	
	Lower limit	**Upper Limit**
Frictional loss in tube connecting three-way valve and cannula hub	1.16×10^{-4}	1.28×10^{-4}
Sudden expansion in cannula hub	3.7×10^{-11}	4.52×10^{-11}
Frictional loss in cannula hub	3.24×10^{-7}	3.58×10^{-7}
Contraction loss in cannula hub	1.01×10^{-12}	1.24×10^{-12}
Contraction loss from cannula hub to tube	1.45×10^{-8}	1.77×10^{-8}
Frictional loss in cannula tube	1.85×10^{-4}	2.04×10^{-4}
Contraction loss from cannula tube to implant tube	5.98×10^{-7}	2.74×10^{-6}
Frictional loss in implant tube	7.64×10^{-3}	3.17×10^{-2}
Change in elevation	- 0.49	- 0.45
Total	**-0.48**	**-0.42**

From Figs. 29 and 30, it is seen that there are residual losses within the setups, and that these losses are relatively constant [within ±0.5 mm Hg] for a set flow rate; and, as mentioned in

the OMEGA product brochure, the transducer measures pressure with a variation of ± 0.1 mm Hg.

When trials were run at 2.5 and 1.5 µl/min, the corresponding pressure readings at the three way valve were about 2.09 ± 0.19 mm of Hg [theoretical range was -0.48 to -0.42 mm Hg] and 1.47 ± 0.19 mm Hg [theoretical range was -0.46 to -0.44 mm Hg], respectively. The measured pressures include the elevation change between the center of the transducer and the Baerveldt tube outlet [as shown in Fig. 14].

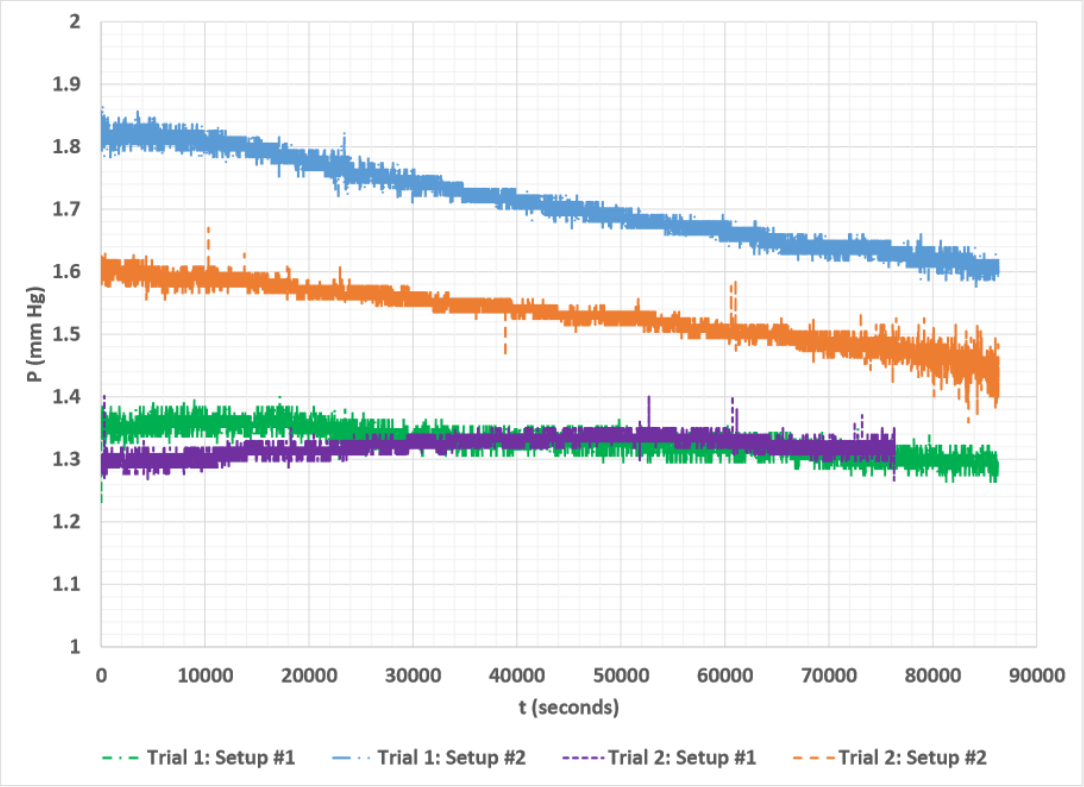

Figure 29: Pressure variations for residual pressure trials at 1.5 µl/min [Dates run: April 25 – 27, 2015]

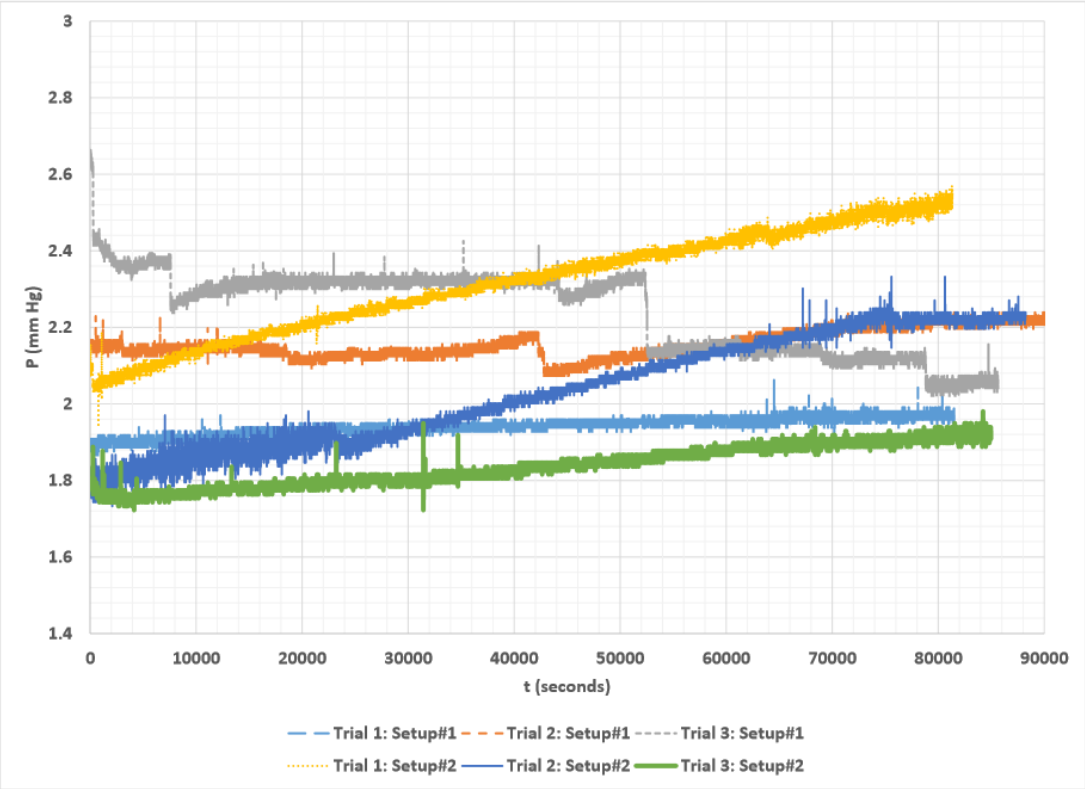

Figure 30: Pressure variations for residual pressure trials at 2.5 µl/min [Dates run: April 4 – 7, 2015]

3.5 Experimental Matrix

The experimental matrix for the insert trials involved 4 parameters: flow rate, diameter, length and suture material, yielding a total of about 30 possible combinations. Since, the initial phase of this research was to develop a reliable experimental setup; it was decided to conduct trials which had clinical relevance [i.e., expected pressures within the range of 4 – 20 mm Hg]. Hence, the trials listed in Table 8 were conducted. 3-0 monofilament and 4-0 braided types of absorbable sutures were selected since using them resulted in pressures which fell within the range of clinical interest [15 – 20 mm Hg]. These trials would help to understand the pressure increase in the BGI tubing when different sutures were inserted. The effects of length, diameter and suture material on the pressure profile would help to determine a suitable material and dimensions to produce the required pressure drop. The suture diameters shown in Table 8 are

based on data found in suture manufacturing standards [27]. The matrix was put together assuming that at least 3 trials were run for each configuration. The results from these trials are discussed in detail in Chapter 4.

Table 9 shows possible variations in the main parameters and the resulting variation in pressure with reference to the base condition [calculated assuming no variation]. It can be seen that the pressure can vary by 200 – 700% if either the tube inside diameter or insert outer diameter are varied. This is the main reason for having a theoretical pressure range instead of a single number.

Table 8: Experimental matrix – list of trials planned

Suture Size	Diameter* (mm)	Length (mm)	Type	Flow rate (µl/min)	# of Trials	Trial duration (hrs)
3-0	0.2 – 0.249	8 ± 0.5	Prolene [Polypropylene]	2.5 ± 0.125	3	~ 24
3-0	0.2 – 0.249	4 ± 0.5		2.5 ± 0.125	3	~ 24
3-0	0.2 – 0.249	8 ± 0.5		1.5 ± 0.0625	3	~ 24
2-0	0.3 – 0.339	4 ± 0.5		2.5 ± 0.125	4	~ 24
3-0	0.2 – 0.249	8 ± 0.5	Monocryl [Poliglecaprone 25]	2.5 ± 0.125	5	~ 24
3-0	0.2 – 0.249	8 ± 0.5		1.5 ± 0.0625	4	~ 24
3-0	0.2 – 0.249	4 ± 0.5	Braided [Polyglactin 910]	2.5 ± 0.125	4	~ 24
4-0	0.15 – 0.199	8 ± 0.5		2.5 ± 0.125	4	~ 24
TOTAL					**30**	

* Sources of diameter data are from Refs. 30 and 32.

If there is a variation in both, the insert's outer diameter and tube's inner diameter, the compounding effect on the theoretical pressure numbers are sizeable. Though flow rate and tube length do not seem to have much of an effect on the overall pressure, they do play a prime role when tubes of much smaller diameter [e.g., 50 – 100 microns] are considered.

Table 9: Variation of theoretical pressure when major parameters change within experimentally possible ranges

	Base condition	**Variation in**			
		Tube inside diameter	**Insert outer diameter**	**Flow rate**	**Tube length**
Tube inner diameter [mm]	0.305	0.305 + 0.025 = 0.330	0.305	0.305	0.305
Insert outer diameter [mm]	0.200	0.200	0.200 + 0.049 = 0.249	0.200	0.200
Flow rate [µl/min]	2.5	2.5	2.5	2.5 + 0.125 = 2.625	2.5
Tube length [mm]	8	8	8	8	8 + 0.5 = 8.5
Calculated pressure [mm Hg]	-0.20	-0.66	1.11	-0.06	-0.18
% decrease in pressure with reference to base condition	--	~230%	~655%	~70%	~10%

The calculated pressure includes a base height difference between the center of the transducer and BGI tube outlet. This is the reason why the calculated pressures are negative when this could not be the case, otherwise.

Chapter 4: Results and Discussion – Short Term Trials

In this chapter, the pressure profiles from the short term trials [discussed under Section 3.5 and in Table 8] with suture inserts, both absorbable and non-absorbable, are presented and analyzed.

4.1 Trials with 3-0 Prolene

3-0 Prolene is a non-absorbable suture made of polypropylene whose nominal outer diameter is 0.2 mm [Table 8]. Sutures of lengths 4 and 8 mm were inserted into BGI tubing of inner diameter 0.305 mm; and experiments were conducted wherein the differential pressure between the three way valve and tube outlet [Fig. 14] was measured over a 24 hour time period for a set flow rate. The first three trials [Table 8] used a flow rate of 2.5 µl/min with an 8 mm suture insert [Fig. 31].

The recorded pressures had an average of 2.84 ± 0.81 mm of Hg, and the theoretical prediction was 0.90 – 2.93 mm Hg. Two of the three trials had very similar pressure plots. In a clinical setting, a variation in pressure of about one to two mm of Hg is not considered significant [33]. However, while trying to characterize the pressure drop of an insert using these experimental setups, the difference between the trials does not help us to statistically analyze the data, even if the variation is about 6%.

The pressures indicated on Fig. 31 naturally include the residual [Section 3.4], which is the pressure recorded when there is no suture in the tube. On average, from Section 3.4, residual pressure was found to be 2.09 ± 0.19 mm Hg. Thus, removing the residual pressure would cause Fig. 31 to range between 0.13 – 1.37 mm Hg. The individual curves in Fig. 31 probably differ from one another because of angle of cut, or burrs, on the edges of the cut sample pieces.

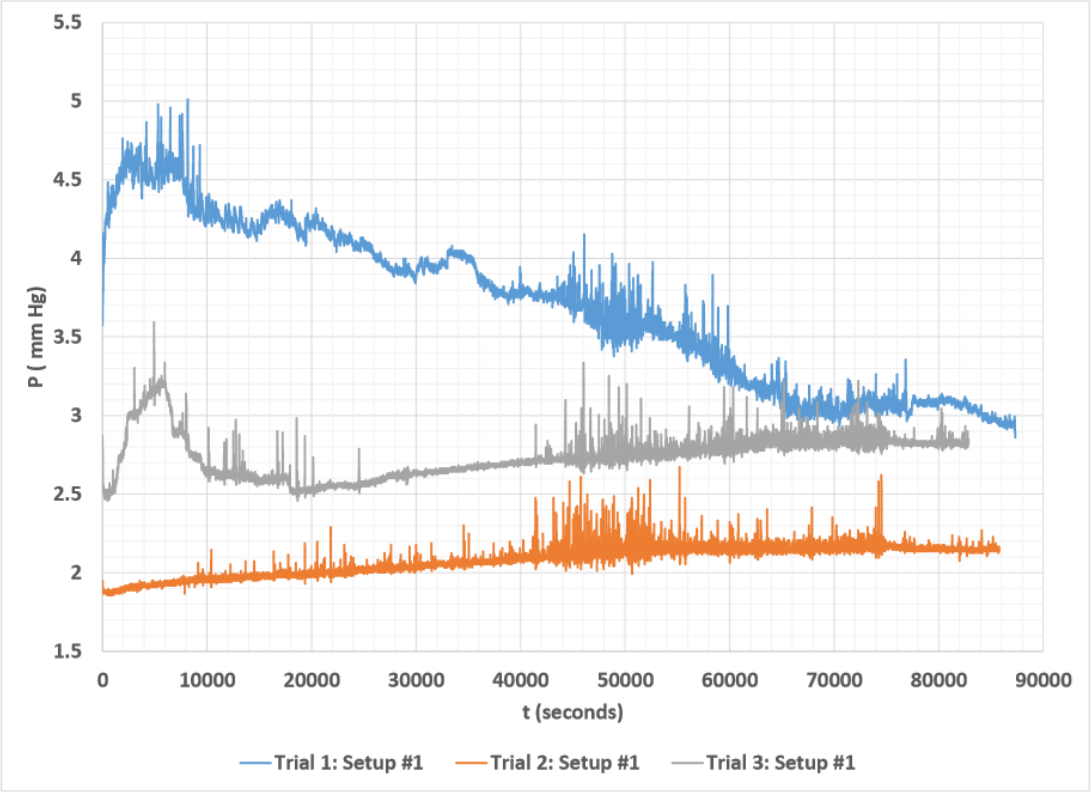

Figure 31: Pressure variations for eight mm 3-0 Prolene insert; flow rate of 2.5 µl/min [Dates run: March 24 – 26, 2015]

The next three trials [Table 8, row 2] were conducted with an insert of the same material as for Fig. 31's trials, but with a shorter length of four mm [results shown in Fig. 32]. From Poiseuille's flow equation [Eq. (1)], one can see that pressure drop is directly proportional to length. Hence, for the same set of parameters, if the insert length is halved, the pressure drop should also decrease by half. Unfortunately, it is not clear if the pressures measured [1.8 to 2.2 mm Hg] are a result of the reduction in length of the insert or are just the residual pressure losses in the system [0 to 2.5 mm Hg, Fig. 30]. Theoretical calculations, considering that the sutures do not swell, showed that the pressures would be within a range of 0.54 – 2.08 mm Hg. However, it is evident that most of the Fig. 32 pressures are lower than what was measured when the insert's length was 8 mm [Fig. 31]; so the trends are correct, but the values are not clearly half. Figure 32 indicates similar spikes in the pressure profile as in Fig. 31, indicating the same possible issues with the way the suture was cut as for Fig. 31. Hence, in order to help clarify this issue, three

more trials were run where the insert length was set at eight mm, but the flow rate was reduced to 1.5 µl/min [Fig. 33]. Though the reduction in flow rate was not exactly half [from 2.5 to 1.5 µl/min], there should have been a proportional decrease [about 0.25 – 1 mm Hg] in measured pressure [from Eq. (2), discussed in Section 2.8].

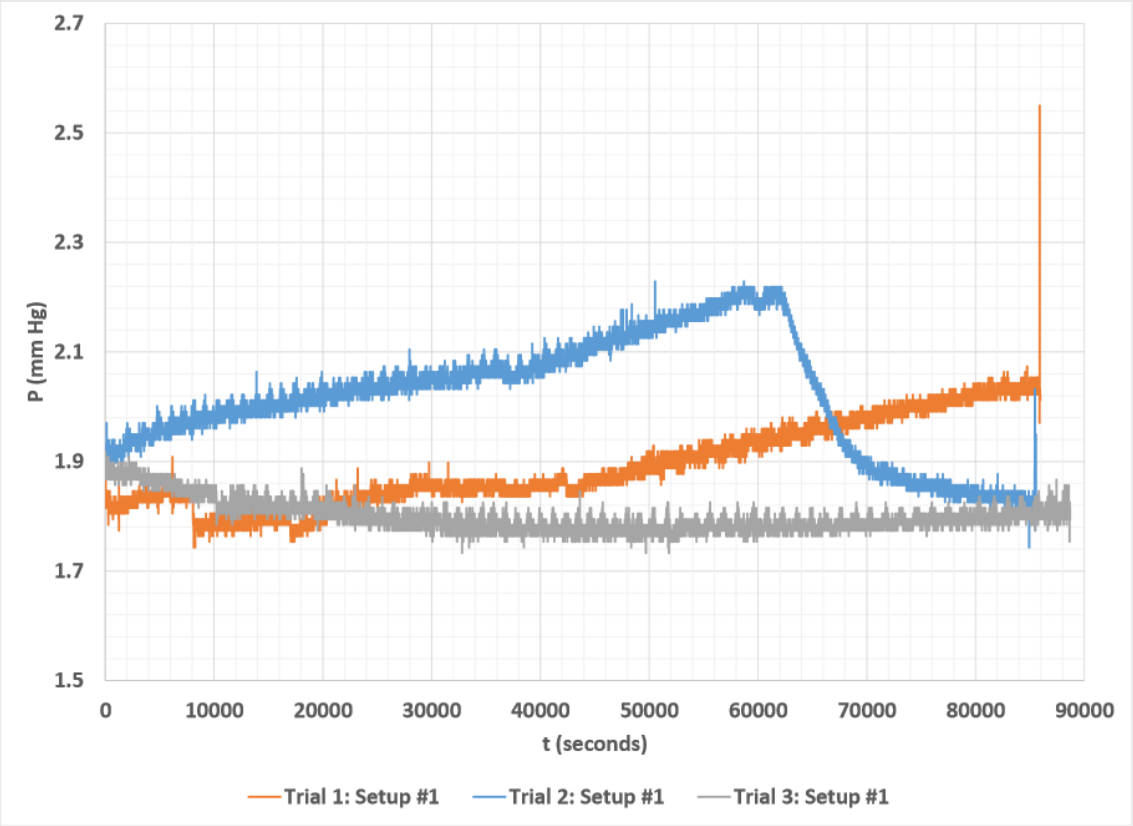

Figure 32: Pressure variations for four mm long 3-0 Prolene insert; flow rate of 2.5 µl/min [Dates run: April 7 – 9, 2015]

Theoretical calculations predicted that, if the sutures do not swell, the pressures would be in the range of 0.22 – 1.29 mm Hg. From Fig. 33, it can be seen that the pressures measured for this trial are very similar to those of the previous trial [Fig. 32] for half of the insert length and higher flow rate. The ratio between the theoretical pressures for Figs. 32 and 33 should ideally be about 1 to 0.83; but the experimental results indicate that there is very little impact due to the reduction of flow rate and increase in length. It could be that the residual pressures dominate, and

the pressures created by the suture insert are relatively unimportant for sutures of this size and material.

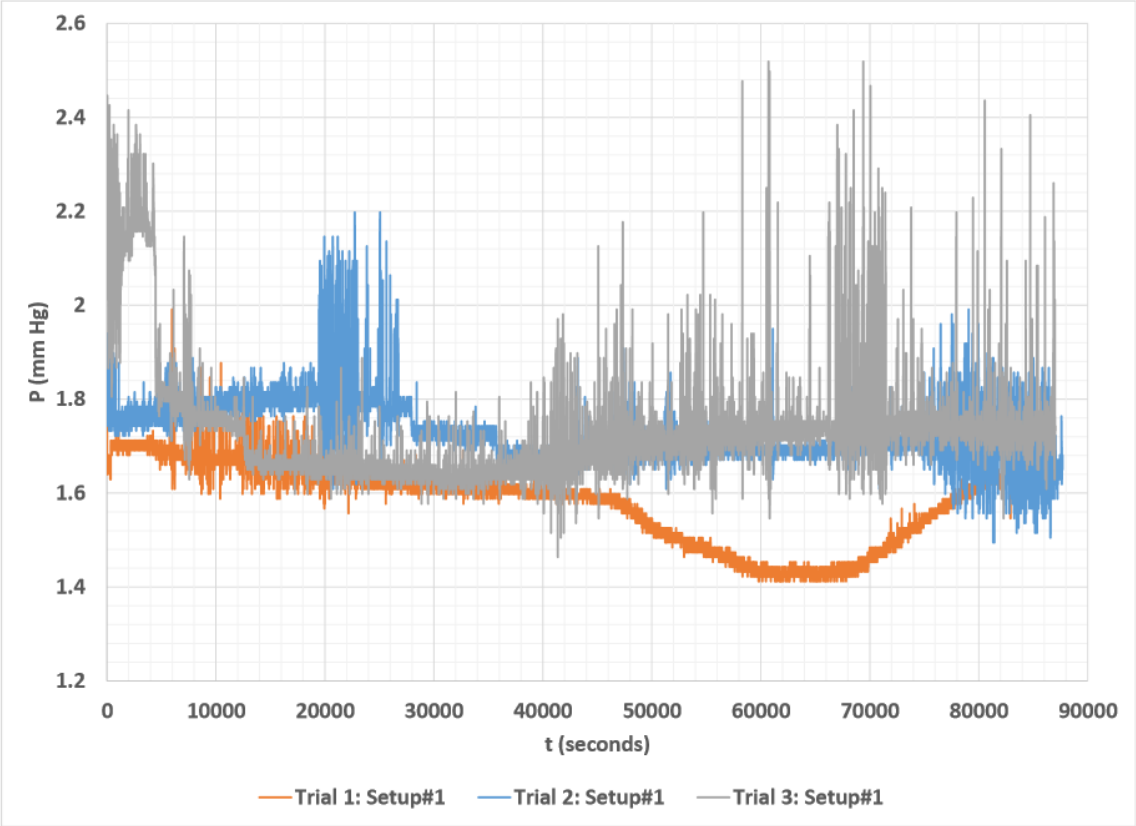

Figure 33: Pressure variations for eight mm long 3-0 Prolene insert; flow rate of 1.5 µl/min [Dates run: March 31 – April 2, 2015]

4.2 Trials with 3-0 Monocryl

3-0 Monocryl is a monofilament synthetic absorbable suture made from a copolymer of glycolide and epsilon-caprolactone [27]. This type of suture starts at the same size [200 microns, Table 8] as 3-0 prolene but expands, by about 100 microns in diameter, when it is submerged or comes in contact with a liquid [34]. The theoretical pressure, assuming no swelling of sutures, was found to be within the range of 0.9 – 2.93 mm Hg. However, if we calculate the theoretical pressures assuming that the sutures swelled, say by about 70 microns in diameter [creating an effective hydraulic diameter for fluid flow of around 100 microns], the resulting theoretical range is 2.01 – 5.75 mm Hg [suture diameter = 200 + 70 (because of swelling) = 270 microns, tube

inner diameter = 305 microns, flow rate = 2.5 µl/min]. This would mean that the measured pressure should be higher than what we observed for 3-0 Prolene, because, when the suture expands, the cross-sectional area for the fluid to flow through would be smaller [smaller annulus] for the Monocryl.

The first set of four trials [Table 8, row 5] were run with an eight mm long insert at a flow rate of 2.5 µl/min. Figure 34 shows that the final pressure in the system at the end of the 24 hour trial was between four and five mm of Hg for all trials. Also, the increasing trend of the curves suggests a gradual increase in pressure due to the swelling of the sutures inserted in the tubes. The increase in the pressure [3.59 ± 0.99 mm Hg] over 3-0 Prolene [2.84 ± 0.81 mm Hg] [Fig. 31] was reasonable considering the fact that these sutures swell based on the theoretical predictions for a suture of bigger diameter.

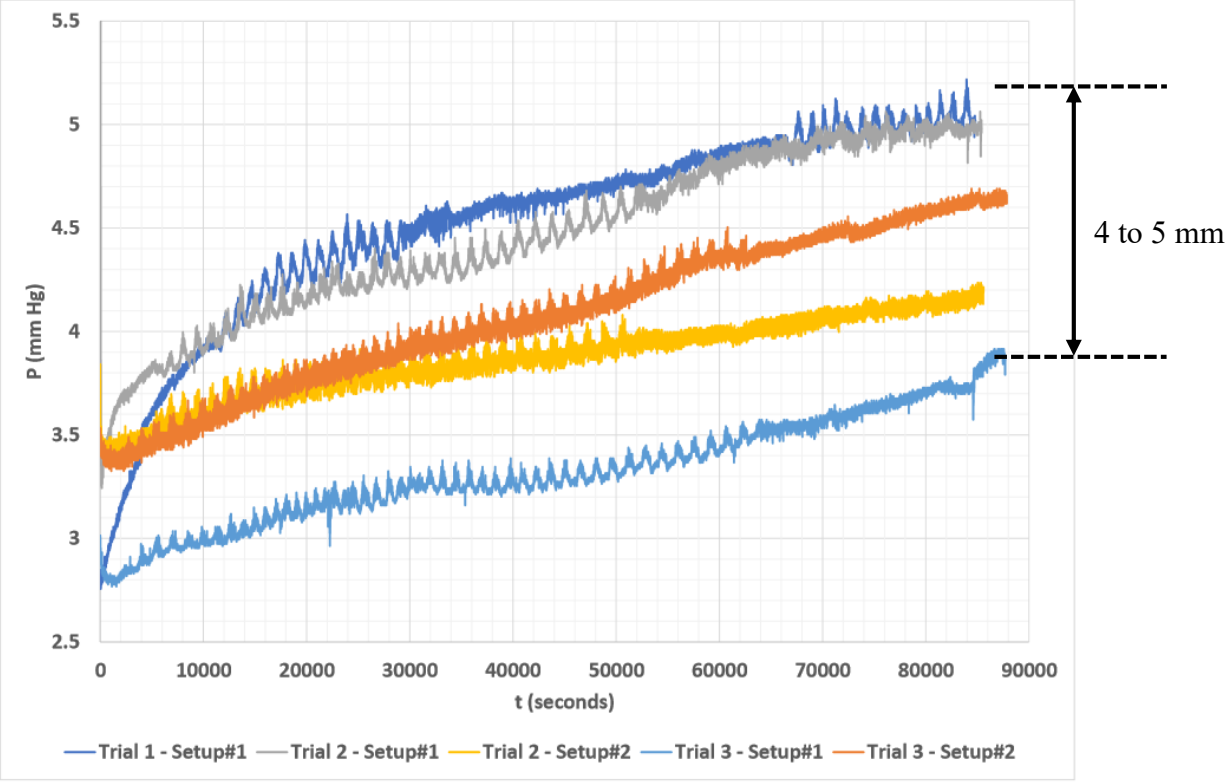

Figure 34: Pressure variations for eight mm long 3-0 Monocryl insert; flow rate of 2.5 µl/min [Dates run: April 10 – 15, 2015]

In order to check for a drop in pressure when the flow rate is reduced, the next four trials were run with an 8 mm long insert at 1.5 µl/min. Unfortunately, the resulting pressure profiles did not have the same pressure trends [rate of increase], and hence the data obtained could not be used to verify the effect of reduction in flow rate on the pressure profile for the absorbable types of sutures. However, it might be inferred that the suture inserts were expanding at different rates because the flow rates were low and the inserts were probably not hydrolyzed evenly. Except for one trial on Fig. 35, the range of pressures was similar to that of Fig. 34.

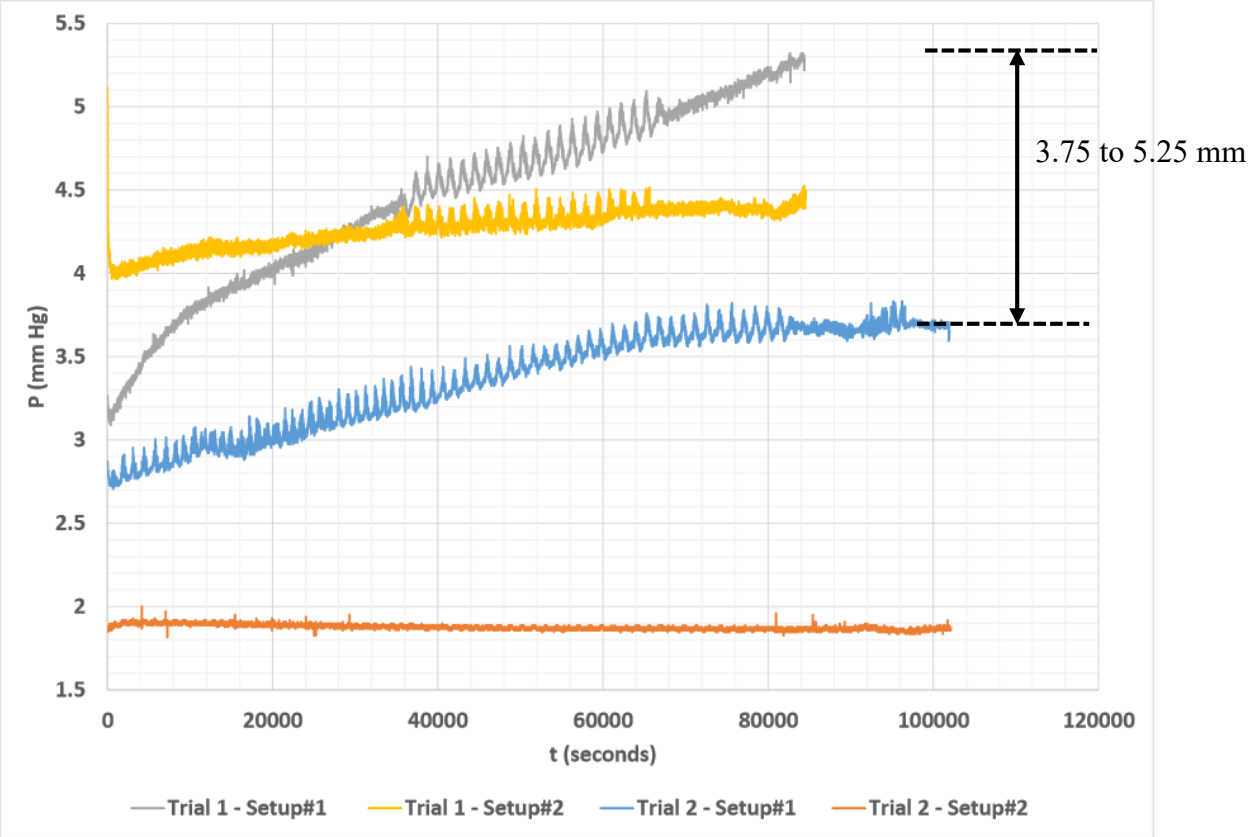

Figure 35: Pressure variations for eight mm long 3-0 Monocryl insert; flow rate of 1.5 µl/min [Dates run: April 16 – 17, 2015]

4.3 Trials with 3-0 Braided

The 3-0 braided suture is a synthetic absorbable suture which is a copolymer of 90% glycolide and 10% L-Lactide, also called Polyglactin [25]. Strands of thin monofilaments are wound together to get the braided look [Fig. 9] [27]. Just as a piece of thread expands when it

comes in contact with water, each of the braided sutures strands swell. That is to say, when fluid is flowing over the suture, it will probably expand and block the whole tube. Therefore, the length used was four mm instead of eight mm and was run at 2.5 µl/min [Fig. 36].

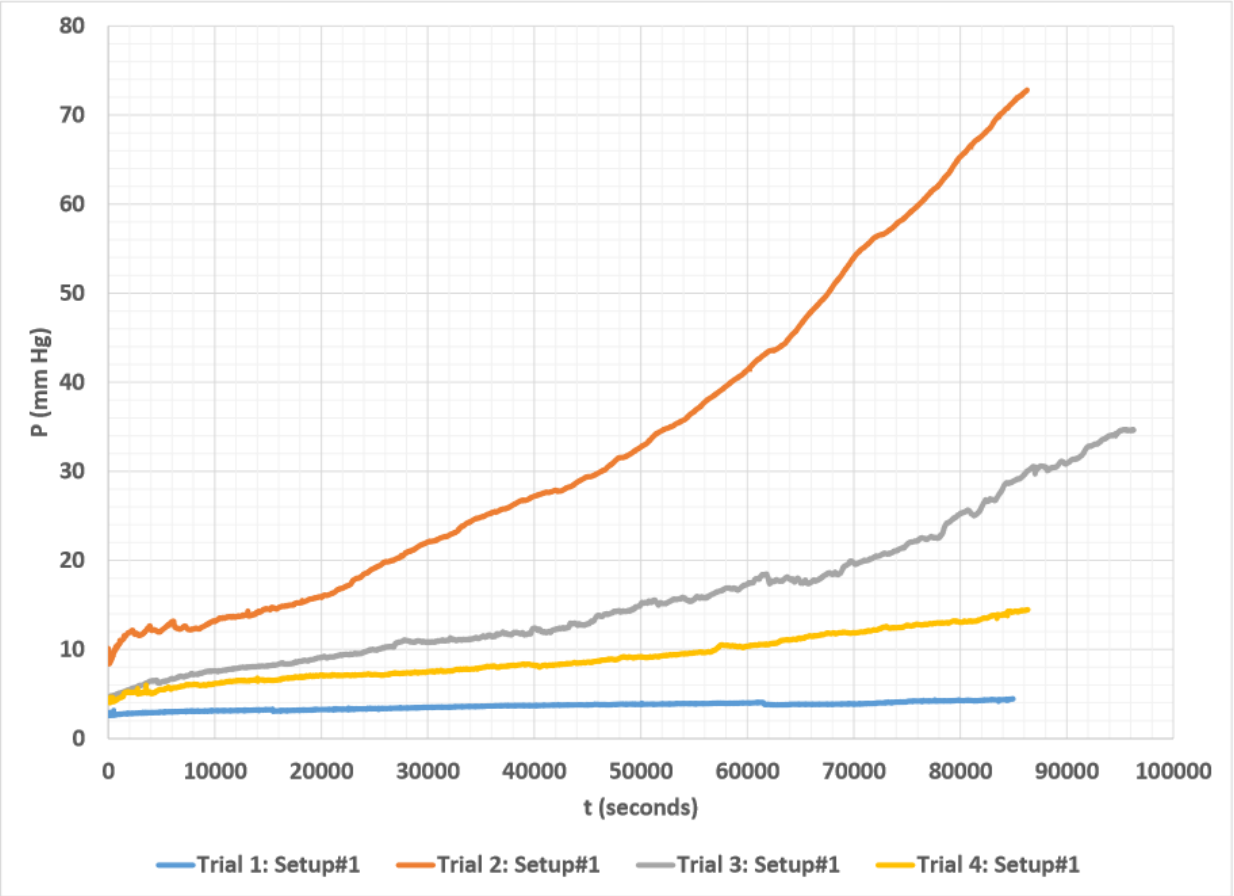

Figure 36: Pressure variations for four mm long 3-0 Polyglactin braided insert; flow rate of 2.5 µl/min [Dates run: February 24 – March 3, 2015]

Though the curves of Fig. 36 are very different from each other, these results help one understand that the pressure can steeply or slowly increase over time. It was later understood that the location of the sample cut from the suture spool could also affect the rate at which the suture expands. To clarify, the suture connected to the suture needle of the spool has an exterior coating. This coating holds the monofilaments together, so that the individual monofilaments don't spread when doctors use them during surgery. The thickness of the coating reduces over the length of the entire spool [27]. This thickness change, in turn, affects the spreading rate of

suture samples that are taken from different locations along the length of the spool. The samples for all of the trials shown herein were taken closer to each other in the spool in an attempt to eliminate the effect of the coating holding the filaments together. It is also possible that edges of the braided sutures were separated or expanded, which could have in turn created a dense porous section for the fluid to flow through the implant tube leading to higher pressures. The individual strands, that are wound together to form the braided suture, could be of different diameters causing non-uniform swelling of the suture, thereby creating a cross-sectional flow area that is not constant throughout the flow path, resulting in higher pressures.

4.4 Trials with 4-0 Braided

The 4-0 braided suture is smaller in diameter than the 3-0 braided suture used in the trials of Fig. 36. The nominal diameter for a 4-0 braided suture is 0.15 mm as compared to 3-0 sutures which have a nominal diameter of 0.2 mm [Table 8]. As explained in Section 4.3, braided sutures tend to expand and partially block the tubes, resulting in porous flow volumes. The results from the trials for 3-0 braided lead to running some trials with 4-0 braided sutures, assuming that 4-0 sutures might not block the tubes as much. The four trials were run with eight mm long inserts of 4-0 braided sutures; at 2.5 µl/min. Figure 37 shows the pressure variation for the four trials that were conducted with this configuration. Three of the four trials showed responses very similar to each other, though the pressure did not rise to the levels seen for trials with 3-0 braided inserts in Fig. 36. This corroborates the assumption that the pressure profile observed for 4-0 braided inserts should be lower than that of 3-0 braided inserts as seen in Fig. 37. One of the four curves is different, possibly because the sample swelled inconsistently due to the coating on the suture [same coating effect as for 3-0 braided].

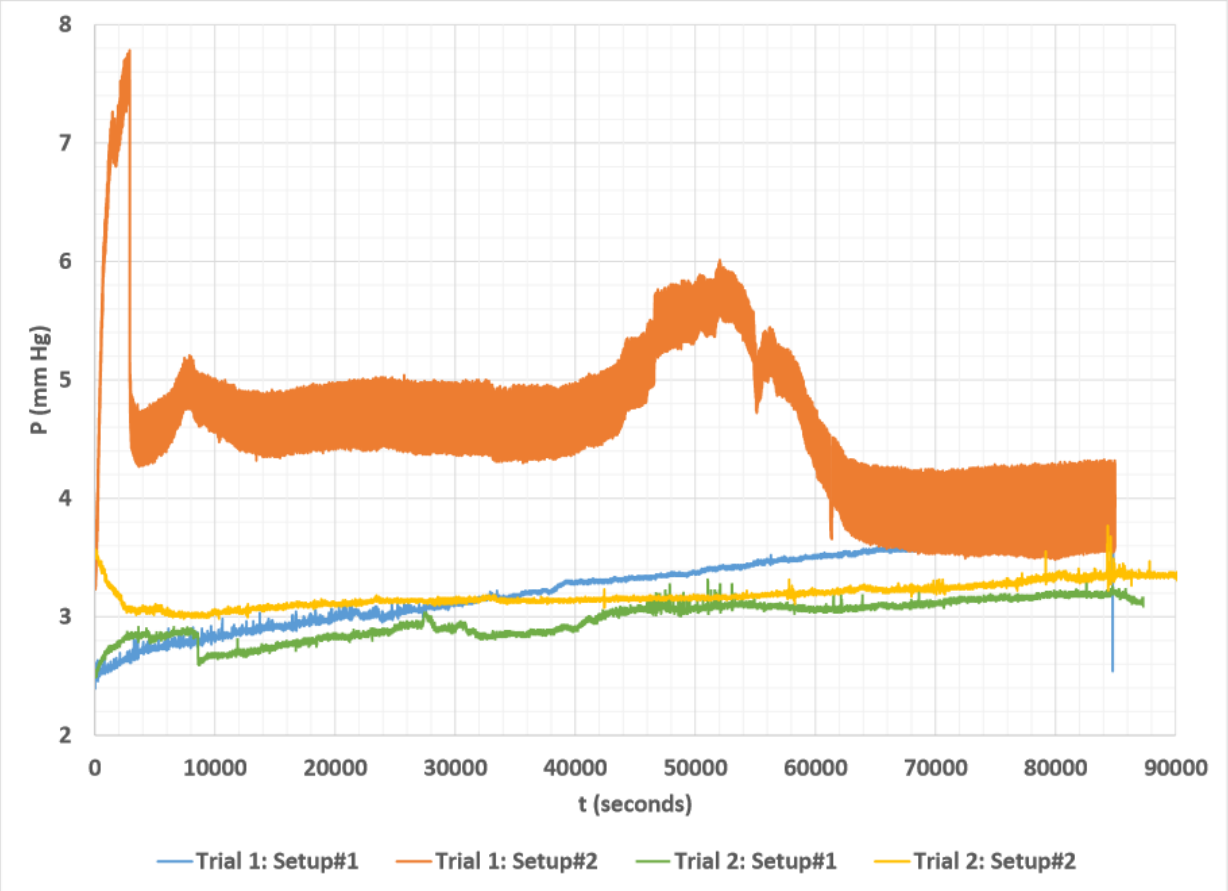

Figure 37: Pressure variations for eight mm long 4-0 polyglactin braided insert; flow rate of 2.5 µl/min [Dates run: April 20 – 22, 2015]

When comparing the pressures from Fig. 37 [between 3 and 5 mm Hg] with those of the 3-0 Prolene trials [2.84 ± 0.81 mm Hg] [Fig. 31], it can be deduced that the average pressures are more or less in the same range. However, the pressure trend is increasing for the 4-0 braided suture insert trials but constant for the 3-0 prolene suture insert trials. If a similar comparison is made between the 3-0 braided and 4-0 braided trials, one can see that the 3-0 braided sutures produced much higher pressures [5 – 80 mm Hg] than did the 4-0 braided suture inserts. The reason for this difference is because a 4-0 suture does not swell as much as a 3-0 suture since their diameters are different. As explained earlier in Section 4.3, the edges of the 3-0 braided sutures could have been separated, resulting in a dense porous cross-section for the fluid to flow through. Also, it could be that the number of strands of monofilaments woven together to create

the 4-0 braided sutures was lower than the number of filaments used to make the 3-0 braided sutures. In short, fewer strands provide lower resistance to flow and cause lower pressure spikes in the system.

4.5 Trials with 2-0 Prolene

From Section 4.1, it can be seen that non-absorbable sutures, like 3-0 Prolene, do not cause much of an effect on the pressure increase in the system. Hence, four trials were run with 2-0 Prolene to see the pressure difference as compared to the trials run with 3-0 Prolene. The nominal diameter for 2-0 Prolene is 0.3 mm [Table 8] which gives a really small clearance/gap when inserted in a tube having an internal diameter of 0.305 mm. It was expected that the measured pressure with this larger insert would be considerably higher than what was observed with 3-0 Prolene. Trials were conducted with four mm long inserts, run at 2.5 µl/min. The theoretical pressure range for this case was 350.9 – 1011.6 mm Hg. Figure 38 shows the pressure variation for different trials with 2-0 Prolene inserted in the tube. The graph bolsters our expectation of increased pressure when an insert of 300 microns is put inside a 305 micron internal diameter tube. The reason that the recorded pressure readings were much lower than the theoretical values could have been the low pressure range of the pressure transducer [0 – 129.3 mm Hg – refer to **Appendix E** for specifications]. The actual diameters of the inserts could have been a little smaller. Even 5 microns could cause a major pressure reduction of 125.6 mm Hg.

Burrs along the edges of the sample might have triggered the difference in peak pressures observed in each trial. Also, the pressure profiles of these non-absorbable sutures seem to exhibit some characteristics of absorbable sutures in the way that the pressure increases over time. This could mean that there were fragments of the suture breaking off and clogging the small annulus flow path, thereby leading to increasing pressures; or these structures might have also swelled by a micron or so, even though they were not supposed to. Also, the tolerance in diameter [± 5

microns] considered for our theoretical calculation might not be correct for the specific sutures used herein, even though the average tolerance is supposed to be ± 5 microns.

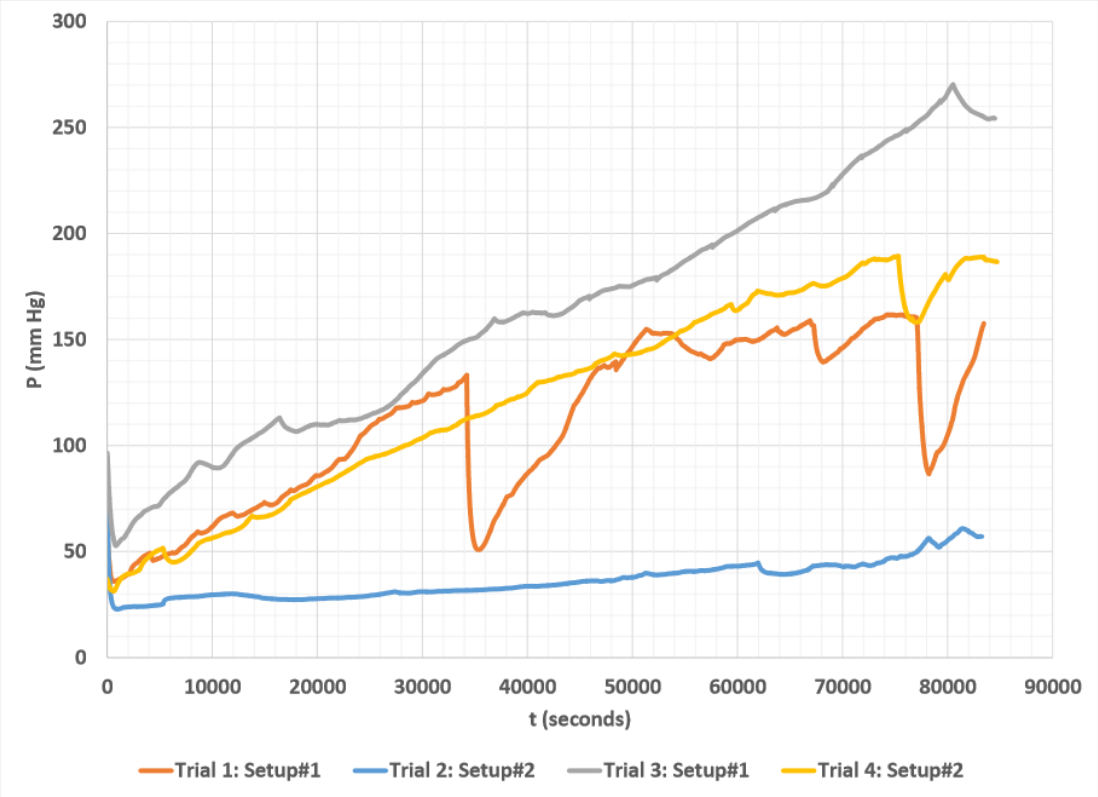

Figure 38: Pressure variations for four mm long 2-0 Prolene insert; flow rate of 2.5 µl/min [Dates run: May 13 – 15, 2015]

4.6 Resistance to Flow

Resistance is defined as ΔP/Q and compared for all of the trials [from Figs. 31 to 37]. From Eq. (2), resistance for annular flow is:

$$R_{flow} = \frac{\Delta P}{Q} = \frac{8\mu L}{\pi\left[r_2^4 - r_1^4 - \frac{\left(r_2^2 - r_1^2\right)^2}{\ln\left(\frac{r_2}{r_1}\right)}\right]} \qquad (3)$$

where,

ΔP Pressure drop [Pa or mm Hg]

Q Fluid flow rate [µl/min or m^3/s]

µ Dynamic viscosity of fluid [Pa.s]

L Length of insert in tube [m]

r_2 Inner radius of tube [m]

r_1 Outer radius of insert [m]

The resistances for all of the trials [from Figs. 31 to 37] were averaged for each time instant and plotted in Figs. 39 and 40. The average of the three or four pressure plots recorded for each configuration was used to determine the average resistance to flow, which is shown in Figs. 39 and 40. Figure 38's data was not included in this plot because the observed pressures were much higher than the clinically relevant range [below 20 mm Hg]. There is not much change in the resistance to flow for 3-0 Prolene [polypropylene] because, when the fluid flows over the surface, there is probably hardly any change in the diameter of the insert.

From Figure 39, for 3-0 Monocryl, one can see that, when the flow rate is almost halved, the resistance to flow increases proportionally for cases when the length of the suture remains the same. But the trends are similar because the rate of swelling is probably similar for both sets of trials [Figs. 34 and 35]. The reason for this trend is that the filaments get hydrolyzed and swell during continuous exposure to any fluid. As the flow rate decreases and pressure drop decreases, and the value of the resistance to flow increases. This can be seen in Fig. 39 where the resistance to flow for 3-0 Monocryl at 1.5 μl/min is higher than that for the trial at 2.5 μl/min.

The 3-0 Polyglactin 910 suture [braided] curve in Fig. 39 has a different trend as compared to those of the other curves because [explained in detail under Section 4.3] these sutures swell much more than 3-0 Monocryl when they come in contact with fluids, creating a dense porous section for the fluid to flow through. The resistance to flow increases with time as the individual strands of the braided sutures swells slowly.

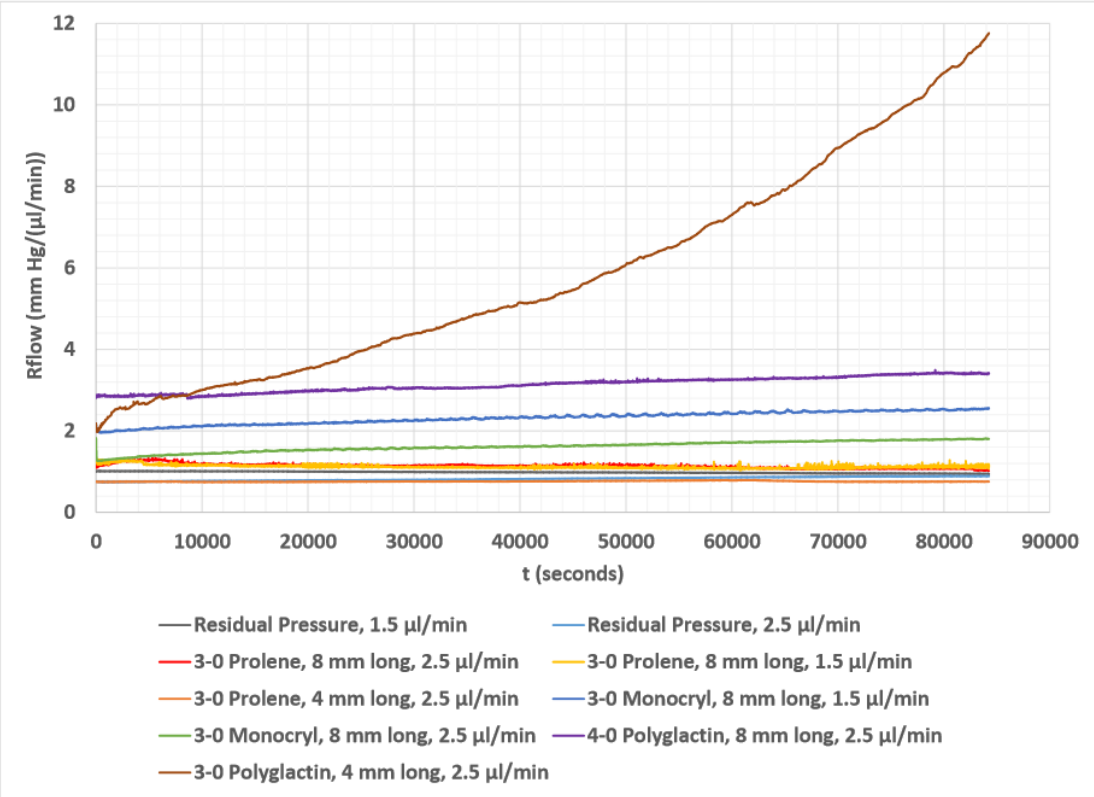

Figure 39: Resistance to flow for various inserts, for 24 hour trials

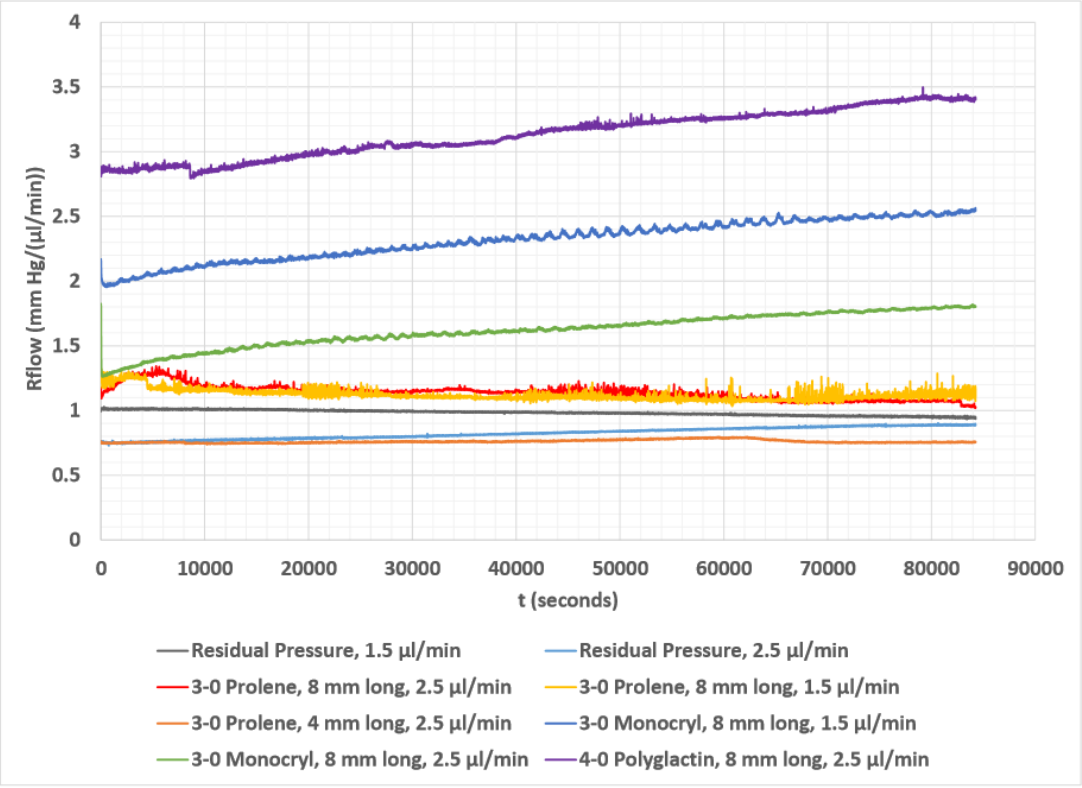

Figure 40: Magnified section of Figure 39

Figures 39 and 40 can be used to better understand the variation of resistance to flow among sutures when similar flow conditions are set. The findings from resistance to flow curves can be summarized as follows:

- Prolene inserts [non-absorbable] have low but constant resistance to flow, since there is no change in the annular flow path [cross-section] over time because the sutures do not swell with continued exposure to water.
- Monofilament Monocryl inserts [absorbable] swell over time and hence the resistance to flow increases by a small amount with time. Annular cross-sectional area decreases as the insert swells.
- Braided Vicryl [Polyglactin 910] inserts [absorbable] also swell over time but may create a porous flow path for the fluid, increasing the amount of fluid coming in contact to the filaments, thereby dramatically increasing the overall resistance to flow. The 3-0 Polyglactin 910 sutures have an increasing resistance to flow because the individual strands in the suture probably swell when they come in contact with fluid and form a dense porous flow area creating an increasing trend in the flow resistance.
- For the same type of suture, when the length is reduced by half, it has been shown that the resistance to flow reduces by roughly half, provided that the flow rate remains approximately constant. This is clear from the RHS of Eq. (3).
- Also, when the flow rate is reduced by half, the resistance to flow remains constant because the pressure drop reduces by a proportional amount. This can be clearly seen because the RHS of Eq. (3) depends only on geometric factors and viscosity, which are constant. However, this does not hold true for absorbable sutures because their dimensions [and observed pressure drop] vary or swell with time; and thus the RHS of Eq. (3) changes.

Chapter 5: Long Term Trials

5.1 Results from Long Term Flow Trials

As mentioned previously [Sections 4.3 and 4.4], on extended exposure to fluids, absorbable sutures deteriorate by a process called hydrolysis [process where the fluid gradually penetrates the suture filaments, producing a breakdown of the suture's polymer chain]. These sutures swell up and slowly begin to erode/deteriorate over time [7 – 10 days for plaingut sutures, 30 – 60 days for both Monocryl and Polyglactin] [27]. This would mean that, when a suture is inserted in a tube and fluid flows through, the suture would first swell, then gradually decrease in size, leading to a sharp initial increase in pressure which would gradually drop to the residual value over time. The plan was to run multiple long-term trials in order to evaluate this prediction. However, only one trial could be run in each of the two setups, with distilled water instead of balanced salt solution. However, a deterioration study external to the two setups was done to compare the effects of using a balanced salt solution [BSS] instead of distilled water [DW].

For the long term trials in the two setups, eight mm long 3-0 Monocryl sutures were inserted in ten mm long implant tubes; and one trial was done using each setup for a period of 30 – 45 days. Figures 41 and 42 show the variation in pressure for Setup #s 1 and 2 for the entire duration of each trial. It can be seen that the pressure fluctuated significantly for reasons unknown at that time. Possible reasons for these fluctuations were later discovered during the stagnant long term trials [Section 5.2]. From the suture manufacturer's website and product catalog, it was understood that the sutures would lose almost 50% of their tensile strength within four weeks [34-36] of being used in surgery.

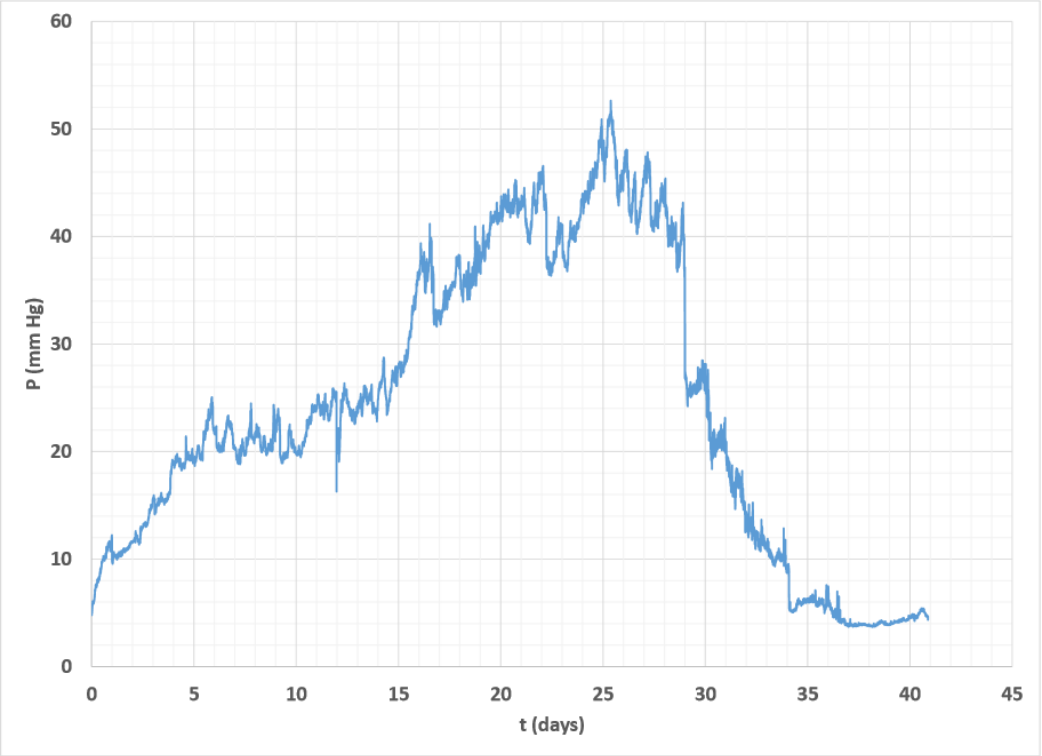

Figure 41: Pressure variations for 8 mm long 3-0 Monocryl insert; and flow rate of 2.5 µl/min [Setup #1] [Dates run: May 18 – June 29, 2015]

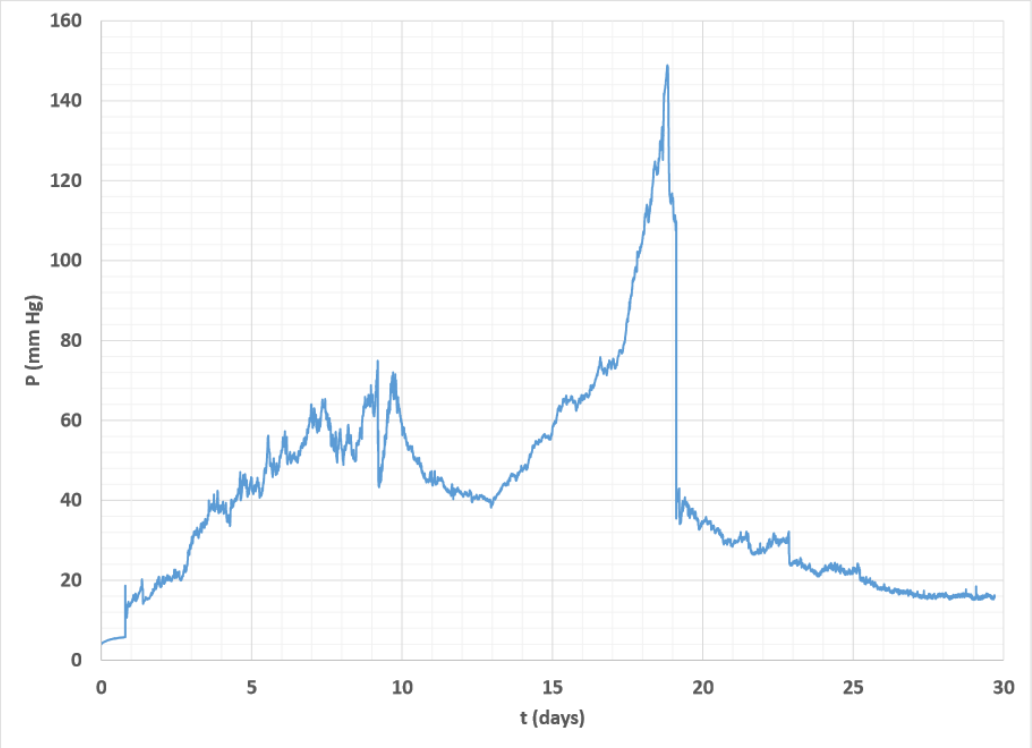

Figure 42: Pressure variations for 8 mm long 3-0 Monocryl insert; and flow rate of 2.5 µl/min [Setup #2] [Dates run: May 28 – June 25, 2015]

Ideally, this means that the pressures should have started to decrease within the four week period. This is because the synthetic absorbable sutures are hydrolyzed when they are exposed to fluid. Ideally, complete absorption of the sutures should take about 60 – 90 days [25, 36].

The pressure fluctuations, as shown in Figs. 41 and 42, could indicate that the suture inserts underwent swelling and deterioration over time. Since it took a long time [about 35 – 40 days] for the pressures to drop to acceptable levels [below 20 mm Hg], it was assumed that this larger-than-expected time might be due to the use of DW. DW, being an inert solution with no salt or acid dissolved in it, does not simulate actual physiologic conditions and does not have a composition similar to that of aqueous humor. So the long term trials were stopped; and a different study was conducted on the dissolution profile of the absorbable sutures in two different fluids – DW and BSS [Section 5.2].

As mentioned earlier, BSS is similar to aqueous humor [produced in the eye] in its composition; and it was hypothesized that the deterioration of the suture would be faster in BSS as compared to DW [36]. The salts and acid concentrations in BSS deteriorate the polymer chains holding the suture together [36]. As explained earlier, absorbable sutures usually first expand in size [diameter and length] by absorbing the fluid in which they are immersed and then start to erode/decrease in size [diameter and length] [34]. An absolute deduction about the pressure variation for long term flow trials cannot be made, since a sufficient number of trials was not conducted. However, with the data available, it can be said that the sutures might have become too large in diameter because the observed pressures reached levels [more than 30 mm Hg] that are not desirable in a clinical situation [where IOP has to be below 20 mm Hg]. It could be that those pressures might reduce to the clinically desired range if absorbable sutures of smaller diameter, say 4-0 Monocryl, were used to run further long term studies.

5.2 Results from Long Term BSS vs DW Trials

Twelve samples of 3-0 monocryl sutures were cut from the spool. Six samples were placed in vials having about two milliliters of DW, and six were immersed in BSS. The vials were secured in small boxes [refer to Figs. 43 and 44]; and beginning on July 2, 2015, they were rocked by hand every day for about 15 – 20 minutes manually in order to include an effect of fluid flow over their surfaces. Though the manual rocking/shaking was not a close approximation to the flow of fluid over suture surfaces at a slow flow rate of 2.5 µl/min, the rocking did help to mimic the effect of fluid movement over the sutures in order to increase the deterioration rate. The plan was to let the suture samples be immersed in stagnant DW or BSS for at least 30 days and determine the time taken for the samples to deteriorate. One sample each for DW and BSS was pulled every week or so to study the variation in diameter and look for effects of deterioration. When each vial was removed from the stack, approximate measurements of the diameter were made, using a microscope with a micrometer scale, and recorded. The micrometer scale had 100 divisions, where each division denoted 0.01 mm. One vial each of DW and BSS was removed at the same time to help compare the dissolution profiles of both samples. Table 10 shows the measurements made over time for all of the samples; and Fig. 45 plots the measured diameters as a function of time.

Figure 43: Interior of box having six vials

Figure 44: Exterior of boxes having six vials each with DW or BSS

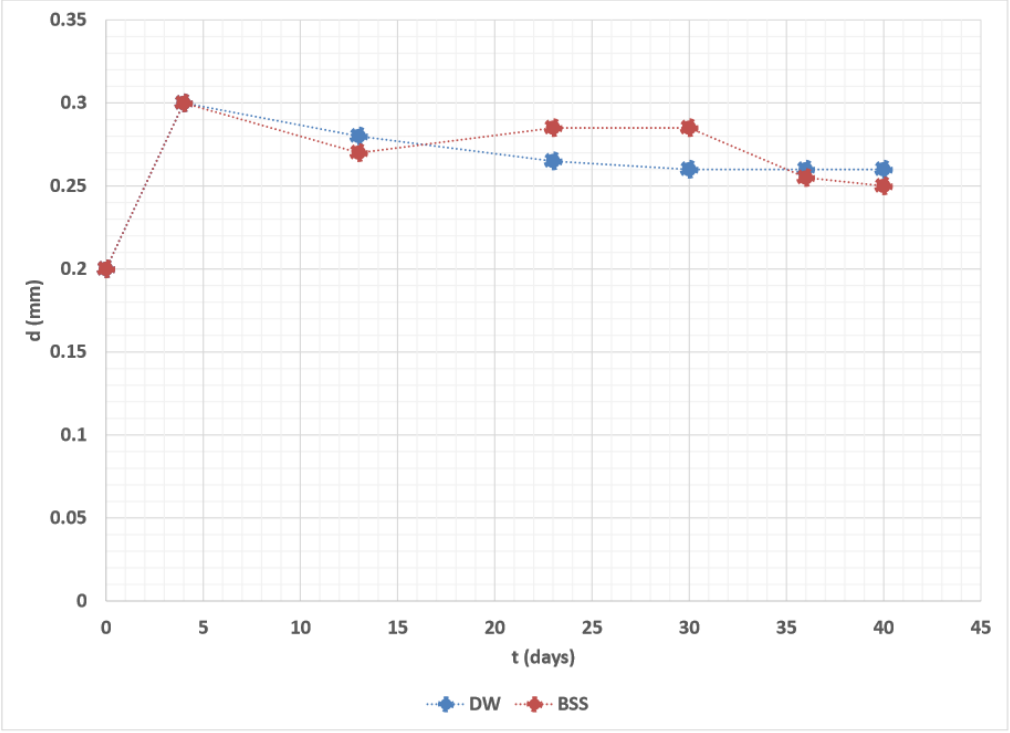

Figure 45: Harvested suture diameters over time

Figures 46 – 50 show the physical changes in the surfaces and textures of the sutures over time. From these figures, it can be seen that the deterioration of the samples immersed in BSS was much faster than that of the samples immersed in DW. The reason why the samples immersed in BSS had greater deterioration rates was because the polymer chains were broken down during hydrolysis [37].

Table 10: Diameter measurements at different time intervals over the 40 day trial

Date	DW sample diameter (mm) ± 0.01 mm	BSS sample diameter (mm) ± 0.01 mm	Observations
Day 0 [7/2/2015]	0.2	0.2	Before immersing the samples.
Day 4 [7/6/2015]	0.3	0.3	Swollen samples.
Day 13 [7/15/2015]	0.28 – 0.3	0.27	Slight discoloration of BSS sample. DW sample was clear. [Fig. 46]
Day 23 [7/25/2015]	0.25 – 0.28	0.27 – 0.3	Flaking on the surface for BSS sample. No flaking on DW sample. [Fig. 47]
Day 30 [8/1/2015]	0.25 – 0.27	0.27 – 0.3	BSS sample broken into two pieces. Flakes all over surface. Disintegrated. DW sample was in the initial stages of flaking. [Fig. 48]
Day 36 [8/7/2015]	0.26	0.25 – 0.26	BSS sample had lacerations all over the surface. Flakes on DW sample. [Fig. 49]
Day 40 [8/11/2015]	0.26	0.25	Both samples showed signs of extensive flaking. DW sample had longer flakes as compared to BSS sample. [Fig. 50]

The ionic solution (BSS) played a major role in accelerating the hydrolysis, and this did not happen in the case of DW. During hydrolysis, the fluid enters into the monofilaments of the suture, internally reacting with the polymer, slowly eroding the suture from inside [25]. From Fig. 46, which was taken 13 days from the start, the BSS sample had striations along the surface, and there were ‘glints’ in the suture suggesting fluid seepage into the monofilaments. This effect was not very prominent in the DW sample, though both samples had absorbed the respective fluids. The BSS sample was slightly discolored [yellowish] as compared to the DW sample. The micrometer scale can be seen behind the suture samples in Fig. 46.

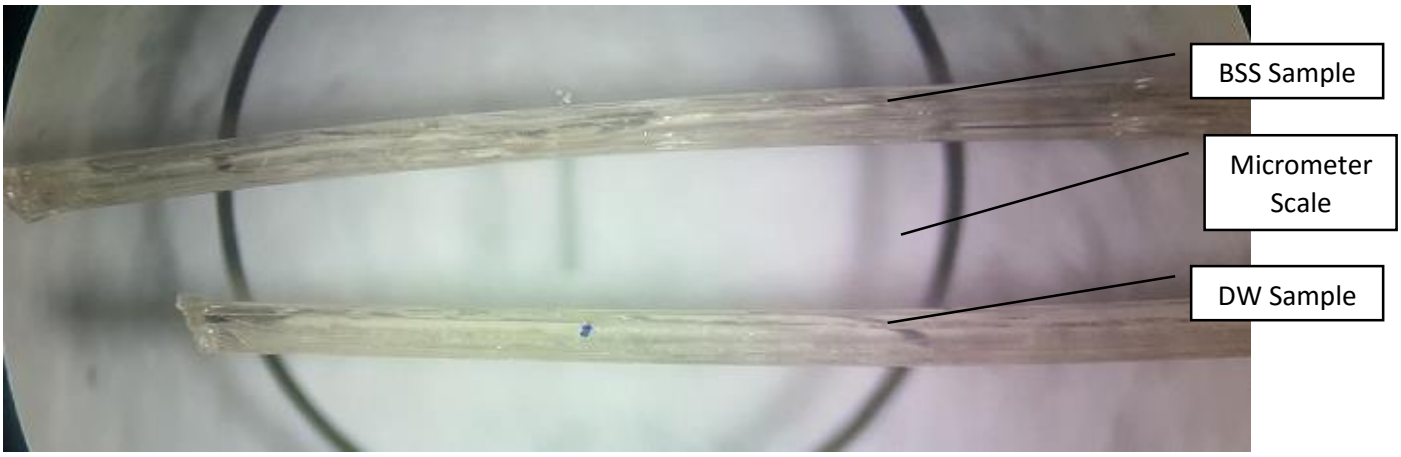

Figure 46: After 13 days – BSS sample on the top, DW sample on the bottom

From Fig. 47, taken after 23 days from the start of the trial, the BSS sample showed greater signs of deterioration, in the form of 'flaking' on the surface. The surface was full of small flakes that curled out. Also the internal part of the suture suggested more seepage of the BSS fluid. The DW sample showed no signs of flaking on the surface but had significant striations along the length of the suture. Both samples were clear when examined under the microscope.

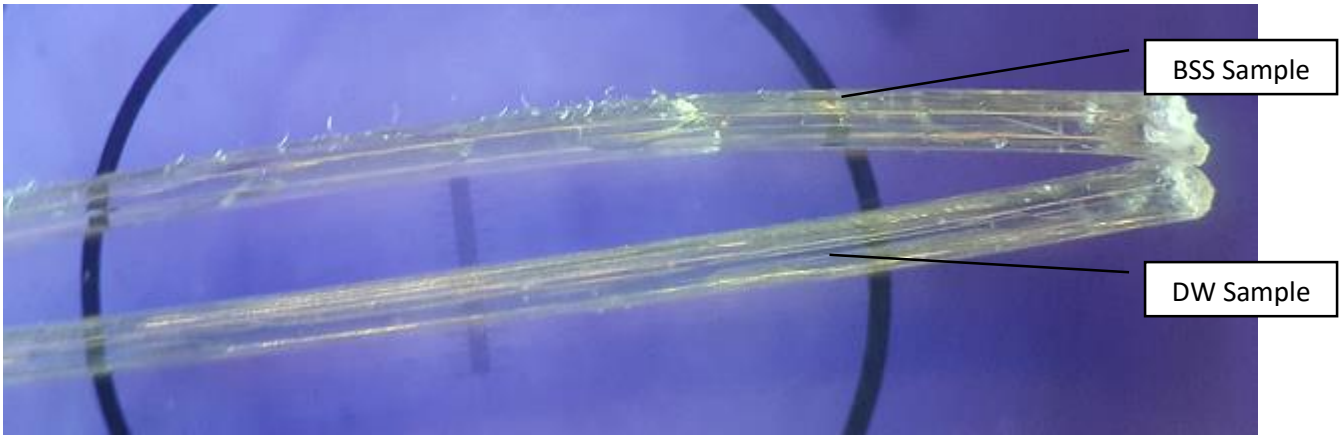

Figure 47: After 23 days – BSS sample with flakes on the top and DW sample on the bottom

In Fig. 48, taken 30 days from the start day, it is clear that the BSS sample was tattered and had started to fall apart. Though no tensile strength tests were conducted, it seems clear that the sample would have very low strength as compared to that of its initial state. One could easily

comprehend the reduction in strength while handling the sample. The DW sample showed very slight signs of flaking on the surface, but it had many striations along its length suggesting fluid seepage into the monofilaments.

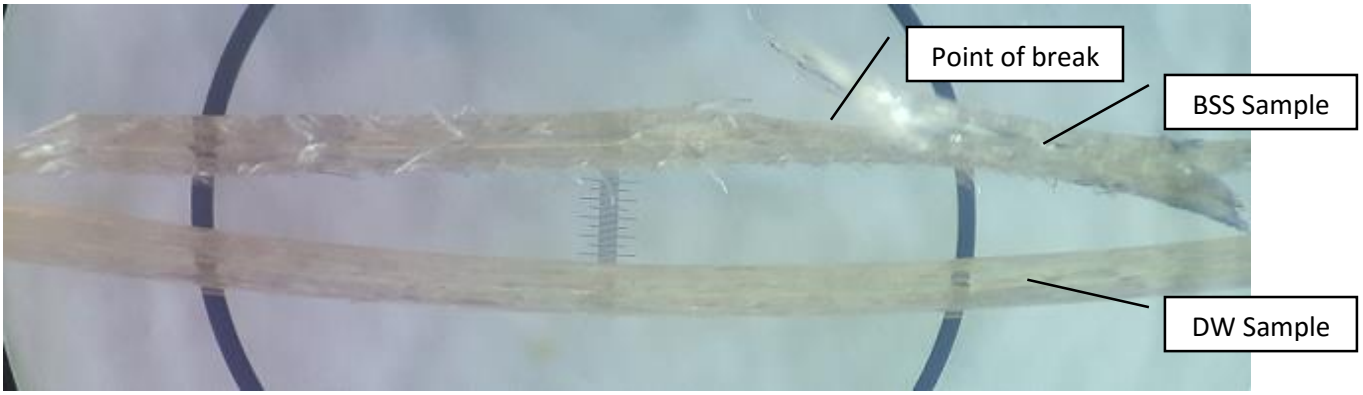

Figure 48: After 30 days – Deteriorating BSS sample on the top and DW sample on the bottom

At the end of 36 days, Fig. 49 show that the BSS sample had flaking and breaks along the length similar to what was seen in Fig. 48. The DW sample was very clear but had straight lines/breaks all along the surface, and also cavities were visible on the inside of the suture, suggesting internal erosion.

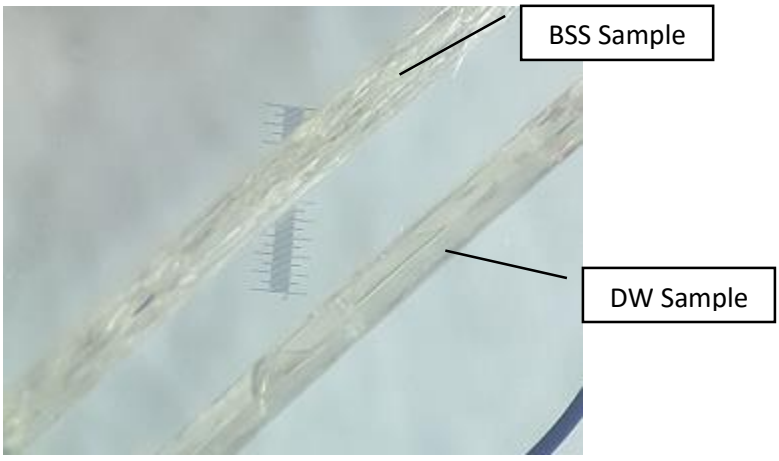

Figure 49: After 36 days – Deterioration is visible in both samples

At 40 days, Fig. 50, one can see that both samples showed flaking on the surface. The flakes on the DW sample were longer in length when compared to those of the BSS sample.

Flaking was denser on the BSS sample as compared with the DW sample, and both samples were slightly discolored.

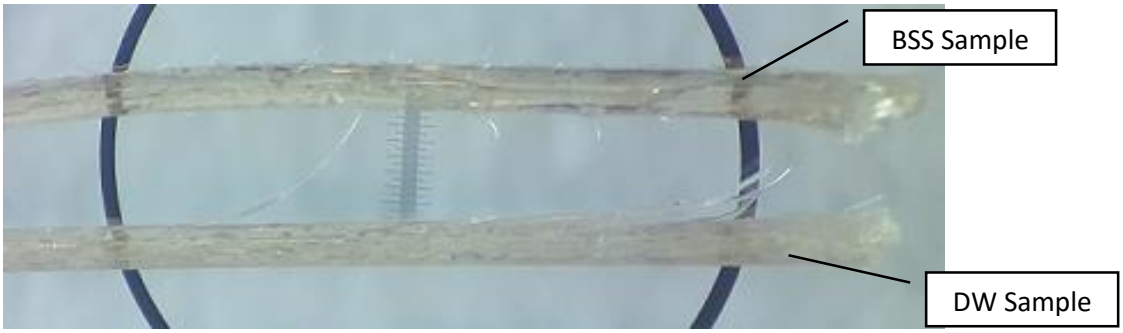

Figure 50: After 40 days – Flakes on both samples

From Figs. 46 – 50, one can see the difference in deterioration rates for both samples, suggesting that the BSS reacts much faster with the suture, whereas the DW takes more time to react. This would be because the different salts present in the BSS help to hydrolyze and erode the suture faster. Hence, from the results of these tests, it would appear to be better to use BSS as the operating fluid for running experiments which involve biodegradable/absorbable materials, in order to more accurately simulate physiologic conditions and to get a clear understanding of the dissolution rates and pressure profiles of suture-like polymer inserts.

However, there is one big problem when it comes to running trials with BSS instead of DW. The BSS is a breeding ground for bacteria/algae, and there would be growth of some sort in the bottle/container in which BSS was stored. Hence, care must be taken to ensure that the bottle/container is cleaned every two weeks and made sterile using an autoclave. In addition to this, an anti-bacterial solution can be added to BSS in order to reduce the rate of bacterial growth.

Another way to check for dissolution rates of sutures in BSS would be to take several samples of sutures and immerse them in DW and BSS. Then, use a lab rocker to provide constant

movement of fluid in the vials. This part of the study was begun on August 1, 2015; and, as of August 14, 2015, there were no significant changes in the measured diameters. However, there could be an effect, because of rocking the samples, on the samples that will be examined around 30 days from the start of the trial. A simple baby seat rocker was being used to simulate constant fluid movement on the sutures in order to check for any changes in dissolution rates under these conditions.

Chapter 6: Conclusions and Recommendation for Future Study

6.1 Conclusions

The long term goal for this research is to help patients affected by glaucoma and who have to undergo surgical implantation of glaucoma drainage devices. Improving the initial effectiveness of BGI is not only a step to improve the device, but also to ensure safety and comfort for patients who need the device.

The main objective of this project was to develop and validate two experimental apparatus to measure the pressure drop along a BGI tube, with and without inserts. These setups will be used in the future to further evaluate the pressure drop resulting from the use of inserts. The current study was focused on benchmarking the experimental setup for the IOP range of 15 – 20 mm Hg. Repeated experiments were conducted with different configurations of inner tube diameter, insert diameter, length of insert and fluid flow rate, in order to produce pressure variations in the clinically relevant range. The experimental measurements of pressure drop for the benchmarking trials were compared with theoretical calculations. The theory predicted that the pressure could vary within a range because of the variation in manufactured tube and insert diameters, control and detection of flow rates [refer to **Appendix L** for data on flow variation], sample lengths and profiles of cut sample edges.

The benchmarking trials with 75 micron inner diameter tubes helped to document that the setups produce results that are different by approximately 1 mm Hg for a 15 mm reading [about 6% variation]. The results from the 75 micron inner diameter tube trials were only used to make this comparison because only these results were close to the clinically relevant pressure drop [between 5 – 20 mm Hg]. It is imperative that there be no difference between the setups in order to achieve complete reproducibility between the setups, but a difference of 1 -2 mm of Hg is not critical in terms of a clinical standpoint. Hence, before further trials are performed, it is

recommended to further characterize the difference between the setups and consider changes to the setups to reduce or eliminate any differences.

The experimental data set for flow through 50 μm inner diameter tubes at 2.5 μl/min gave pressure drops ranging from 97 to 105 mm Hg [101.5 ± 3.2 mm Hg], and were close to the upper limit of the theoretical range of 48.2 – 103.2 mm Hg. In the case of the trials conducted with 75 μm inner diameter tubes and flow at 2.5 μl/min, the observed pressures of 14.5 – 15.8 mm Hg [15.0 ± 0.4 mm Hg] were within the 9.2 – 16.8 mm Hg theoretically predicted range. However, for the experiments conducted with the 75 μm diameter tubes at 1.25 μl/min flow rate, the observed pressures, 8.2 – 8.6 mm Hg [8.4 ± 0.2 mm Hg], were higher than the upper limit of the predicted pressure range of 3.7 – 7.6 mm Hg. Since the upper limit of the predicted pressure range and the lower limit of the observed pressures were close, there may have been other small factors such as room temperature, relative humidity, error in measuring the elevation difference between transducer and outlet, pressure transducer measurement error, and/or surface roughness of the tubes, which could have contributed to this minor difference.

The annular flow benchmarking trials produced results [2.98 ± 0.32 mm Hg] that were within the theoretically predicted pressure range of 0.13 – 3.23 mm Hg, for a flow rate of 10 μl/min. The lower limit of the theoretical range was calculated for a wire insert of diameter 265 microns and a needle inner diameter of 345 microns at a flow rate of 9.5 μl/min. The upper limit of the theoretical range was calculated for a wire insert of diameter 275 microns and a needle inner diameter of 335 microns at a flow rate of 10.5 μl/min. The next most critical part of this research would be to benchmark the setup by simulating annular flow that would produce pressures in the clinically relevant pressure range of 15 to 20 mm Hg with flow rate of 2.5 μl/min. Though the observed pressures for the annular flow benchmarking trials [2.98 ± 0.32 mm Hg] were lower than the clinically relevant pressure range [5 – 20 mm Hg], the results indicated

that the experimental setups can produce pressures within the predicted theoretical pressure range. Though the effects of eccentricity were not considered when calculating the theoretical pressures, it is noted that the effect of eccentricity is a major factor that would help understand the variation of pressure for annular flow.

In an attempt to understand the pressure response of flow through tubes with suture inserts, trials were conducted using different types of sutures. The properties that were varied were: the suture being absorbable/non-absorbable, fluid flow rates of 1.5 and 2.5 μl/min, suture lengths of 4 and 8 mm, and suture diameters of 0.15, 0.2, and 0.3 mm. The results showed that the pressure profiles of tubes with absorbable suture inserts increased over time [3 – 5 mm Hg], probably because these sutures expanded when hydrolyzed. In contrast, the pressure profiles for tubes with non-absorbable suture inserts demonstrated a reasonably steady pressure [1.5 - 3 mm Hg]. A comparison of absorbable and non-absorbable suture data confirms that using absorbable sutures could result in a much higher pressure drop. This being said, it is evident that the two setups assembled for this thesis can be used to verify the pressure response of different types of inserts, when they are placed within tubes of dimensions similar to those of Baerveldt Implant tubes.

For every suture insert trial, each type of suture offered a different resistance to fluid flow. For example, absorbable sutures appeared to swell over time and created an increasing pressure drop [3-0 Monocryl, 8 mm long, 2.5 μl/min – 3.59 ± 0.99 mm Hg; 3-0 VICRYL Braided, 4 mm long, 2.5 μl/min – 5.07 ± 2.66 mm Hg] as compared to non-absorbable sutures [3-0 Prolene, 8 mm long, 2.5 μl/min – 2.84 ± 0.81 mm Hg]. This led to a comparison of the different trials using a resistance to flow variation chart. From this chart, it can be seen that the non-absorbable sutures had a reasonably steady and constant resistance to flow [around 1.2 mm Hg/(μl/min)] as compared to absorbable sutures. Though a constant flow resistance is good, it

does not address the issue at hand, which is to maintain pressures of at least 5 mm Hg in real life situations. The achieved pressure drop was small [less than clinically relevant pressure range of 5 – 20 mm Hg], and the insert would be permanently lodged in the BGI tubing. If a non-absorbable suture were used in the BGI tubing, it could lead to complications in the long run because it would not be biodegradable. When scar tissue grew over the implant, the suture could cause additional pressure drop issues. The scar tissue alone creates sufficient flow resistance to help maintain the IOP above 5 mm Hg, so having a non-biodegradable insert in the BGI tubes could create a larger increase in the IOP than desired. This could create discomfort for the patient and could cause more damage to the optic nerve than help, if the IOP increased beyond 20 mm Hg. Also, if the sutures were pushed out of the tubing and into the eye, that suture could cause irritation and discomfort for patients. All of these factors indicate that a biodegradable polymer [absorbable suture] is preferred because the polymer could deteriorate and dissolve, even if it became dislodged from the tubing.

The long term trials, both using the experimental setups and using stagnant fluid in vials, helped understand the pressure response and degradation profile of absorbable sutures [specifically, Monocryl] over time. Monocryl sutures deteriorate when they hydrolyze and appear to undergo bulk internal erosion that might not be a suitable characteristic for glaucoma related applications. This is because the observed pressures are much higher [4 – 150 mm Hg] than the clinically relevant range. Also, when the sutures undergo bulk erosion, layers of the polymer flake and tend to “fall off”. This could in turn block the tubes and result in temporary spikes in IOP. It might be better if a different polymer could be identified for further studies.

Another important finding is the effect of the type of fluid used to run these trials on the dissolution rate of the biodegradable sutures. Though DW and BSS are similar fluids, the small concentrations of salts and acids in BSS made the sutures deteriorate within 23 days as compared

to DW, where it took over 30 days for the sutures to deteriorate. These preliminary studies indicate that future experiments should be conducted using BSS in order to best mimic physiological conditions in the BGI.

The results from this thesis have helped solidify the basic modelling of micro-fluid flow and validated the experimental setups that can be used to conduct further studies. In the long run, these setups can be used to test various degradable inserts that would help to improve the initial effectiveness of the BGI.

6.2 Recommendations for Future Study

Based upon the results made available from this research and the fact that the setups produced different results, there is a large scope for further studies. Some of these studies are described in the following.

1. With the data available from the long term trials using stagnant DW with inserts in 2 ml vials, it would be beneficial if similar trials were performed for different types of absorbable sutures, probably for a number of samples, in order to get a statistically better data set for evaluation. For these trials, it would be best to induce continuous movement in order to simulate flow over the sutures similar to what might occur for sutures in BGI tubes. These trials have been initiated using a rocker/mixer, but have not been completed.
2. A different polymer, other than the bulk eroding sutures used in this thesis, could be used to study the effects that erosion modes [surface vs. bulk] could have on the pressure profile.
3. To confirm that the results from the experiments proposed in items (1) and (2) match physiological conditions, experiments should be conducted using BSS instead of DW.
4. If long term experiments are conducted with BSS instead of DW, determine ways to eliminate bacterial growth in BSS.

5. Because the suture diameters are either 200 or 300 μm in diameter and there is nothing commercially available in between, trials should be conducted with tubes of smaller inner diameter using the standard/available suture sizes that would produce pressures in the clinically relevant range.
6. Determine if pre-hydrating 200 μm diameter absorbable sutures for a considerable length of time [say a week] before conducting trials has positive effects on the observed pressures during long term trials, i.e., resulting in pressures being in the physiologic range.
7. To make it easier to test tubes of desired lengths [8 to 10 mm], modify the experimental setup using better tube connections so that the head losses due to friction in the long connecting tubes and expansions can be eliminated and making sure that the setups produce identical results. For example, the use of connections that do not have abrupt changes in diameter, should help to eliminate losses due to expansion and contraction. Also, tubes of shorter length [to eliminate frictional losses] and smaller diameter [to eliminate losses due to sudden expansion or contraction] could be used to connect the major components of the setup.
8. Conduct experiments by changing both the elevation of the reservoir and collection trough, to check for variations in the observed pressure readings. Ideally, when the elevation of the reservoir is increased, the pump should require less power to pump the fluid and vice versa. When the elevation of the collection trough is increased with respect to the pressure transducer, then the observed pressure would be higher and vice versa.

References

1. **Glaucoma implant surgery** [http://www.glaucoma.org/treatment/glaucoma-implants.php], **Glaucoma Research Foundation**, Accessed on: June 22, 2015.
2. **Health Concerns - Glaucoma** [http://www.lef.org//Protocols/Eye-Ear/Glaucoma/Page-01], **Life Extensions**, Accessed on: August 8, 2015.
3. **Diseases and Conditions - Glaucoma** [http://www.mayoclinic.org/diseases-conditions/glaucoma/basics/definition/con-20024042], **Mayo Clinic**, Accessed on: June 22, 2015.
4. **Facts about Glaucoma** [https://nei.nih.gov/health/glaucoma/glaucoma_facts], **National Eye Institute**, Accessed on: July 1, 2015.
5. **Glaucoma Drainage Devices** [http://eyewiki.aao.org/Glaucoma_Drainage_Devices], **Eye Wiki**, Accessed on: June 22, 2015.
6. Vanbuskirk EM, Cioffi GA: **Glaucomatous Optic Neuropathy**. *American Journal of Ophthalmology* 1992, **113**(4):447-452.
7. Leydhecker W: **The Intraocular Pressure: Clinical Aspects**. *Experimental Eye Research* 1975, **20**(2):175-176.
8. Robinson JC: **Chandler and Grant's Glaucoma**. *Archives of Ophthalmology* 1998, **116**(11):1552-1552.
9. **Glaucoma and Your Eyes** [http://www.webmd.com/eye-health/glaucoma-eyes], **Web MD**, Accessed on: June 6, 2015.
10. Johnston M, Grant WM: **Pressure-Dependent Changes in Structures of Aqueous Outflow System of Human and Monkey Eyes**. *American Journal of Ophthalmology* 1973, **75**(3):365-383.
11. **Portfolio** [http://www.dnaillustrations.com/inside-art.html], **DNA Illustrations**, Accessed on: August 8, 2015.
12. Prata Jr JA, Mérmoud A, LaBree L, Minckler DS: **In Vitro and In Vivo Flow Characteristics of Glaucoma Drainage Implants**. *Ophthalmology* 1995, **102**(6):894-904.
13. **Baerveldt® BG 101-350 Glaucoma Implant** [http://www.amo-inc.com/products/cataract/glaucoma-implants/baerveldt-bg-101-350-glaucoma-implant], Accessed on: June 22, 2015.
14. **Plain Film Imaging of Baerveldt Glaucoma Drainage Implants** [http://www.ajnr.org/content/23/6/935.figures-only], **American Journal of Neuroradiology**, Accessed on: June 22, 2015.
15. Wilson MR, Mendis U, Smith SD, Paliwal A: **Ahmed Glaucoma Valve Implant vs Trabeculectomy in the Surgical Treatment of Glaucoma: A Randomized Clinical Trial**. *American Journal of Ophthalmology* 2000, **130**(3):267-273.
16. Tong L, Frazao K, LaBree L, Varma R: **Intraocular Pressure Control and Complications with Two-Stage Insertion of the Baerveldt Implant**. *Ophthalmology* 2003, **110**(2):353-358.
17. Budenz DL, Barton K, Gedde SJ, Feuer WJ, Schiffman J, Costa VP, Godfrey DG, Buys YM: **Ahmed Baerveldt Comparison Study: Five-Year Treatment Outcomes in the Ahmed Baerveldt Comparison Study**. *Ophthalmology* 2015, **122**(2):308-316.
18. Christakis PG, Tsai JC, Kalenak JW, Zurakowski D, Cantor LB, Kammer JA, Ahmed IIK: **The Ahmed Versus Baerveldt Study**. *Ophthalmology* 2013, **120**(11):2232-2240.
19. Britt MT, LaBree LD, Lloyd MA, Minckler DS, Heuer DK, Baerveldt G, Varma R: **Randomized Clinical Trial of the 350-mm2 Versus the 500-mm2 Baerveldt Implant: Longer Term Results**. *Ophthalmology* 1999, **106**(12):2312-2318.
20. Manring N: **Hydraulic Control Systems**, 1st ed: Wiley; 2005.
21. Conlisk AT: **Essentials of Micro- and NanoFluidics**, 1st ed. USA: Cambridge University Press; 2013.

22. **Laminar Flow in Pipes and Annuli** [http://infohost.nmt.edu/~petro/faculty/Nguyen/PE311/Presentations/C4/2_LaminarFlowPipes&Annuli_Newtonian.ppt], **New Mexico Technology**, Accessed on: May 20, 2015.
23. Miller RW: **Flow Measurement Engineering Handbook**, 3rd ed: McGraw-Hill Education; 1996.
24. Myers P, Conlisk T: **Essentials of Micro- and Nanofluidics. With Applications to the Biological and Chemical Sciences**. *Chromatographia* 2014, **77**(7-8):643-643.
25. **Suture Characteristics** [http://www.suru.com/sut_charac.htm], **SURU International Pvt. Ltd.**, Accessed on: August 5, 2015.
26. **Information about Sutures in the Operating Room** [http://www.surgical-instrument-pictures.com/suture.html], **Surgical Instrument Pictures**, Accessed on: June 27, 2015.
27. **Ethicon Product Catalog** [http://www.ecatalog.ethicon.com/sutures-absorbable], **Ethicon**, Accessed on: June 27, 2015.
28. **PneuWave Pump** [http://www.mycorsolutions.com/pneuwave.html], **CorSolutions Ltd.**, Accessed on: June 27, 2015.
29. **High Accuracy Pressure Transducers** [http://www.omega.com/pressure/pdf/PX429_SERIES.pdf], **Omega Engineering**, Accessed on: August 25, 2014.
30. **Data Loggers** [http://www.omega.com/das/pdf/OM-CP-VOLT101A_SERIES.pdf], **Omega Engineering**, Accessed on: August 24, 2015.
31. **SGE Analytical Science - LC PEEKsil Tubing** [http://www.sge.com/products/gc-lc-supplies/lc-supplies/lc-peeksil-tubing3], **Trajan Sci Med**, Accessed on: August 1, 2015.
32. **Ceramic Column Cutter** [http://www.thermoscientific.com/content/dam/tfs/ATG/CMD/CMD%20Documents/Application%20&%20Technical%20Notes/Chromatography/GC%20HPLC%20and%20UHPLC%20Columns%20and%20Accessories/GC%20Columns/TN-GC-Column-Cutting-TN20778_E.pdf], **Fisher Scientific**, Accessed on: May 20, 2015
33. Munden P, Associate Professor, Department of Ophthalmology, **KU Medical Center**, Discussed on: November 2014, 7400 State Line Road, First Floor, Prairie Village, Kansas 66208, E-Mail ID: pmunden@kumc.edu.
34. Fitz BD, Jamiolkowski DD: **Hydrolysis Profiling: An In Vitro Methodology to Predict In Vivo Absorption Time**. *Journal of Biomedical Materials Research Part B-Applied Biomaterials* 2013, **101B**(6):1014-1022.
35. Alexis F: **Factors Affecting the Degradation and Drug-Release Mechanism of Poly(lactic acid) and Poly (lactic acid)-co-(glycolic acid)**. *Polymer International* 2005, **54**(1):36-46.
36. Tomihata K, Suzuki M, Ikada Y: **The pH Dependence of Monofilament Sutures on Hydrolytic Degradation**. *Biomedical Materials Research* 2001, **58**(5):511-518.
37. Casalini T, Masi M, Perale G: **Drug Eluting Sutures: A Model for In Vivo Estimations**. *International Journal of Pharmaceutics* 2012, **429**(1-2):148-157.
38. **Human Eye Anatomy: Parts of the Eye** [http://www.allaboutvision.com/resources/anatomy.htm], **All About Vision**, Accessed on: August 8, 2015.
39. Mays LW: **Water Resources Engineering**, 2nd ed: John Wiley & Sons; 2010.

APPENDICES

Appendix A: Medical Terminology

To better understand the causes and difference between the various types of glaucoma, it is essential to define the medical terminology used in this thesis. Following are explanations of some medical terms used herein.

Aqueous Humor

Aqueous humor is a fluid, rich in nutrients and electrolytes, produced to nourish the cornea and the lens [38]. Figure A.1 shows the front of the eye, where aqueous humor forms, and the normal flow direction [2]. From Fig. A.1, it can be seen that aqueous humor is produced in the ciliary body behind the iris and flows over the iris, finally draining into the trabecular meshwork.

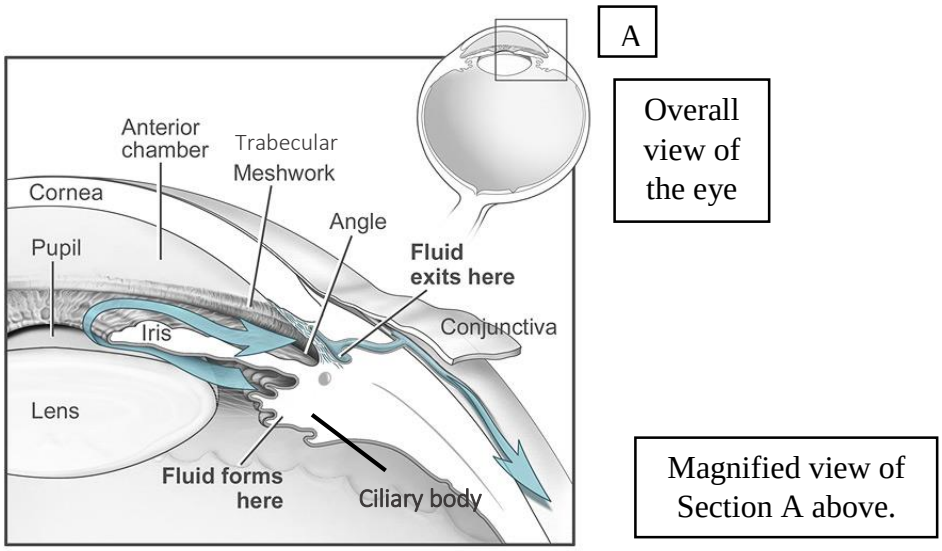

Figure A.1: Formation of aqueous humor and normal flow [reproduced from Ref. 2]

Anterior Chamber, Angle and Trabecular Meshwork

The anterior chamber is the part of the eye behind the cornea and in front of the iris and lens [Fig. A.1]. The anterior chamber angle and trabecular meshwork are located where the cornea and iris meet [as seen in Fig. A.1]. The trabecular meshwork is important because aqueous

humor drains out of the eye through it. Any unusual flow restrictions within the meshwork could result in an increase in IOP causing damage to the optic nerve [5].

Bleb Size

The hole that is surgically made in the eye in order to insert the implant tubing into the eye [5].

Choroid

The choroid is the layer of blood vessels located between the sclera and the retina. They provide nourishment to the back area of the eye [Fig. A.2] [38].

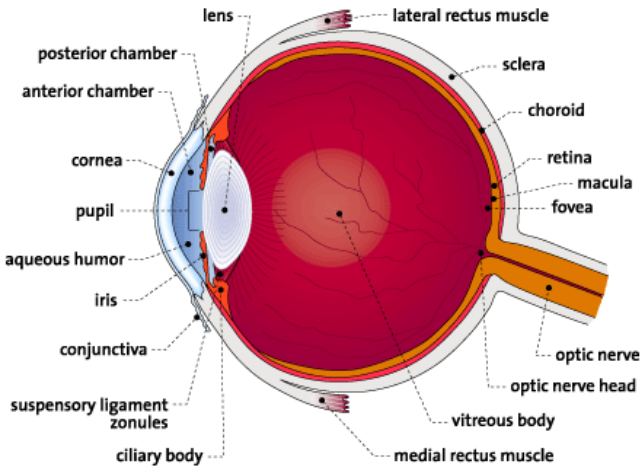

Figure A.2: Anatomy of the eye [reproduced from Ref. 37]

Ciliary Body

The ciliary body [Fig. A.2] is the part of the eye between the iris and choroid. The main functions of the ciliary body are producing aqueous humor and holding the lens in place [38].

Conjunctival Scarring

Formed as a result of the body's natural healing process by creating scar tissue around an incision, and scar tissue may close up the drainage channels, causing IOP in the eye to rebuild [1].

Cornea

The clear part of the eye covering the iris and the pupil [Fig. A.2]. The cornea lets the light into the eye, permitting sight [38].

Hydrolysis

A process where fluid gradually penetrates the individual filaments of a suture, instigating a breakdown of the suture's polymer chains [25].

Hypotony

This condition results when the IOP is very low, in the range 0 – 5 mm of Hg. Patients with BGI and other non-valved implants, which do not have added flow regulators, have a higher risk of their IOPs dropping below 5 mm of Hg right after the surgical implant procedure. Hypotony results in corneal decomposition, accelerated cataract formation and discomfort [5].

Intraocular Pressure

Intraocular pressure is the fluid pressure in the eye. A healthy IOP is the result of the equilibrium between the amount of aqueous humor being produced within the eye and the physiologic outflow of the fluid from the eye. The nominal range of IOP is between 8 and 20 mm Hg. When the outflow of aqueous humor is impeded, the pressure inside the eye begins to increase in order to maintain a constant flow rate. The optic nerve, being the weakest area in the eye, is most vulnerable to damage due to this elevated pressure. Continuous increase of pressure and damage to the optic nerve can lead to permanent vision loss [1].

Iris

The iris is the colored part of the eye surrounding the pupil. This pigmented membrane lies between the cornea and the lens. The iris acts as a diaphragm to widen or narrow the pupil, controlling the amount of light that enters the eye [Fig. A.2] [38].

Optic Nerve

The optic nerve carries the nerves impulses from photoreceptor cells in the retina to the visual cortex in the brain [Fig. A.2] [38].

Posterior Chamber

The posterior chamber is the space filled with aqueous humor behind the iris and adjacent to the lens [Fig. A.2] [38].

Retina

The sensory membrane that lines the eye [Fig. A.2]. It receives images formed by the lens and converts them into signals that reach the brain by way of the optic nerve [38].

Sclera

The outer coating of the eyeball that forms the visible white of the eye and surrounds the optic nerve at the back of the eyeball [Fig. A.2] [38].

Trabecular Meshwork

The area of tissue in the eye located around the base of the cornea, near the ciliary body [Fig. A.1]. It allows drainage of the aqueous humor from the eye via the anterior chamber [38]. Under normal conditions, its resistance to flow helps to maintain the IOP within the nominal 8 – 20 mm Hg range.

Appendix B: List of Components in Setup

The two setups were comprised of many components. Listed below are the main items in each setup. See Figures 12 – 14 for pictures of the setups.

Table B.1: Major components of Setup #1

Description	Make/Model	Serial #/Part #	Specifications
Pump	CorSolutions – PneuWaveMicroPump	S/N: 20141231.3 P/N: CS3900r5 – 1 CH	0 – 50 µl/min [±5%]
Pressure Transducer	Omega – PX429-2.5GV	S/N: 419411	0 – 2.5 psi [±0.2 psi]
Data Logger	Omega – OM-CP-VOLT101A-160MV	S/N: P44261	4 readings per second – 1 reading per 24 hrs
500 ml Glass Bottle	Sigma Aldrich - CLS13955000		500 ml
Connector Cable for Transducer	Omega – CA-329-4PC24-015		15 feet long
Power Supply	Hewlett Packard	S/N: E3630A	10 V DC supply
Tubing	BD Medical		IV Tubing – ID 0.5”, 6” long
PEEK Tubing	CorSolutions		ID 0.05”, 1’ long
Needle Connector	BD Medical	Part #: 305156	22 Gauge, 1 ¼” long
Caulk			
Rubber Connector	Cover for leads of multimeter		Approx. 4” long Approx. 1” diameter

Table B.2: Major components of Setup #2

Description	Make/Model	Serial #/Part #	Specifications
Pump	CorSolutions – PneuWaveMicroPump	S/N: 20140701.3 KU Med P/N: 227494	0 – 50 µl/min [±5%]
Pressure Transducer	Omega – PX429-2.5GV	S/N: 419345	0 – 2.5 psi [±0.2 psi]
Data Logger	Omega – OM-CP-VOLT101A-160MV	S/N: P59725	4 readings per second – 1 reading for 24 hrs
500 mL Glass Bottle	Sigma Aldrich - CLS13955000		500 ml
Connector Cable for Transducer	Omega – CA-329-4PC24-015		15 feet long
Power supply	Hewlett Packard	S/N: E3630A	10 V DC supply
Tubing	BD Medical		IV Tubing – ID 0.5”, 6” long
PEEK Tubing	CorSolutions		ID 0.05”, 1’ long
Needle Connector	BD Medical	Part #: 305156	22 Gauge, 1 ¼” long
Caulk			
Rubber Connector	Cover for leads of multimeter		Approx. 4” long Approx. 1” diameter

Table B.3 lists the other components utilized to measure, analyze and prepare suture samples used in the various trials. These items were either borrowed from within the department or bought from vendors.

Table B.3: Other components used in the experimental setup

Description	Make/Model	Serial #/Part #	Specifications
Microscope	Baush & Lomb		10X – 40X Magnification
Baby Seat Rocker	Redmon Rock On Car Seat Rocker	4000	11.5” x 12” x 3”
Stage Micrometer Scale	OMAX Microscope Net	CS-A36CALM1	1 mm width, having 0.01 mm divisions
Ruler			300 mm ruler with 1 mm divisions
Superglue	KrazyGlue		0.18 oz
Glass Vials	MHB	VSC-1/12	1 Dram, pack of 12
Medical Grade Connecting Tubes	BD Medical		6 inch long 0.5” inch diameter
Medical Grade Tweezers	BD Medical		Stainless steel 6” long
Medical Grade Scissors	BD Medical		Stainless steel 6” long

Appendix C: PneuWave Pump Specifications

The specifications below were taken from Corsolutions – PneuWave Micro Pump brochure [28]

Flow specifications

Flow rate range	0.1 to 50 µl/min
Pressure range	0.01 to 14.5 psi
Accuracy of flow measurement	0.5% of set point or 0.15% of full scale
Repeatability below full scale [flow]	0.01% of full scale
Flow detection response time	40 msec
Flow rate stability	Down to 0.1% control volume [relative to fluid type, tubing and system set-up]
Operating temperatures	10 to 50 °C
Fluid connector type	UNF ¼ - 28 flat bottom
Flow sensor materials	Quartz Glass, PEEK™, Teflon®, Tefzel®
Flow sensor inner diameter	430 µm
Flow sensor internal volume	5.1 µl

Pressure specifications

Pressure range with internal compressor	0 – 1 bar ± 0.15%
Response time	down to 10 msec

Appendix D: PneuWave Pump Software User Manual

The following procedure and pictures were developed by Ajay Ramani in order to help other graduate students working on this setup. To record the pump pressure data, follow the steps below. It would be better to review the entire procedure before performing it for the first time. Currently, a single computer is used to control both the pumps which means that trials running in both the setups must start and stop at the same time. In the future, if two independent computers controlled the pumps separately, then the trials in each setup could be performed for different periods of time.

1. Start the computer connected to the pump. On the desktop, open the application with the name ‘CorSolutions PneuWave’ [Fig. D.1]. Make sure the pumps are switched on before opening the PneuWave software.

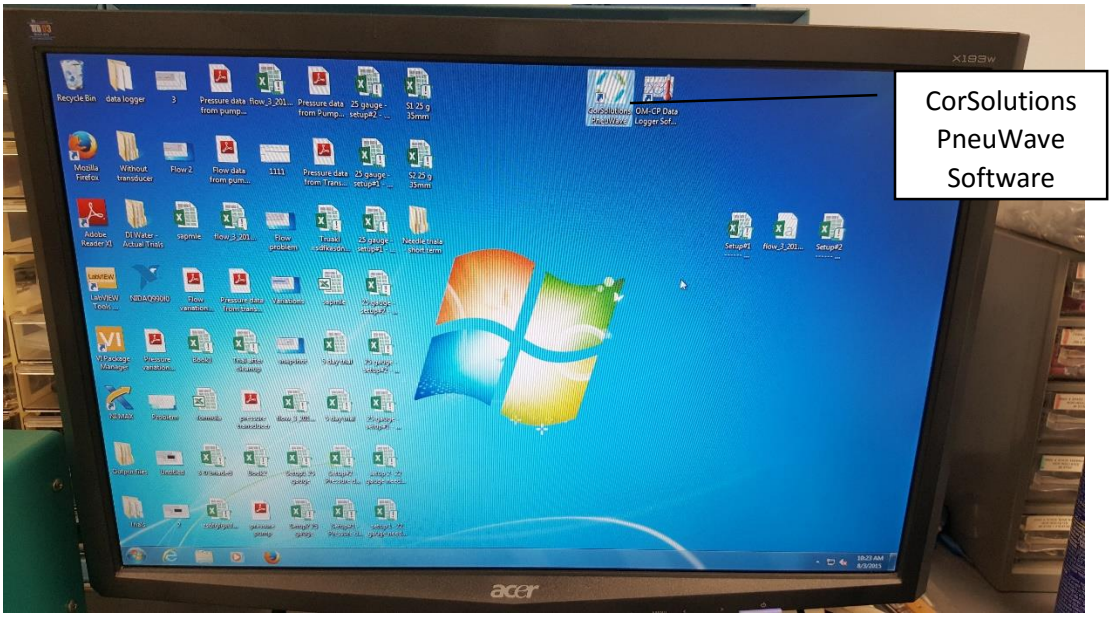

Figure D.1: Desktop showing PneuWave pump software

2. The software scans all of the ports and a dialog box pops up. Check/Select ‘COM3’ & ‘COM4’. COM3 refers to Pump 1 and COM4 refers to Pump 2 [Fig. D.2].

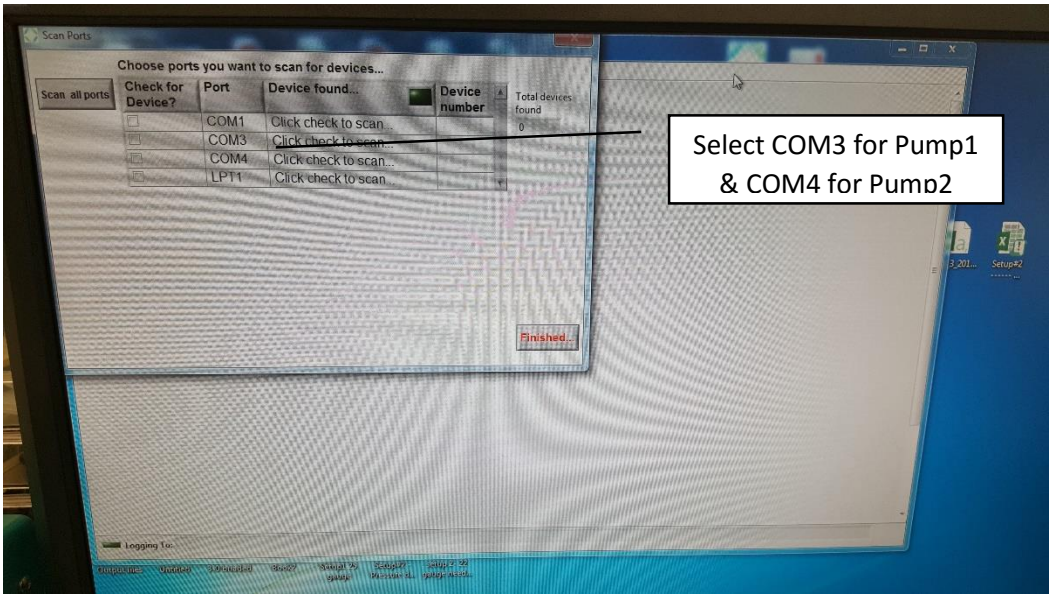

Figure D.2: Select COM3 & COM4

3. After selecting the pump, click ‘Finished’ [Fig. D.3].

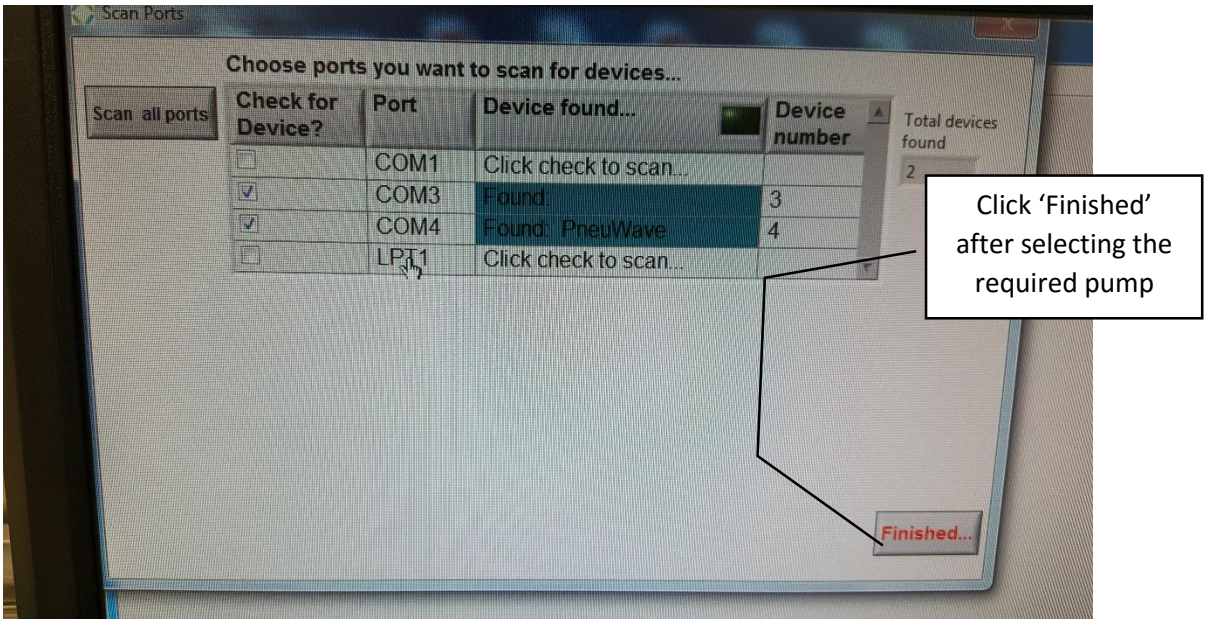

Figure D.3: Select 'Finished'

4. The next screen has the real time graphical input of each pump, the control mode they are in, and the set point [Fig. D.4].

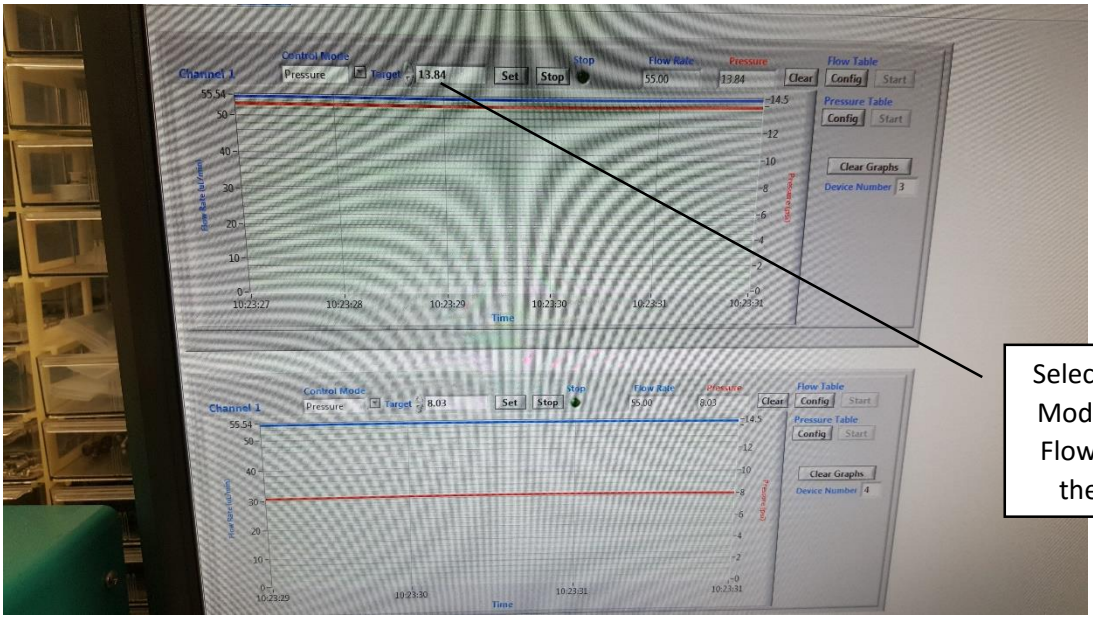

Figure D.4: Mode selection

5. Select the required ‘Control Mode’, which is usually the ‘Flow’ mode. Set the required flow rate [e.g., 2.5 µl/min] and click ‘Set’. The pump takes 10 – 15 minutes to achieve the required flow rate [Fig. D.4].
6. Once the pump has settled down and it is time to record data, select ‘Logging’ menu in the tool bar and select the rate as 1 second. The range available for rate of data capture is 0.1 second, 0.5 second, 1 second, 5 seconds, and 10 seconds. Select ‘Enable’ under ‘Logging’ menu to start recording data [Figs. D.5 and D.6].

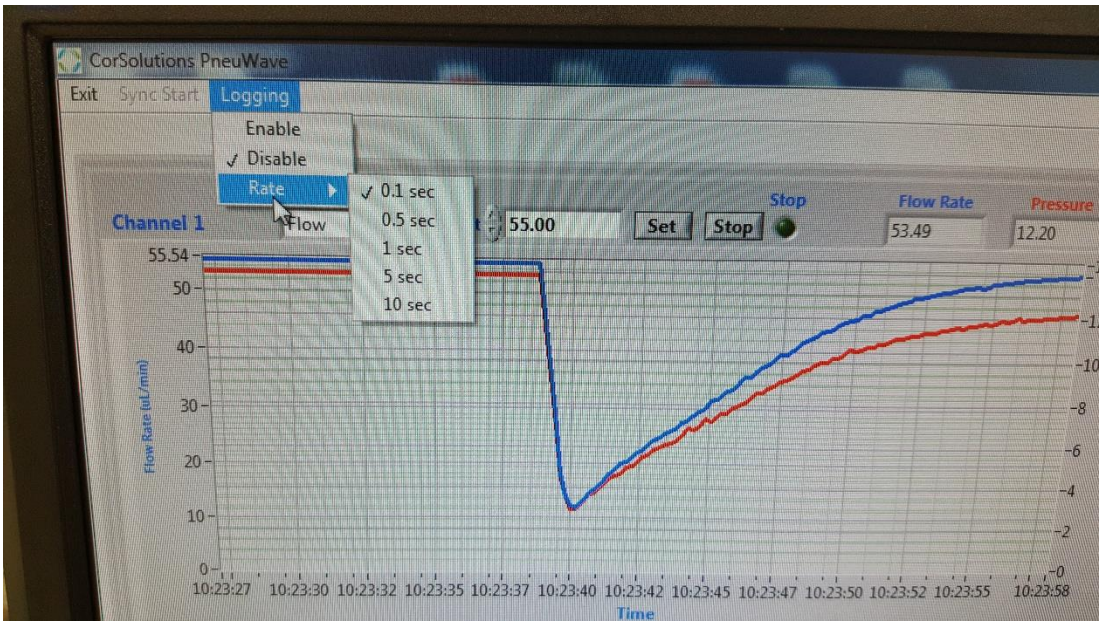

Figure D.5: Data logging rate options

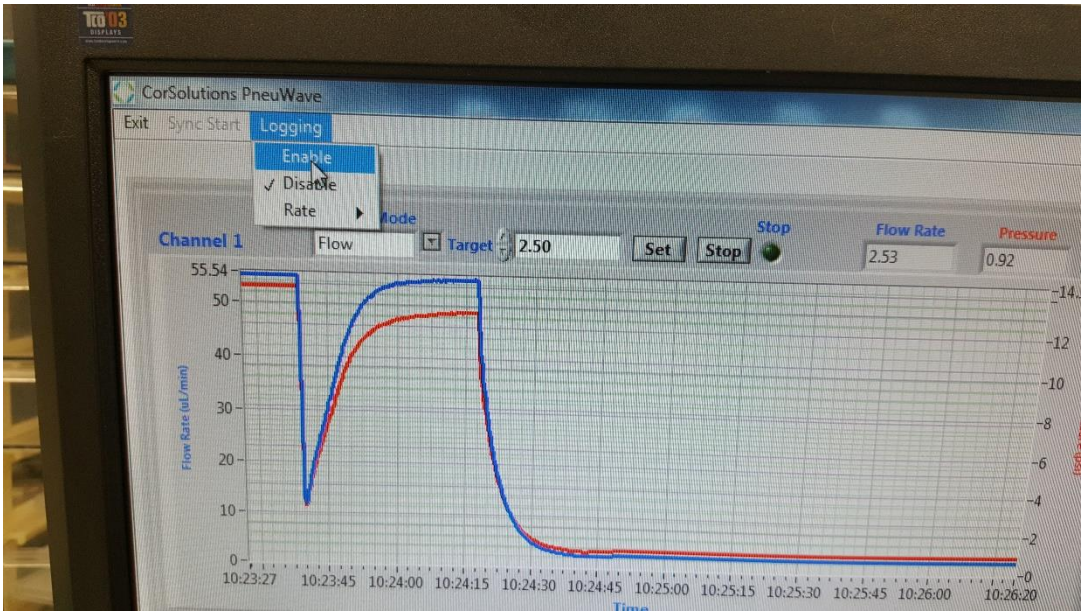

Figure D.6: To start data logging, select 'Enable'

7. A prompt appears on the lower left corner of the window, displaying the location where the data is being recorded [Fig. D.7].

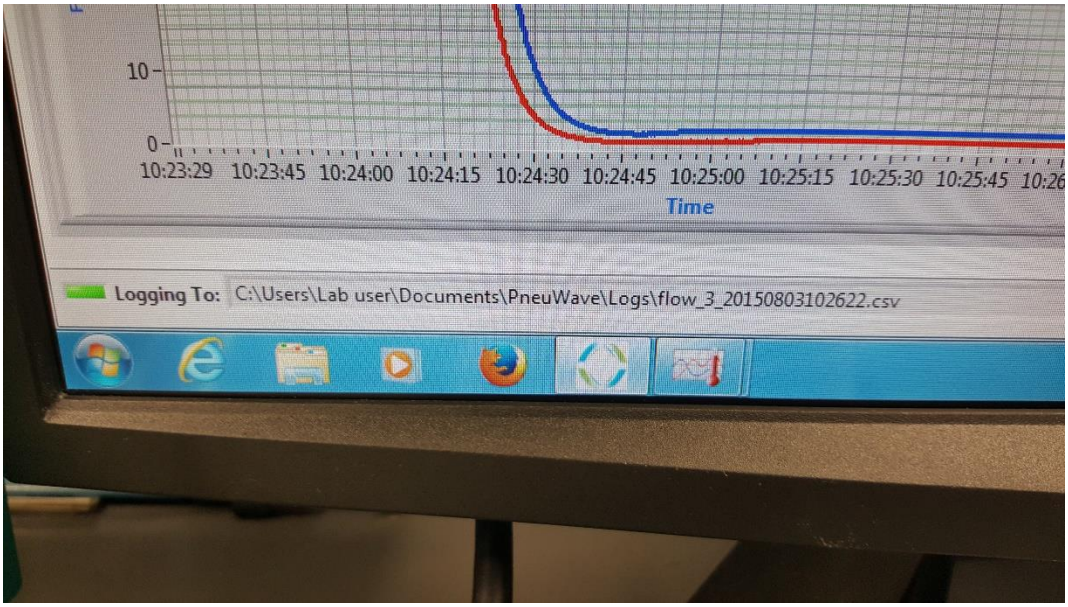

Figure D.7: Data logging confirmation

8. When the trial is done, click 'Exit' on the tool bar [upper left of the screen] to stop the data recording [Fig. D.5].

9. The data gets exported as a "*.csv" file and has columns which are labeled in Fig. D.8.

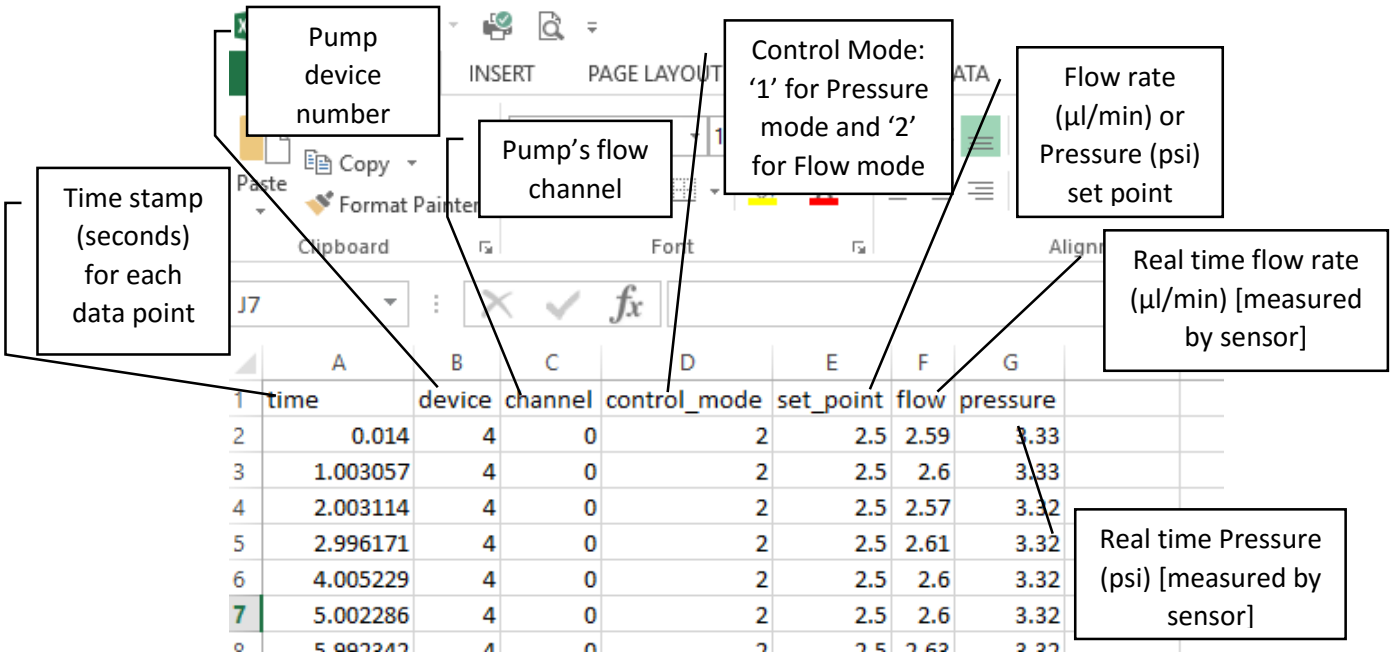

Figure D. 8: Snapshot of output data file

Appendix E: Omega Pressure Transducer Specifications

The specifications below were reproduced from Omega's Pressure transducer brochure [29]. Based on the target operational pressure range of the application, a transducer that would operate between 0 – 50 mm Hg [0 – 1 psi] was needed. However, in case the pressure in the setup should exceed this range, it should be possible to record and identify the reason because the selected transducer can measure up to 2.5 psi [160 mm Hg]. The specifications are:

Model	PX429 – 2.5 GV
Pressure range	0 – 2.5 psi
Input	DC only; 5 – 10 V operating range
Output range	0 – 100 mVdc
Accuracy	± 0.08% BFS – Best Fit Straight line [combined non-linearity, hysteresis and non-repeatability]
Zero Balance	± 0.5% FS typical, 1% max [1% typical, 2% max for 2.5 PSI and below]
Span Setting	± 0.5% FS typical, 1% max [1% typical, 2% max for 2.5 PSI and below]. Calibrated in vertical direction with fitting down
Long term stability	± 0.1% BFS typical [1 year]
Durability	1 million data points, typical

Appendix F: OMEGA Data Logging Software User Manual

The following procedure and pictures were developed by Ajay Ramani in order to help other graduate students working on this setup. To record the transducer pressure data, follow steps 1 – 12 on the following pages. The transducer and pump data logging cannot be started at the same time. The Pneuwave data logger is started first and then the OMEGA data logger. The OMEGA data logger uses the absolute clock time of the computer whereas the PneuWave data logger calculates time based on the instant the data logging is started. There is usually a gap of about 30 seconds of recorded data between the two loggers. The method adopted to avoid any mismatch between the loggers is to set the pump at a higher flow rate and reduce it to the required level and use this peak in flow rate and pressure graph as a reference point while analyzing the data.

1. Connect the Data Logger to the computer using the connector cable [Figs. F.1 and F.2].

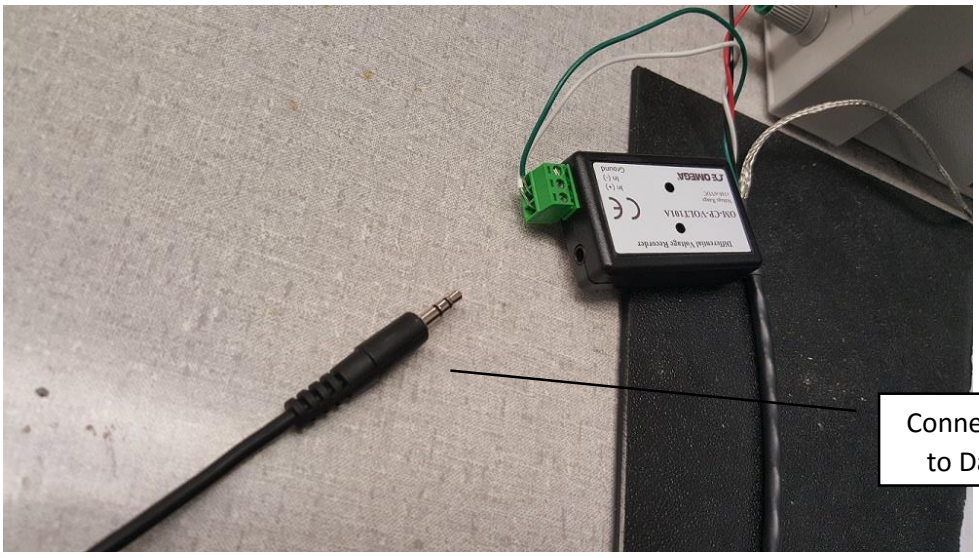

Figure F.1: Data logger and connecting cable

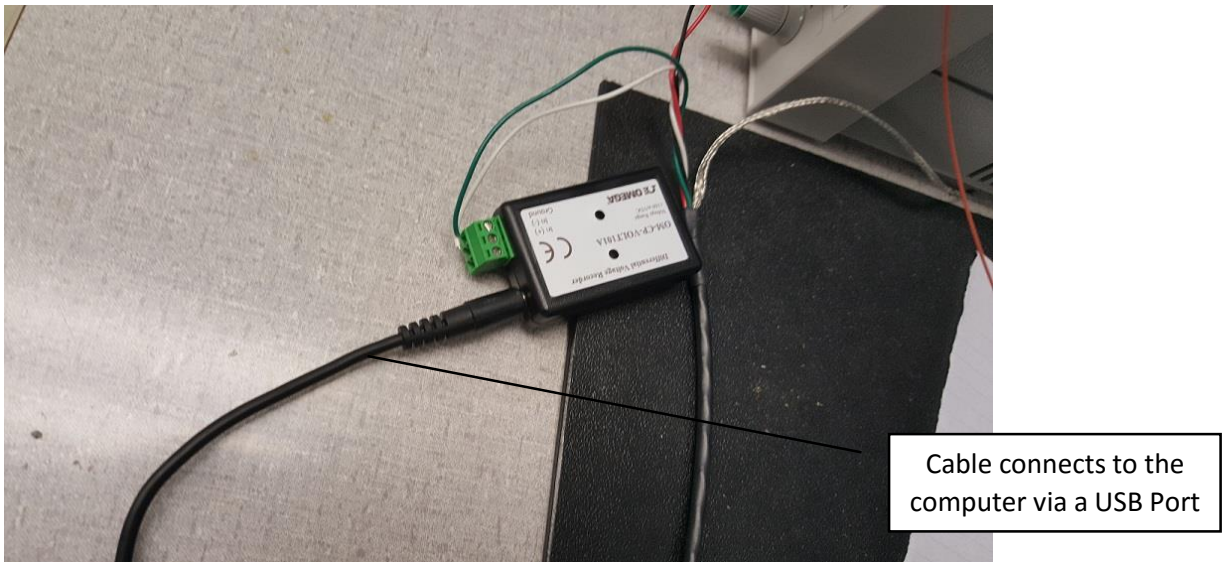

Figure F.2: Connected data logger

2. On the desktop, open the application with the name ‘OM-CP Data Logger Software’ [Figs. F.3 and F.4].

Figure F.3: Desktop logo of data logging software

Figure F.4: Prompt when user interface opens

3. To start logging data, select the ‘Device’ tab, click on ‘Custom Start’ [Fig. F.5]. Always run the experiments using ‘Custom Start’ because the other ‘Starts’ require the data logger to be connected to the computer at all times, which drains the 3.5 V battery in a month.

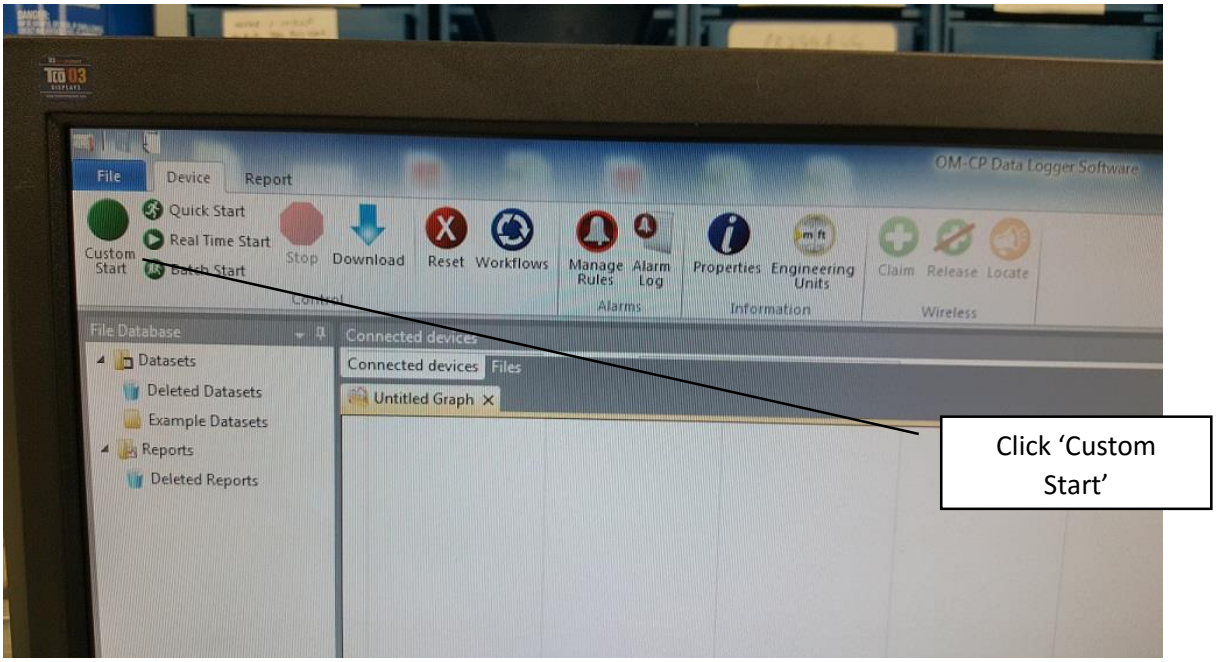

Figure F.5: Select 'Custom Start'

4. A dialog box pops up. Select the required start method [usually ‘Now’], stop method [usually ‘Manual’], and reading interval [usually 1 second]. Click ‘Start’ [Fig. F.6].

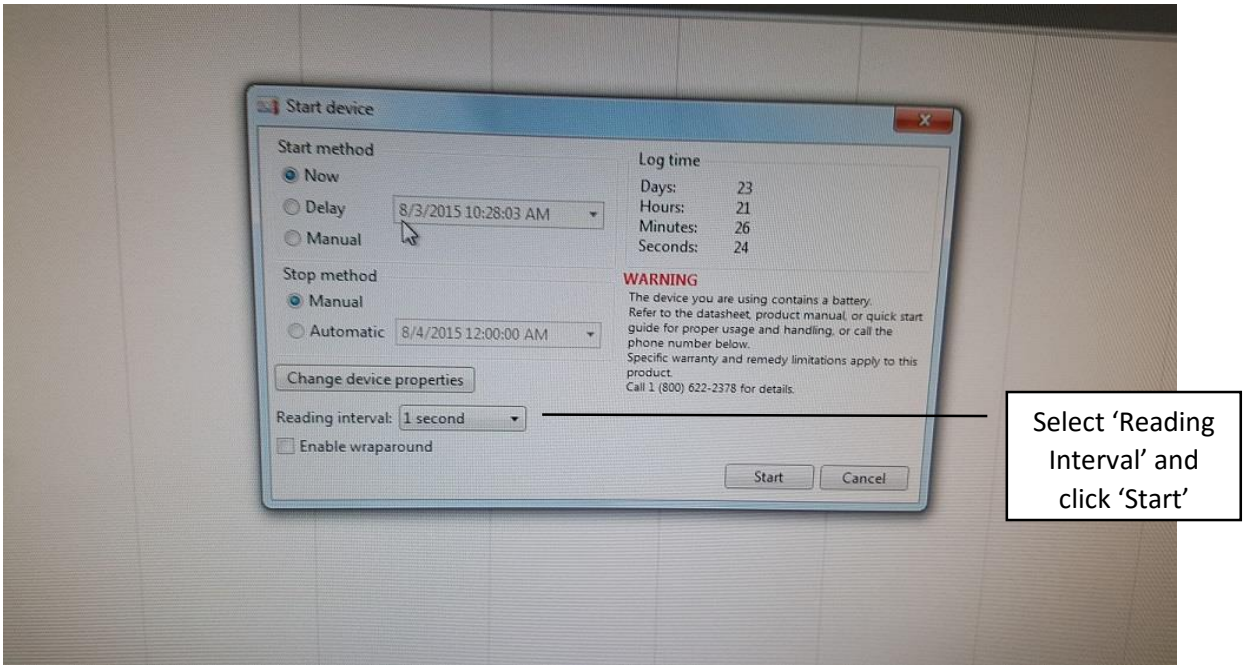

Figure F.6: Select reading interval

5. Once the Data Logger starts logging, the screen looks like Fig. F.7.

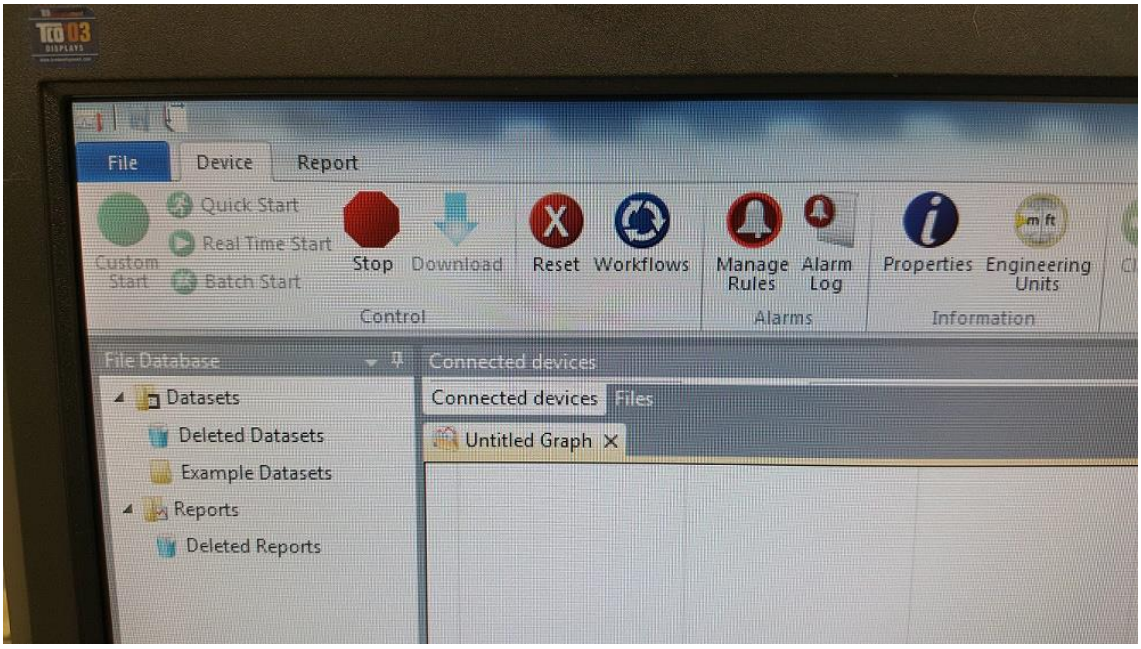

Figure F.7: After data logging begins

6. When the trial is done, click the ‘Stop’ button on the tool bar [Fig. F.7]. Then, click ‘Download’ to download the data from the last trial [Fig. F.8].

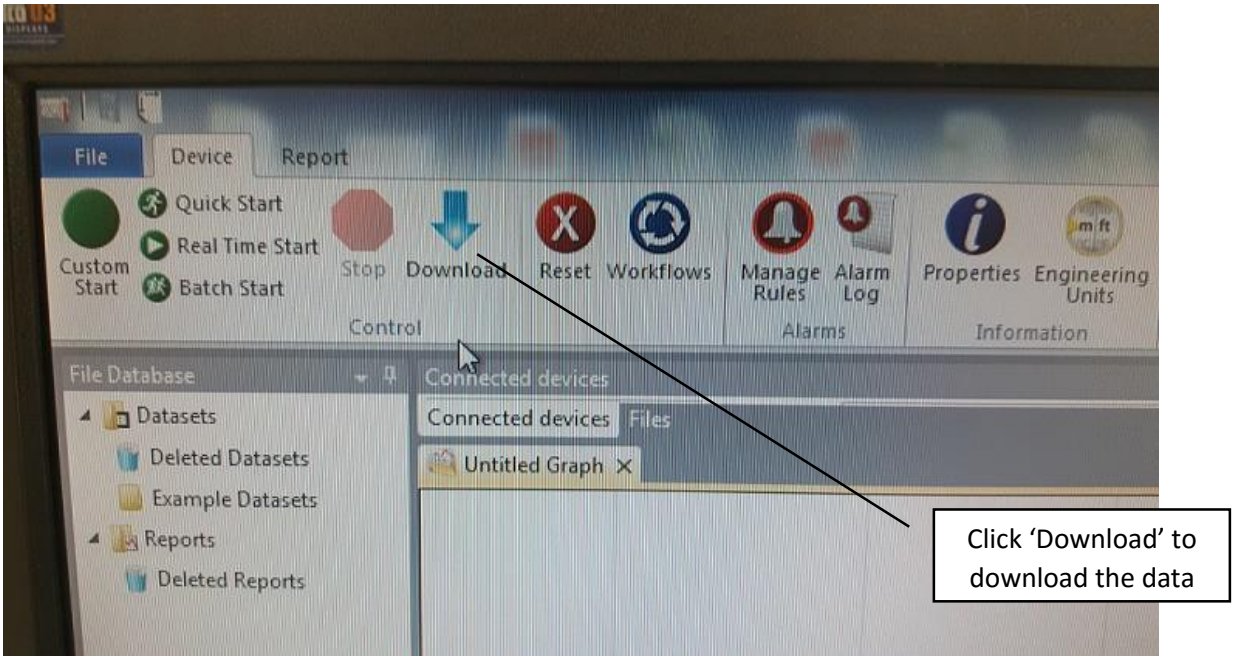

Figure F.8: To download data, click 'Download'

7. A dialog box pops up prompting the user to enter a file name. Click OK after entering a file name [Fig. F.9]. After the file gets downloaded, you will be able to see the tranducer’s recorded voltage readings plotted vs. time as shown in Fig. F.10.

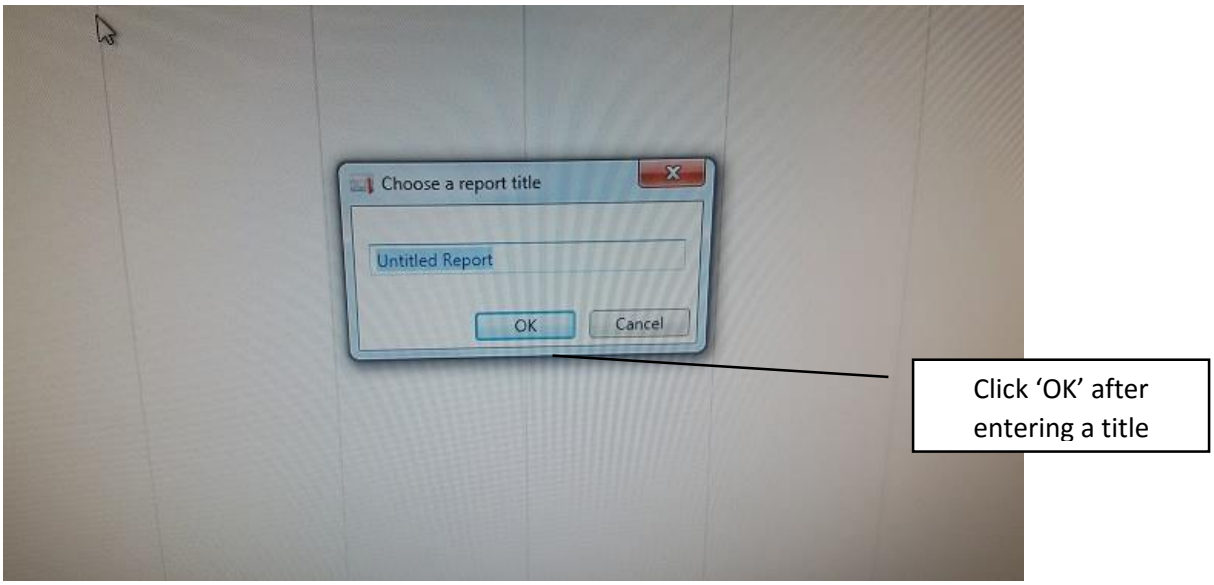

Figure F.9: Dialog box prompt

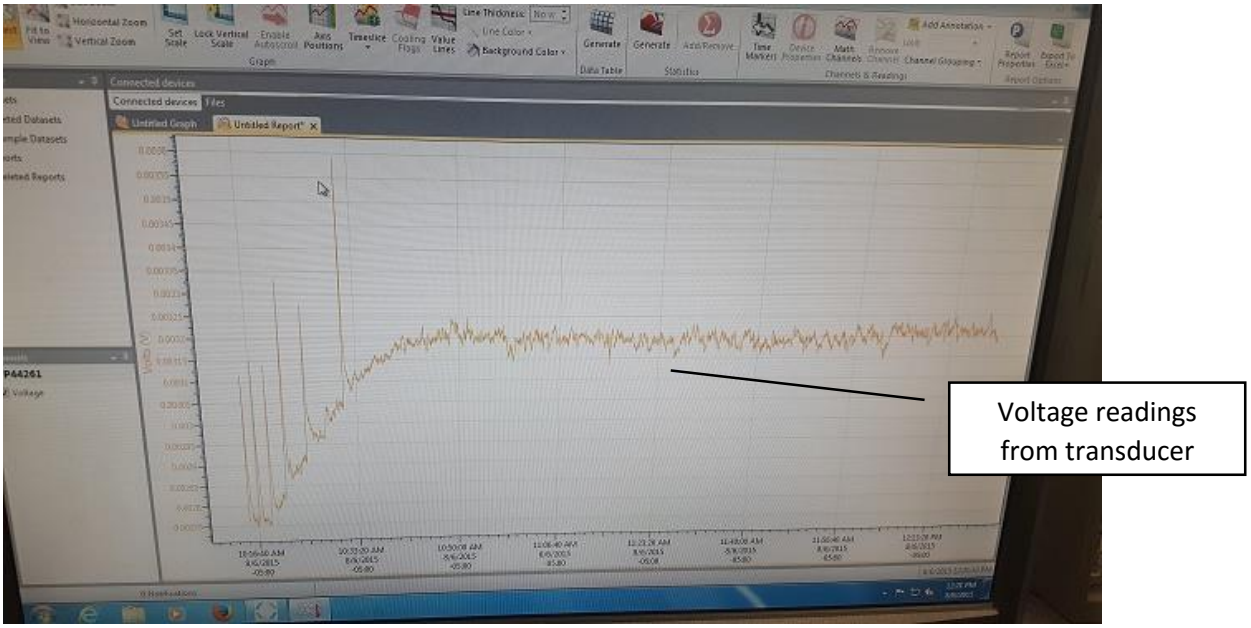

Figure F.10: Typical pressure data

8. To export the data to an Excel file, click on ‘Export to Excel sheet’ button in the top right corner of the window [Fig. F.11].

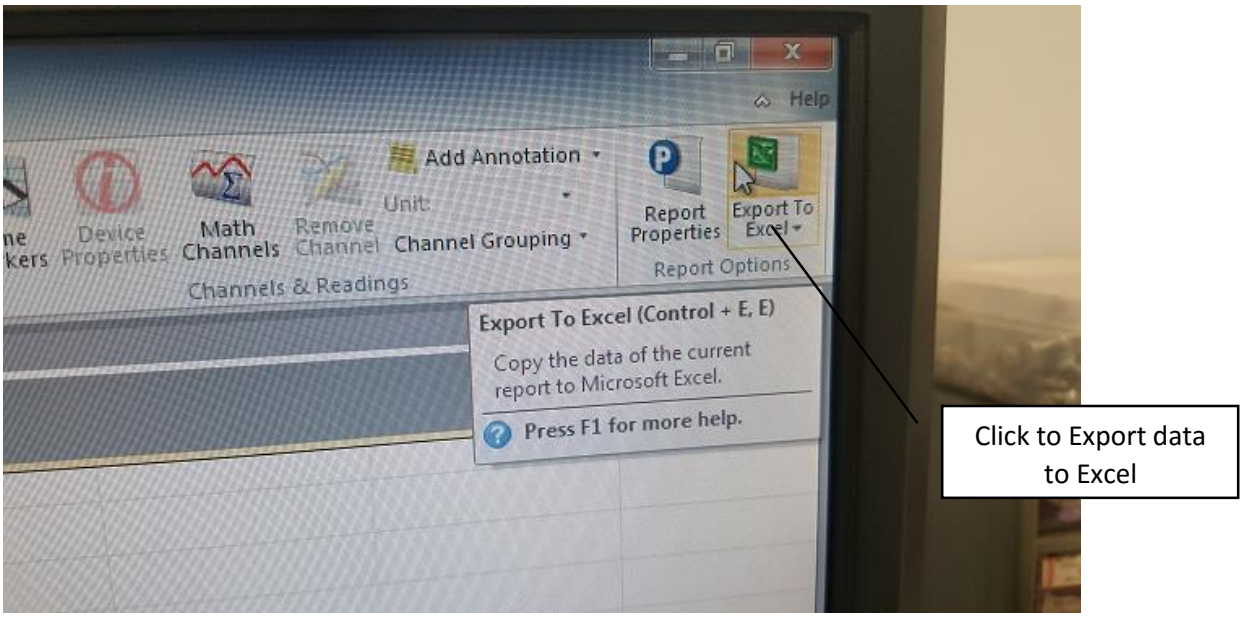

Figure F.11: To export data file

9. While the file is being exported, a prompt appears asking if a chart is required or not [Fig. F.12]. Usually not required.

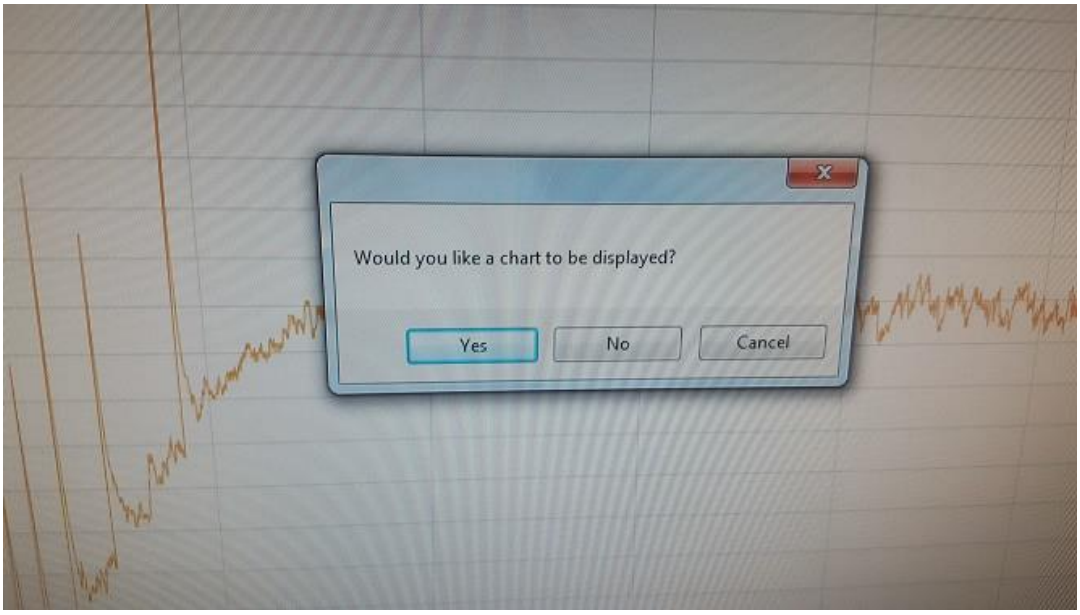

Figure F.12: Dialog box prompt

10. An Excel file shows the data recorded by the Logger. Save the file to the required location [user's choice] [Fig. F.13]. The exported data file includes information about the transducer device, date and time of data logging, and the real time voltage readings measured from the transducer.

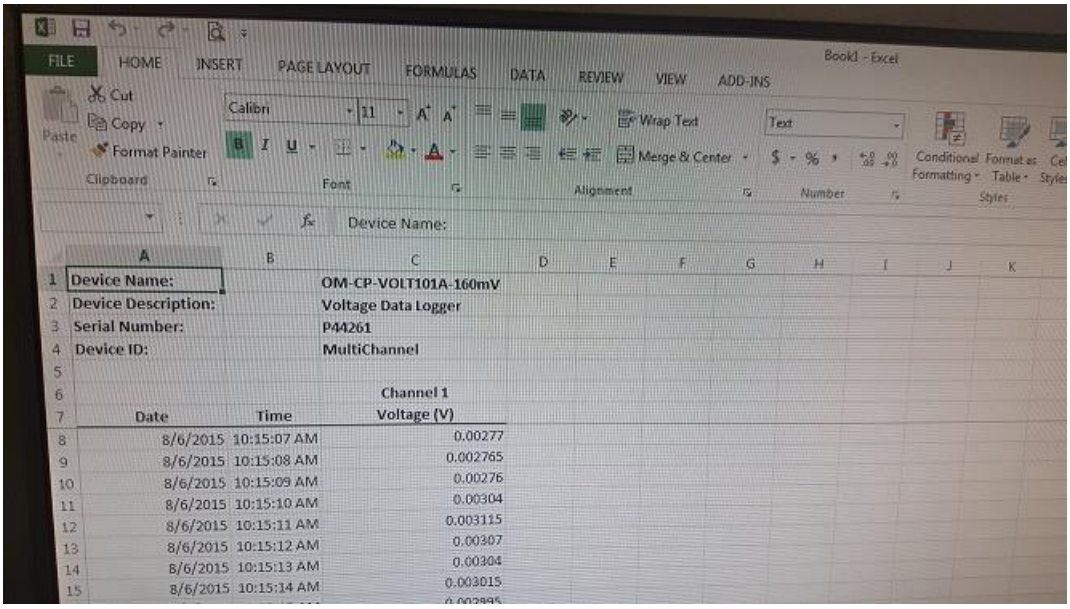

Figure F.13: Sample data log Excel file

11. Also save the Data Logger file when exiting the program [Fig. F.14] because the file can be used as a back up for the Excel file exported from the software.

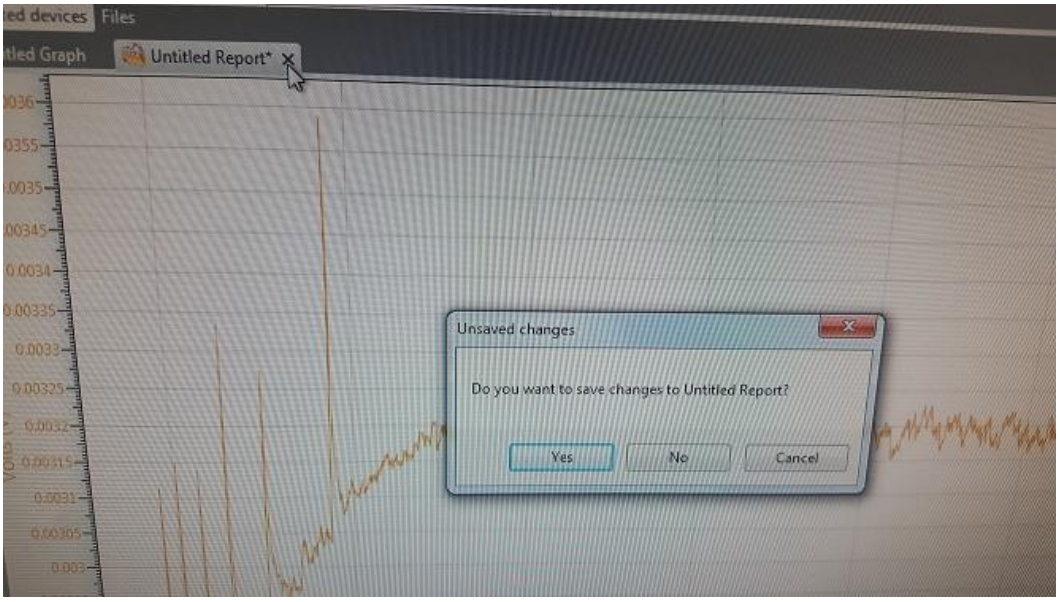

Figure F.14: Save the report every time

12. Note that the program has to be closed and reopened every time the user switches between the two data loggers. The only difficulty that this causes is the fact that the trials running in both the setups cannot be stopped at the same time instant. Data is not lost because the software prompts to save any unsaved data file when the user attempts to close the software. If separate computers were used for each setup, an additional USB connector cable would need to be procured.

Appendix G: Data Logger Specifications

The specifications below were taken from Omega's Data Logger brochure [30]. Based on the 45 day data logging requirements of the experiments, it was decided to use this type of data logger [long term data logging].

Model	OM-CP-VOLT 101A – 160 MV
Voltage range	± 160 mV
Voltage resolution	5 μV
Calibrated accuracy	± 0.01% of reading
Input impedance	> 1 MΩ
Overload protection	± 5V
Input type	Differential
Time accuracy	± 1 minute/month
Reading rate	From 4 readings per second [4 Hz] to 1 reading per 24 hrs

Appendix H: Transducer Data Logger – Voltage to Pressure Conversion Equation

From the Calibration Sheet provided for the transducer [29], a calibration curve was plotted and a linear equation fit was used to determine the conversion equation.

Table H.1: Pressure vs. output voltage reading [calibration sheet]

Pressure (psi)	Voltage (mV)
0	-0.023
1.25	49.977
2.5	99.981
1.25	49.974
0	-0.025

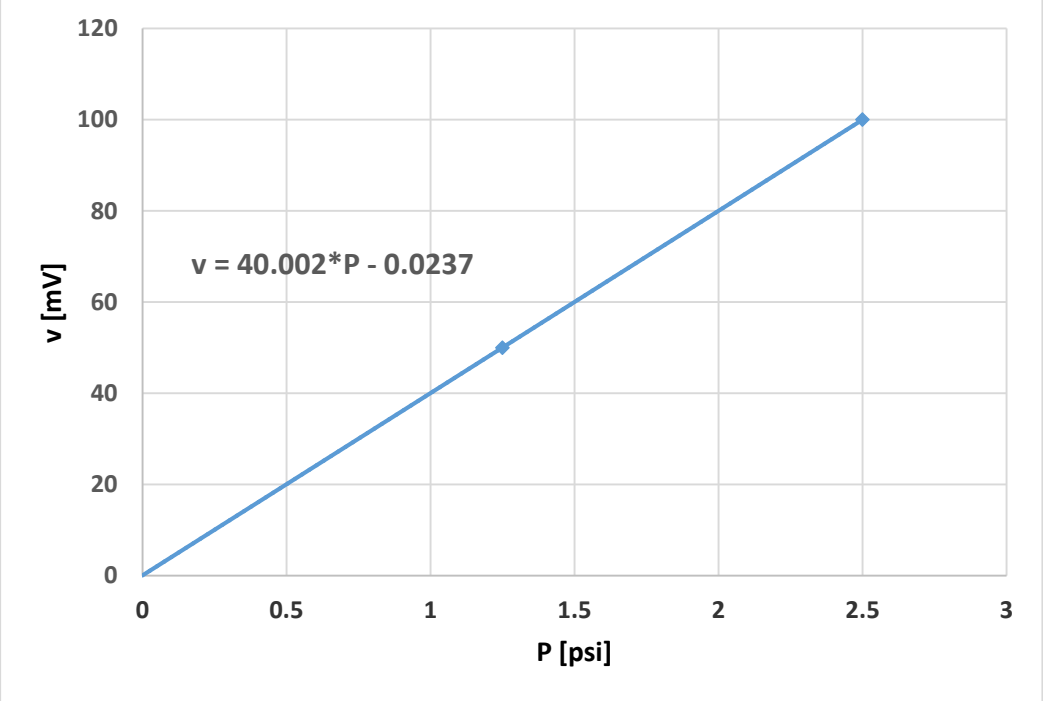

Figure H.1: Output Voltage vs. Pressure calibration curve

Appendix I: Theoretical Pressure Calculation

I.1 Flow through tube – Poiseuille's Law

From Eq. (1) [Section 2.8.1], Table I.1.1 was generated. For a set flow rate and length of tube, the inner radius of the tube is increased by a user-determined value, and the corresponding pressure drop is calculated automatically. The fluid flow rate [µl/min], inner radius of tube [mm] and tube length [mm] are the three values input by the user. The pressure drop is calculated using Eq. (1). Table I.1.1 was used to calculate that a tube of inner diameter 75 microns and length of 35 mm would produce a pressure drop of ~ 15 mm.

Table I.1.1: Variation of pressure drop with diameter of tube

Q, Flow rate					
2.5	µl/min	Tube Length	35	mm	
4.1667E-08	l/s		0.035	m	
4.1667E-11	m^3/s	Dynamic Viscosity At 20°C	1.00E-03	Pa.s	

Inner Radius of tube (mm)	Inner Diameter of tube (m)	Cross-sectional area of tube (m^2)	Pressure drop, ΔP (Pa)	Pressure drop, ΔP (mm of Hg)
0.02	0.00004	1.26E-09	23,256.5	174.4
0.021	0.000042	1.39E-09	19,133.2	143.5
0.022	0.000044	1.52E-09	15,884.5	119.1
0.023	0.000046	1.66E-09	13,297.0	99.7
0.024	0.000048	1.81E-09	11,215.5	84.1
0.025	0.00005	1.96E-09	9,525.9	71.4
0.026	0.000052	2.12E-09	8,142.8	61.1
0.027	0.000054	2.29E-09	7,001.8	52.5
0.028	0.000056	2.46E-09	6,053.9	45.4
0.029	0.000058	2.64E-09	5,261.1	39.5
0.03	0.00006	2.83E-09	4,593.9	34.5
0.031	0.000062	3.02E-09	4,029.2	30.2
0.032	0.000064	3.22E-09	3,548.7	26.6
0.033	0.000066	3.42E-09	3,137.7	23.5
0.034	0.000068	3.63E-09	2,784.5	20.9
0.035	0.00007	3.85E-09	2,479.7	18.6
0.036	0.000072	4.07E-09	2,215.4	16.6
0.037	0.000074	4.30E-09	1,985.4	14.9

I.2 Flow through tube with insert – Modified Poiseuille's Law

From Eq. (2) [Section 2.8.2], Table I.2.1 was generated. This equation is used to predict the pressure drop across a tube having an insert in the tube, assuming that the tube and insert are concentric. The flow rate [µl/min], radii [mm] of tube and insert, and insert length [mm] are the only values input by the user. The modified Poiseuille's law of Eq. (2) was used to calculate the pressure drop [refer to Fig. 8, in Section 2.8.2]. The highlighted portion in Table I.2.1 shows that the pressure drop for 10 µl/min annular flow through a 15 mm long tube with inner radius of 0.1685 mm [or needle with diameter of 0.337 mm], having an insert with a radius of 0.1435 mm [or wire insert diameter of 0.287 mm], should be ~ 15 mm Hg.

Table I.2.1: Variation of pressure drop with diameter of insert

Q, Flow rate		Dynamic Viscosity At 20°C	1.00E-03 Pa.s
10	µl/min		
1.66667E-07	l/s	Insert Length	15 mm
1.66667E-10	m^3/s		0.015 m

Inner Radius of tube, r_2 (mm)	Outer radius of insert, r_1 (mm)	Pressure drop, ΔP (Pa)	Pressure drop, ΔP (mm of Hg)
0.1685	0.1435	1,961.9	14.7
0.1685	0.14475	2,279.2	17.1
0.1685	0.146	2,670.1	20.0
0.1685	0.14725	3,157.1	23.7
0.1685	0.1485	3,772.0	28.3
0.1685	0.14975	4,560.0	34.2
0.1685	0.151	5,586.9	41.9
0.1685	0.15225	6,950.9	52.1
0.1685	0.1535	8,803.3	66.0
0.1685	0.15475	11,385.2	85.4
0.1685	0.156	15,095.6	113.2
0.1685	0.15725	20,628.3	154.7
0.1685	0.1585	29,259.3	219.5
0.1685	0.15975	43,510.1	326.4
0.1685	0.161	68,831.1	516.3
0.1685	0.16225	118,492.0	888.8
0.1685	0.1635	230,560.3	1,729.3
0.1685	0.16475	544,466.9	4,083.8
0.1685	0.166	1,830,717.5	13,731.5

I.3 Flow through Annulus with Eccentricity – Annular Leakage Equation

One of the most useful applications of the low-Reynolds number flow equation for hydraulic control systems is the annular leakage equation [20, 23, 24]. This is a general equation that can be applied when the following conditions are met:

1. Flow is occurring within a circular tube having a solid round insert [Fig. I.3.1].
2. The center of the insert is not the center of the tube [off-center].
3. The flow is fully developed and at low Reynolds number [Re<<1].
4. Eccentricity ratio [$\varepsilon = e / (r_2 - r_1)$] is between 0 and 1.

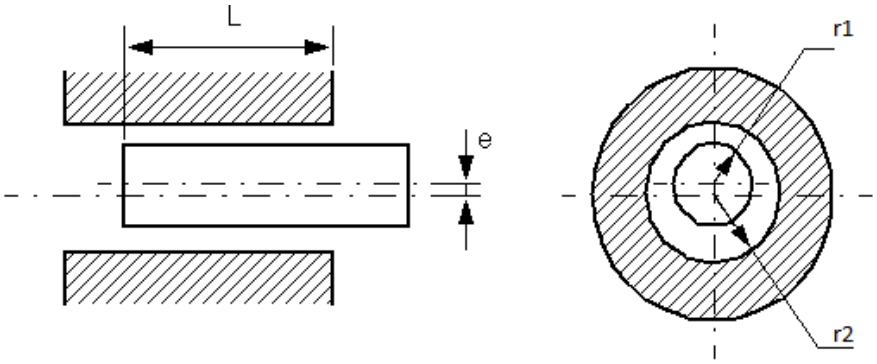

Figure I.3.1: Schematic of an annular leakage path [reproduced from Ref. 20]

The flow – pressure equation for this case is [20]:

$$Q = \frac{\pi r_2 (r_2 - r_1)^3}{6\mu L}\left(1 + \frac{3}{2}\varepsilon^2\right)\Delta P \qquad \text{(I.1)}$$

where, $\varepsilon = \frac{e}{r_2 - r_1}$ (I.2)

It is very rare that the insert and tube are concentric. In most cases they are eccentric. The above equation could be used to account for the difference in pressure drop because of the eccentricity. However, Eq. (I.1) does not reduce to Eq. (2) when e = 0, but becomes

$$Q = \frac{\pi r_2 (r_2 - r_1)^3}{6\mu L}\Delta P \qquad \text{(I.3)}$$

For example, one could calculate the pressure drop for flow of water through a tube of diameter 0.337 mm with a concentric insert of 0.25 mm, length of insert in the tube being 10 mm, and flow rate of 2.5 μl/min. From Eq. (I.3), the pressure drop is calculated to be 0.64 mm Hg, whereas the pressure drop calculated using Eq. (2) is 2.98 mm Hg. There is a 78% difference between the calculated theoretical pressures; and hence Eq. (I.1) cannot be used to calculate the effects of eccentricity on the pressure drop. Another form of the Poiseuille's law must be identified that incorporates the effects of eccentricity and reduces to Eq. (2) when eccentricity is zero.

From the derivation for the annular leakage equation, the pressure drop relation [when e = 0] was found to be [20]:

$$\Delta P = \frac{12Q\,\mu\,L}{\pi\,(r_2-r_1)^3(r_2+r_1)} \tag{I.4}$$

where, r_2 denotes the inner radius of the tube and r_1 denotes the outer radius of the insert. To arrive at Eq. (I.3), Ref. [20] assumed that the gap between the tube and insert was small, i.e., $(r_2 + r_1) \cong 2\,r_2$, in Eq. (I.4); but this approximation was only applied to the term $(r_2 + r_1)$ in Eq. (I.4). To understand this effect with e=0, the ratio of the annular leakage equation to Poiseuille's law (Eq. (2)) was studied for two cases. The first case analyzed the direct ratio of Eq. (I.3) to Eq. (2), yielding

$$\frac{\Delta\text{P calculated from Eq. (I.3) when e=0}}{\Delta\text{P calculated from Eq. (2)}} = \frac{3\left[r_2^4-r_1^4-\frac{\left(r_2^2-r_1^2\right)^2}{ln\left(\frac{r_2}{r_1}\right)}\right]}{4(r_2)(r_2-r_1)^3} \tag{I.5}$$

The second case analyzed the direct ratio of Eq. (I.4) to Eq. (2), and slight simplification of the ratio yields Eq. (I.6).

$$\frac{\Delta P \text{ calculated from Eq. (I.4) when e=0}}{\Delta P \text{ calculated from Eq. (2)}} = \frac{3\left[r_2^4 - r_1^4 - \frac{\left(r_2^2 - r_1^2\right)^2}{ln\left(\frac{r_2}{r_1}\right)}\right]}{2(r_2+r_1)(r_2-r_1)^3} \qquad \text{(I.6)}$$

Analyzing the ratio between the pressure drops calculated using Eqs. (2) and (I.1) with zero eccentricity [Fig. I.3.2], it was determined that, when the radius of the insert approaches the inner radius of the tube, the pressure drop ratio goes to 1.0 for Eq. (I.5) and Eq. (I.6). Figure I.3.2 shows a plot of Eq. (I.5) and Eq. (I.6) against the ratio of the radii.

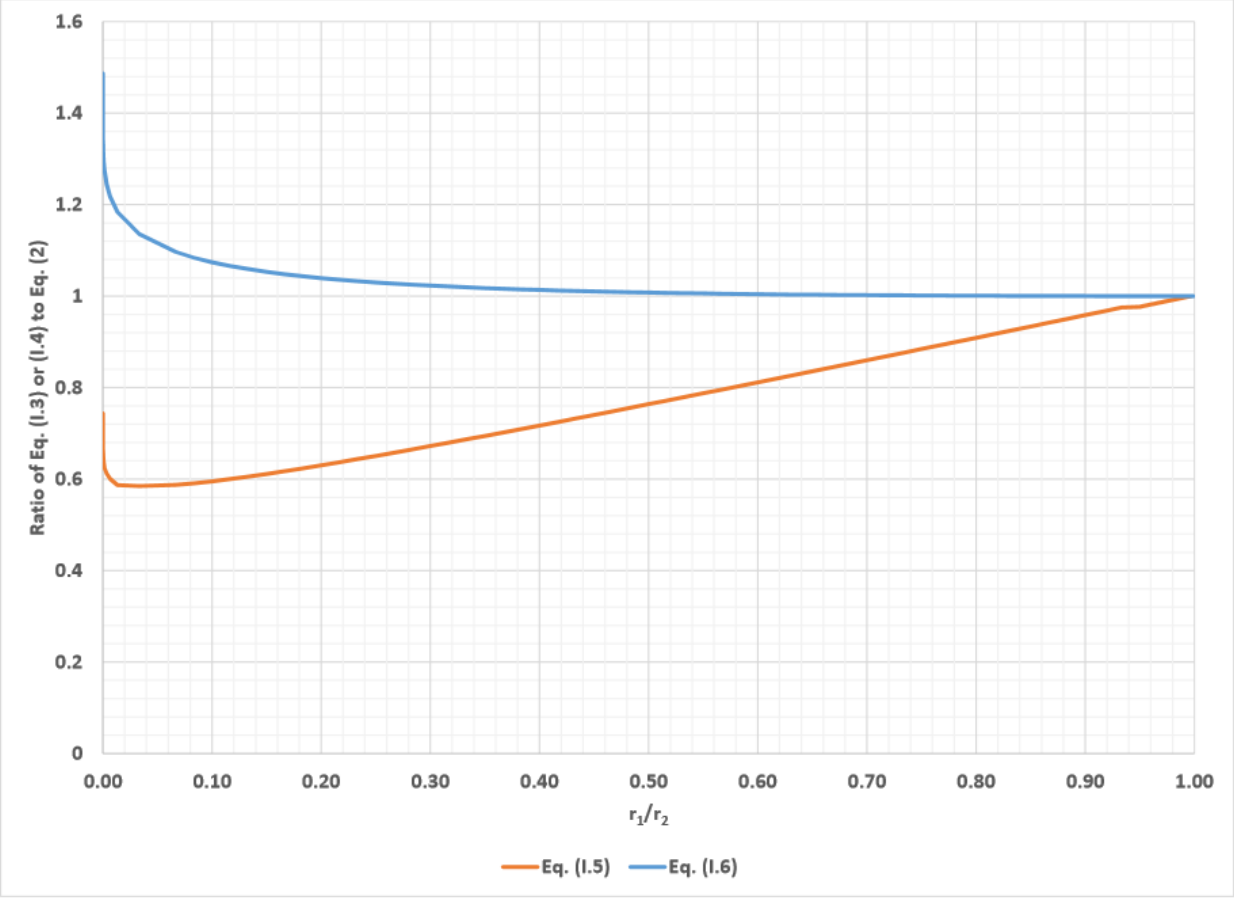

Figure I.3.2: Variation of the ratios between the pressure drops calculated from modified Poiseuille's law and Annular Leakage equation when e = 0

From Fig. I.3.2, it can be seen that when annular leakage equation's assumption that the inner tube radius is approximately equal to the outer radius of the insert is used, at low ratios of the two radii, the annular leakage equation predicts a pressure drop, higher by at least 20% of the

pressure drop calculated by Eq. (2) alone. In contrast, if the radii are assumed to be different, then the pressure drop calculated from the annular leakage equation is less by almost 40% than the actual pressure drop. This indicates that the annular leakage equation is not the best equation to use when considering eccentricity because the equation cannot predict pressure drop at zero eccentricity correctly. No other reference equations were found to check the annular leakage equation for cases with eccentricity.

Appendix J: Theoretical Calculation – Benchmarking Experiments

J.1 Flow through tube

This section shows the sample calculations for the head loss between the three-way valve and the fused silica tube outlet. Based on Dr. Kieweg's and Ajay Ramani's Excel file [Table J.1.2], the theoretical pressure ranges were calculated. Figure J.1.1 shows the different losses that are accounted for in the calculation spreadsheet [Table J.1.2] and the section in which they occur. In Table J.1.2, a user inputs the flow rate with tolerance [in µl/min], tube diameter with tolerance [m], tube length [m], height of the water in the collection trough [m], and elevation difference between the center of the transducer and the outlet [m]. The head losses from Sections A to C are calculated [Fig J.1.1] and displayed on the lower right side of Table J.1.2, along with total head loss. The lower and upper limits of the theoretical pressure range can be calculated by alternately entering '-1' or '+1' next to the tube diameter and flow rate variance sections in Table J.1.2.

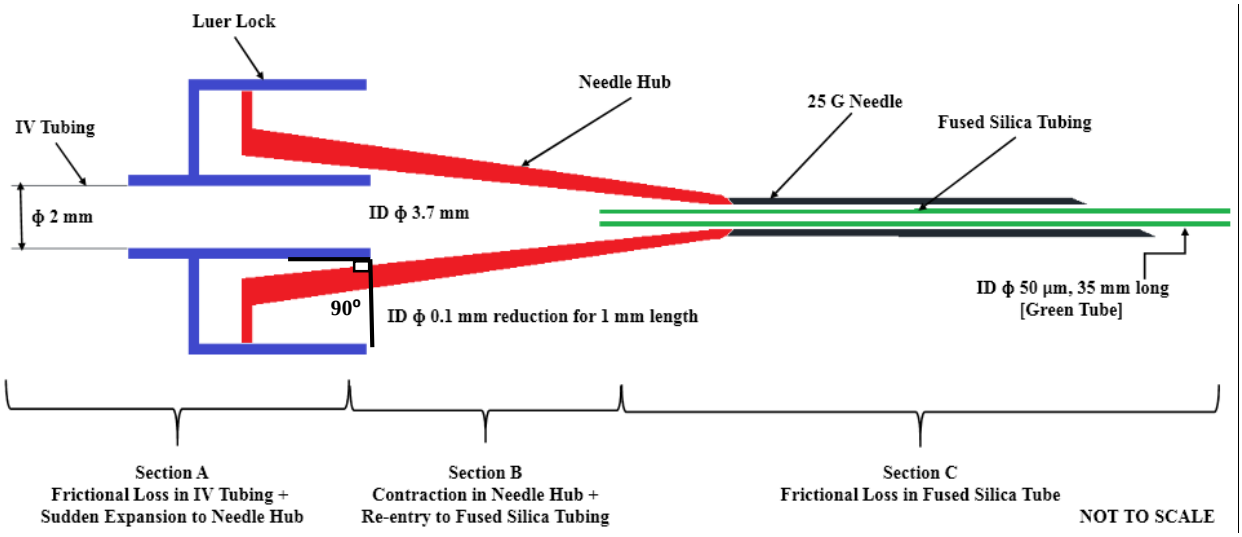

Figure J.1.1: Schematic of losses for the sections and connections of the needle-tube trials

Table J.1.1 shows the how the contraction coefficient was calculated. The ratios of the diameters of the tube sections and the needle hub angle were used to calculate the contraction coefficient from Table J.1.1 [39]. The ratio d/D [or b/B] shown in Table J.1.1 denotes the ratio between the smaller diameter tube and the larger diameter tube, which in our case is the ratio

between the diameter of the IV tubing and diameter of the needle hub. The angle is measured at the expansion or the point where the tubes of the two diameters meet. From Figure J.1.1, we can see that the angle is 90° for this case. The head loss for each section of Fig. J.1.1 was calculated as shown in Table J.1.2. The elevation change between the transducer and outlet was subtracted from the total loss since the center of the transducer was at a higher elevation than the outlet. Sample calculations in Section J.2 go over the manual calculation of all of the sections separately, providing a benchmark for the Excel calculator.

Table J.1.1: Coefficients of Jet Contraction [reproduced from Ref. 38]

COEFFICIENTS OF JET CONTRACTION FOR THE TWO-DIMENSIONAL BOUNDARY CHARACTERISTICS OF FIG. 30

$\frac{d}{D}$ or $\frac{b}{B}$	$\beta = 45°$ C_c	$\beta = 90°$ C_c	$\beta = 135°$ C_c	$\beta = 180°$ C_c
0.0	0.746	0.611	0.537	0.500
0.1	0.747	0.612	0.546	0.513
0.2	0.747	0.616	0.555	0.528
0.3	0.748	0.622	0.566	0.544
0.4	0.749	0.631	0.580	0.564
0.5	0.752	0.644	0.599	0.586
0.6	0.758	0.662	0.620	0.613
0.7	0.768	0.687	0.652	0.646
0.8	0.789	0.722	0.698	0.691
0.9	0.829	0.781	0.761	0.760
1.0	1.000	1.000	1.000	1.000

The following are the assumptions made for these calculations because accurate measurement devices were not available at that time:

1. The diameter where the luer lock meets the hub is 3.7 mm.
2. The hub's diameter reduces by 0.1 mm for every 1 mm of length.
3. The length of Section B is 4 to 5 mm.
4. For conical sections, where there is a smooth reduction in diameter, k_m values were found to be less than or equal to 0.02. k_m was assumed to be 0.02 since this would be the worst case scenario and because the contraction in this section does not affect the overall head loss [39].

Table J.1.2: Theoretical pressure drop range calculation for flow through tubes – break down

Change sample D or Q, or their variability, or assumed parameters in BLUE Boxed Areas.

		Uses values With Variation	*Enter Nominal*		*Enter Variation in Dia. Or Q:*	*Enter Change to 1 or -1 for up or down*		
PeekSil or Peek Tube Diameter	D (m)	0.000075	0.000075	Tube Dia. Var (m)	4.00E-06	0		
PeekSil or Peek Tube Length	L (m)	0.035000				*enter 0: no chg.*		
Flow rate	Q µl/min	2.5	2.5	Q Var. (µl/min)	0.125	0	0.003700	Inlet diameter, D3 (m), to needle hub cone
	Q	4.16667E-08	l/s			*max p (-1 and 1)*	0.0033	Outlet diameter, D4 (m), of needle hub at tube re-entrant
	Q	4.16667E-11	m^3/s			*min p (+1 and -1)*	0.004	Length, L3 (m) of conical contraction of needle hub
Kinematic Viscosity, water, 20 Deg. C	v	1.00E-06	m^2/s				2.00E-02	Assumed loss coefficient in conical section
gravitational constant	g	9.81	m/s^2				*(These effects very negligible. Also calc friction loss here using ave dia of conical section.)*	

	Height of water in trough (m)	0.005								
	Elevation dec.: trans. to outlet (m)	0.028								
	Length of IV tubing (m)	0.1524								
	Section 3 Conical Shape of Needle Hub - estimates:									

Tube inner diameter, length and flow rate info

loss type:		*major*	*minor*	*minor & major*	*minor*	*major*	*elevation*		
Section		A	A	B	B	C	C		
	Section	Friction: Three way valve to Needle Hub	Sudden Expansion into Needle Hub	Needle Hub conical contraction & friction	Re-entry into Needle	Friction: Silica tube (peeksil)	Elevation Change b/t transducer and outlet	TOTALS	
Diameter	D (m)	0.002000	0.003700	0.003500	0.000075	0.000075			
Area of cross section	A (m^2)	3.14E-06	1.08E-05	9.62E-06	4.42E-09	4.42E-09			
Reynolds #	Re	0.02642		0.01510		0.70454			
Friction factor	f	2,422		4,239		91			
Velocity	V_x (m/s)	1.33E-05	3.88E-06	4.33E-06	9.43E-03	9.43E-03			
Length of section	L (m)	0.1524		0.0040		0.0350			
fL/D factor	fL/D	184,586		4,845		42,392			
Head loss due to friction (major)	h_f (m)	1.65E-06		4.63E-09		1.92E-01		*Total head loss due to friction (m)*	0.19219
Loss coefficient	k_m		7.90E-01	2.00E-02	9.98E-01				
Head loss due to minor losses	h_m (m)		6.05E-13	1.91E-14	4.52E-06			*Total head loss due to contraction (m)*	4.52E-06
Head loss due to elevation	h_{diff} (m)						-2.30E-02	*Total head loss due to elevation (m)*	-2.30E-02
% of total head loss		*0.00098%*	*0.00000%*	*0.00000%*	*0.00267%*	*113.58983%*	*-13.59348%*		
section total head loss (m)		1.65E-06	6.05E-13	4.63E-09	4.52E-06	1.92E-01	-2.30E-02	*Total head loss (m)*	1.69E-01
section total head loss (psi)		2.35E-06	8.60E-13	6.59E-09	6.43E-06	2.73E-01	-3.27E-02	*Total head loss (psi)*	2.406E-01
section total head loss (mm of Hg)		1.22E-04	4.45E-11	3.41E-07	3.33E-04	1.41E+01	-1.69E+00	*Total head loss (mm of Hg)*	**12.44**

Table J.1.2 has several section numbers shown along with the type of losses. Dr. Kieweg modified the original Excel sheet developed by Ajay Ramani to get a clear view of the main factors that contribute to the overall head loss. A user inputs the tube inner diameter, the diameter tolerance, length of tube and flow rate at the corresponding highlighted sections. The losses for each section are calculated. The overall head loss [major and minor] is calculated, and the elevation difference between the transducer and tube outlet is deducted to yield the net theoretical head loss for that configuration. To get the entire theoretical range, the cells next to the diameter and flow tolerances [default values are 0] are changed to -1 or +1 to vary the diameter and flow rate. This process of changing the values yields the theoretical range.

J.2 Sample calculation of theoretical pressure drop for flow through tube

These sample calculations were performed in order to confirm that the Excel sheets are computing values correctly. This calculation was done for Q = 2.5 µl/min, D = 75 µm. No variation in diameter or flow rate was considered. This calculation is for the same input parameters as in Table J.1.2. All formulas are reproduced from "Hydraulic Control Systems" by Noah D. Manring [20]. There might be a slight difference in the final value calculated manually because of rounding-off digits; but the closeness of the two results helps to confirm the accuracy of the Excel calculator.

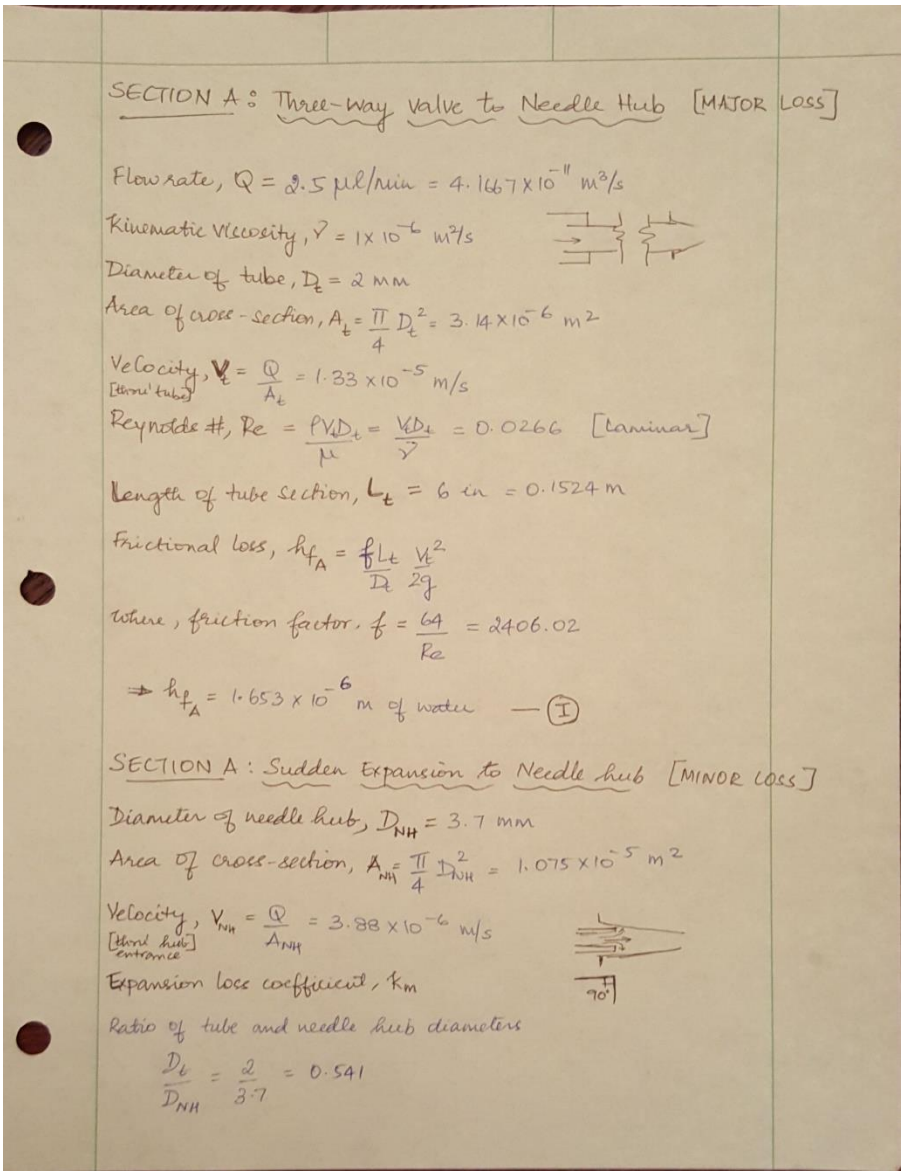

SECTION A : Three-way valve to Needle Hub [MAJOR LOSS]

Flow rate, $Q = 2.5\ \mu l/min = 4.1667 \times 10^{-11}\ m^3/s$

Kinematic viscosity, $\nu = 1 \times 10^{-6}\ m^2/s$

Diameter of tube, $D_t = 2\ mm$

Area of cross-section, $A_t = \frac{\pi}{4} D_t^2 = 3.14 \times 10^{-6}\ m^2$

Velocity [through tube], $V_t = \frac{Q}{A_t} = 1.33 \times 10^{-5}\ m/s$

Reynolds #, $Re = \frac{\rho V_t D_t}{\mu} = \frac{V_t D_t}{\nu} = 0.0266$ [Laminar]

Length of tube section, $L_t = 6\ in = 0.1524\ m$

Frictional loss, $h_{f_A} = \frac{f L_t}{D_t} \frac{V_t^2}{2g}$

where, friction factor, $f = \frac{64}{Re} = 2406.02$

$\Rightarrow h_{f_A} = 1.653 \times 10^{-6}\ m$ of water — (I)

SECTION A : Sudden Expansion to Needle hub [MINOR LOSS]

Diameter of needle hub, $D_{NH} = 3.7\ mm$

Area of cross-section, $A_{NH} = \frac{\pi}{4} D_{NH}^2 = 1.075 \times 10^{-5}\ m^2$

Velocity [through hub entrance], $V_{NH} = \frac{Q}{A_{NH}} = 3.88 \times 10^{-6}\ m/s$

Expansion loss coefficient, k_m

Ratio of tube and needle hub diameters

$\frac{D_t}{D_{NH}} = \frac{2}{3.7} = 0.541$

From Table J.1.1, where the ratio b/B or d/D denote the D_t/D_{NH} and $\beta = 90°$ [Because of a sharp change in diameter & angle between tube outlet and needle hub is 90°]

∴ By interpolating, we determine C_c [expansion/contraction coefficient]

D_t/D_{NH}	$\beta = 90°$ C_c	
0.5	0.644	
0.541	?	⇒ 0.6514
0.6	0.662	

$$k_m = \left[\frac{1}{C_c}\frac{A_t}{A_{NH}} - 1\right]^2 = 0.79$$

Head loss due to sudden expansion; $h_{m_A} = k_m \frac{V_{NH}^2}{2g} = 6.062 \times 10^{-13}$ m of water — (II)

SECTION B: Contraction in needle hub [MAJOR & MINOR LOSS]

Average diameter in the conical hub, $D_H = 3.5$ mm

Area of cross-section, $A_H = \frac{\pi}{4} D_H^2 = 9.62 \times 10^{-6}$ m²

Velocity [in the hub], $V_H = \frac{Q}{A_H} = 4.33 \times 10^{-6}$ m/s

Reynolds #, $Re = \frac{V_H D_H}{\nu} = 0.01516$ [Laminar]

Friction factor, $f = \frac{64}{Re} = 4,221.6$

Length of hub section, $L_H = 4$ mm

Frictional loss, $h_{f_B} = \frac{f L_H}{D_H} \frac{V_H^2}{2g} = 4.61 \times 10^{-9}$ m of water

For a smooth conical section, it was learnt that the coefficient of contraction is below 0.02, because of the smooth transition in diameter. [Reference: "Water Resources Engineering" by L.W. Mays, 2010]

$\therefore k_m = 0.02$ [Worst-case scenario] or "highest loss" case

∴ Head loss due to contraction, $h_{m_B} = k_m \frac{V_H^2}{2g} = 1.91 \times 10^{-14}$ m of water (III)

SECTION B: Re-Entry to tube in needle [MINOR LOSS]

Diameter of PEEKsil tube, $D_p = 0.075$ mm [or 0.050 mm - depending on tube diameter]

Area of cross-section, $A_p = \frac{\pi}{4} D_p^2$

$= 4.42 \times 10^{-9}$ m²

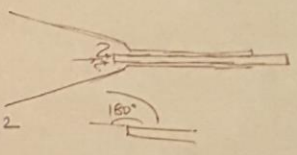

Velocity at point of re-entry, $V_p = \frac{Q}{A_p} = 9.43 \times 10^{-3}$ m/s

From Table J.1.1, where the ratio b/B (or d/D) denotes the ratio D_t/D_H and $\beta = 180°$ [Angle between tube and needle]

By interpolating, we can determine C_c

D_t/D_H	$\beta = 180°$ C_c
0	0.5
0.02143	→ ? 0.5028
0.1	0.513

$$k_m = \left[\frac{1}{C_c} \frac{A_p}{A_H} - 1\right]^2 = 0.998$$

Head loss due to fluid re-entry, $h_{m_B} = k_m \frac{V_p^2}{2g} = 4.52 \times 10^{-6}$ m of water — (IV)

SECTION C: Frictional loss in PEEKsil tube [MAJOR LOSS]

Diameter of PEEKsil tube, $D_p = 0.075$ mm

Area of cross-section, $A_p = \frac{\pi}{4} D_p^2 = 4.42 \times 10^{-9}$ m^2

Velocity, $V_p = \frac{Q}{A_p} = 9.43 \times 10^{-3}$ m/s

Reynolds #, $Re = \frac{V_p D_p}{\nu} = 0.7073$ [Laminar]

Friction factor, $f = \frac{64}{Re} = 90.49$

Length of tube, $L_p = 35$ mm

Head loss due to friction, $h_{fc} = \frac{f L_p}{D_p} \frac{V_p^2}{2g} = 0.1914$ m of water — (V)

Total Head loss in the setup = 0.19141 m of water
[Sum of (I) to (V)]

Difference in elevation b/w transducer & outlet = 28 − 5 = 23 mm

Net loss = $0.19141 - 23 \times 10^{-3}$ = 0.1684 m of water
= 0.239 psi
= 12.38 mm Hg

J.3 Flow through tube with insert

This section shows the sample calculations for the head loss between the three-way valve and the fused silica tube outlet. Based on Dr. Kieweg's and Ajay Ramani's Excel file [Table J.3.1], the theoretical pressure ranges were calculated. Figure J.3.1 shows the sources of the different losses that are accounted for in the calculation spreadsheet [Table J.3.1] and the section in which these losses occur.

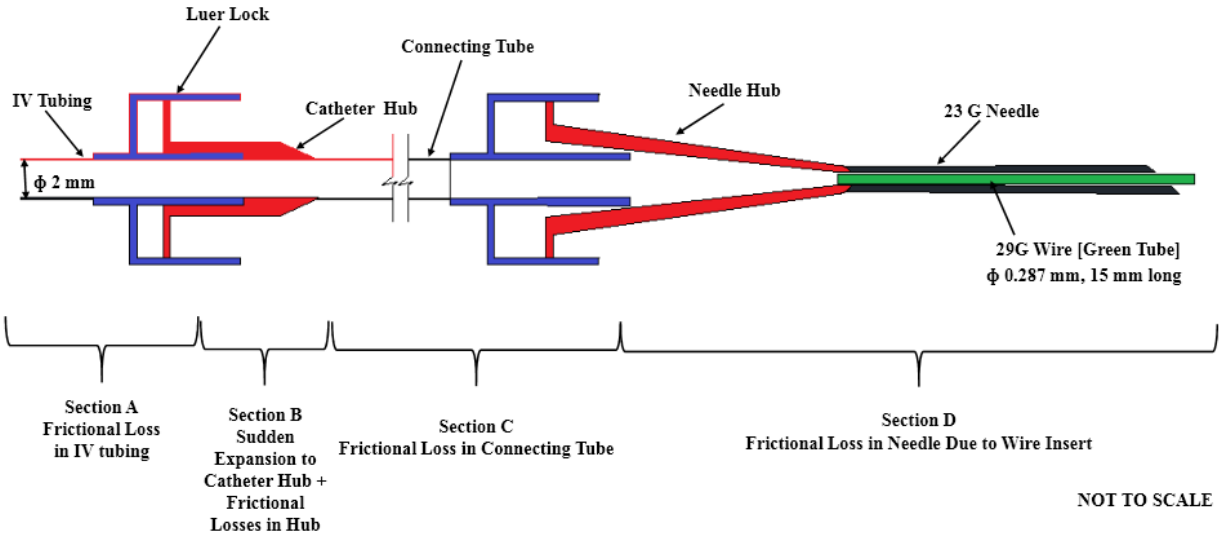

Figure J.3.1: Schematic of losses along the connections - for flow through annulus

The following are the assumptions made for these calculations because accurate measurement devices to measure length and angle were not available at that time.

1. The diameter where the luer lock of the connecting tube meets the hub is 3.7 mm.
2. The hub's diameter reduces by 0.1 mm for every 1 mm of length.
3. For conical sections, where there is a smooth reduction in diameter, k_m values were found to be less than or equal to 0.02. k_m was assumed to be 0.02 since this would be the worst case scenario and because the contraction in this section does not affect the overall head loss [39].

Table J.3.1: Theoretical pressure drop range calculation for annular flow – break down

		Uses values With Variation	Enter Nominal		Variation in Dia. Or Q:	Change to 1 or -1 for up or down			
Insert Diameter	d (m)	0.000272	0.000272	Tube Dia. Var (m)	5.00E-06	0		Elevation dec.: trans. to outlet (m)	0.028
Needle Inner diameter	D (m)	0.000357	0.000357	Tube Dia. Var (m)	5.00E-06	0		Length of IV tubing (m)	0.1524
Insert Length	L (m)	0.015000				enter 0: no chg.		Height of water in trough (m)	0.005
Flow rate	Q µl/min	10	10	Q Var. (µl/min)	0.5	0	0.004000	*Section 3 Cannula Hub - estimates:* Inlet diameter, D_{CH} (m), to catherter hub cone	
	Q	1.66667E-07	l/s			max p (-1 and 1)	0.0037	Outlet diameter, D_{NH} (m), of needle hub at tube re-entrant	
	Q	1.66667E-10	m^3/s			min p (+1 and -1)	0.005	Length, L_{CH} (m) of conical contraction of needle hub	
Kinematic Viscosity, water, 20 Deg. C	v	1.00E-06	m^2/s				2.00E-02	Assumed loss coefficient in conical section	
gravitational constant	g	9.81	m/s^2					*(These effects very negligible. Also calc friction loss here using ave dia of conical section.)*	
Dynamic Viscosity, water, 20 Deg. C	µ	1.00E-03	Pa.s.						

	loss type:	major	minor	minor & major	minor	major	elevation		
	Section	A	B	B	C	D	6		
	Section	Friction: Three way valve to catheter Hub	Sudden Expansion into catheter Hub	Catheter Hub conical contraction & friction	Frictional loss in Connecting tube	Friction: Wire inserted into the needle	Elevation Change b/t transducer and outlet	TOTALS	
Diameter	D (m)	0.002000	0.004000	0.003700	0.002000	0.000231			
Area of cross section	A (m^2)	3.14E-06	1.26E-05	1.08E-05	3.14E-06	4.20E-08			
Reynolds #	Re	0.10568		0.05712	0.10568	0.91409			
Friction factor	f	606		1,120	606	70			
Velocity	V_x (m/s)	5.31E-05	1.33E-05	1.55E-05	5.31E-05	3.97E-03			
Length of section	L (m)	0.1524		0.0050	0.3500	0.0150			
fL/D factor	fL/D	46,147		1,514	105,980	4,542			
Head loss due to friction (major)	h_f (m)	6.62E-06		1.85E-08	1.52E-05	4.04E-02		*Total head loss due to friction (m)*	4.04E-02
Loss coefficient	k_m		3.76E-01	2.00E-02					
Head loss due to minor losses	h_m (m)		3.37E-12	2.45E-13				*Total head loss due to contraction (m)*	3.62E-12
Head loss due to elevation	h_{diff} (m)						-2.30E-02	*Total head loss due to elevation (m)*	-2.30E-02
% of total head loss		*0.0381%*	*0.0000%*	*0.0001%*	*0.0874%*	*232.1553%*	*-132.2809%*		
section total head loss (m)		6.62E-06	3.37E-12	1.85E-08	1.52E-05	4.04E-02	-2.30E-02	*Total head loss (m)*	1.74E-02
section total head loss (psi)		9.41E-06	4.79E-12	2.64E-08	2.16E-05	5.74E-02	-3.27E-02	*Total head loss (psi)*	2.472E-02
section total head loss (mm of Hg)		4.87E-04	2.48E-10	1.36E-06	1.12E-03	2.97E+00	-1.69E+00	*Total head loss (mm of Hg)*	**1.28**

Table J.3.1 has several section numbers shown along with the type of losses. Dr. Kieweg modified the original Excel sheet developed by Ajay Ramani to get a clear view of the main factors that contribute to the overall head loss. A user inputs the tube inner diameter, the insert outer diameter, the diameter tolerances, length of tube and flow rate in the corresponding highlighted sections. The losses for each section are calculated. The overall head loss [major and minor] is calculated and the elevation difference between the transducer and tube outlet is deducted to yield the net theoretical head loss for that configuration. To get the entire theoretical range, the cells next to the diameter and flow tolerances [default values are 0] are changed to -1 or +1 to vary the diameter and flow rate. This process of changing the values yields the theoretical range.

J.4 Sample calculation of theoretical pressure drop for flow through annulus

These sample calculations were performed in order to confirm that the Excel sheets [Table J.3.1] are computing the values correctly. This calculation was done for Q = 10 µl/min, needle inner diameter = 357 µm, insert outer diameter = 272 mm. Variations in diameter and flow rate are not considered in this calculation but in Table J.3.1. The following gives a manual calculation of the pressure drop break down shown in Table J.3.1. All formulas are reproduced from "Hydraulic Control Systems" by Noah D. Manring [20].

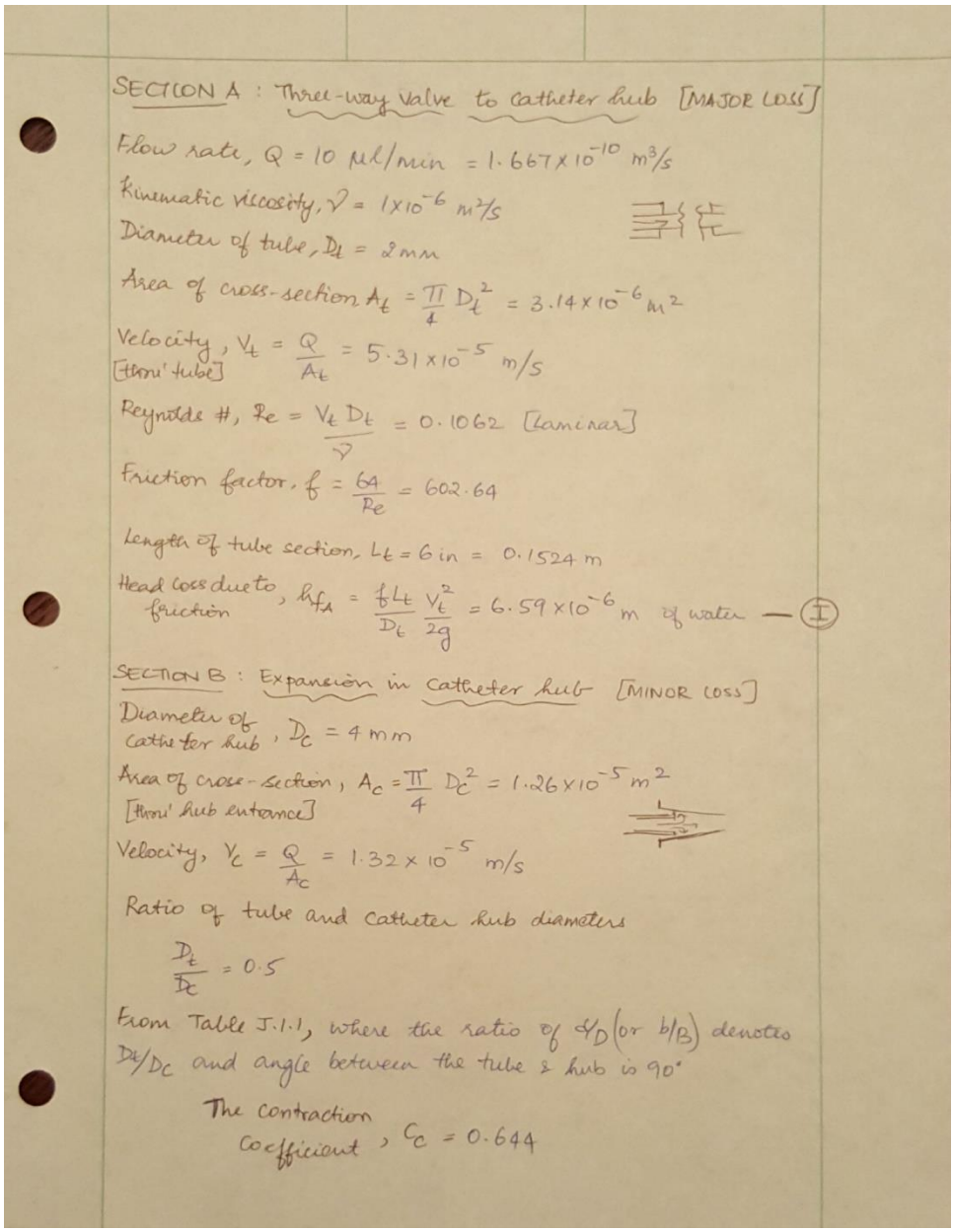

SECTION A : Three-way valve to catheter hub [MAJOR LOSS]

Flow rate, $Q = 10\ \mu l/min = 1.667 \times 10^{-10}\ m^3/s$

Kinematic viscosity, $\nu = 1 \times 10^{-6}\ m^2/s$

Diameter of tube, $D_t = 2mm$

Area of cross-section $A_t = \frac{\pi}{4} D_t^2 = 3.14 \times 10^{-6}\ m^2$

Velocity, $V_t = \frac{Q}{A_t} = 5.31 \times 10^{-5}\ m/s$ [thro' tube]

Reynolds #, $Re = \frac{V_t D_t}{\nu} = 0.1062$ [Laminar]

Friction factor, $f = \frac{64}{Re} = 602.64$

Length of tube section, $L_t = 6\ in = 0.1524\ m$

Head loss due to friction, $h_{f_t} = \frac{f L_t}{D_t} \frac{V_t^2}{2g} = 6.59 \times 10^{-6}\ m$ of water — (1)

SECTION B : Expansion in catheter hub [MINOR LOSS]

Diameter of catheter hub, $D_c = 4\ mm$

Area of cross-section, $A_c = \frac{\pi}{4} D_c^2 = 1.26 \times 10^{-5}\ m^2$ [thro' hub entrance]

Velocity, $V_c = \frac{Q}{A_c} = 1.32 \times 10^{-5}\ m/s$

Ratio of tube and catheter hub diameters

$\frac{D_t}{D_c} = 0.5$

From Table J.1.1, where the ratio of d/D (or b/B) denotes D_t/D_c and angle between the tube & hub is 90°

The contraction coefficient, $C_c = 0.644$

∴ The Expansion loss coefficient, $k_m = \left[\frac{1}{C_c}\frac{A_t}{A_c} - 1\right]^2$

$= 0.376$

Head loss due to expansion, $h_{m_B} = k_m \frac{V_c^2}{2g} = 3.34 \times 10^{-12}$ m of water — (II)

SECTION B: Catheter hub contraction & friction loss [MAJOR & MINOR LOSS]

Diameter of conical hub, $D_{CH} = 3.7$ mm

Length of this section, $L_{CH} = 5$ mm

Area of cross-section, $A_{CH} = \frac{\pi}{4} D_{CH}^2 = 1.075 \times 10^{-5}$ m²

Velocity, $V_{CH} = \frac{Q}{A_{CH}} = 1.55 \times 10^{-5}$ m/s
[Flow' conical hub]

Reynolds #, $Re = \frac{V_{CH} D_{CH}}{\nu} = 0.05735$ [Laminar]

Friction factor, $f = \frac{64}{Re} = 1115.95$

Head loss due to friction, $h_{f_B} = \frac{f L_{CH}}{D_{CH}} \frac{V_{CH}^2}{2g} = 1.85 \times 10^{-8}$ m of water — (III)

for a smooth conical section, it was learnt that the coefficient of contraction is below 0.02 due to the smooth transition in diameter [Reference: "Water Resources Engineering", by L.W. Mays, 2010]

∴ $k_m = 0.02$ [Worst case scenario]

Head loss due to contraction, $h_{m_B} = k_m \frac{V_{CH}^2}{2g} = 2.45 \times 10^{-13}$ m of water — (IV)

SECTION C: Frictional losses in connecting tube [MAJOR LOSS]

Diameter of connecting tube, $D_t = 2$ mm

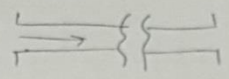

Length of this section, $L_t = 350$ mm

Area of cross section, $A_t = \frac{\pi}{4} D_t^2 = 3.14 \times 10^{-6}$ m^2

Velocity [thru' tube], $V_t = \frac{Q}{A_t} = 5.31 \times 10^{-5}$ m/s

Reynolds #, $Re = \frac{V_t D_t}{\nu} = 0.1062$

Friction factor, $f = \frac{64}{Re} = 602.64$

Head loss due to friction, $h_{fc} = \frac{f L_t}{D_t} \frac{V_t^2}{2g} = 1.52 \times 10^{-5}$ m of water — (V)

SECTION D: Loss in tube due to insert [MAJOR LOSS]

Diameter of insert, $d = 0.272$ mm $\Rightarrow r_1 = 0.136$ mm

Diameter (inner) of needle, $D = 0.357$ mm $\Rightarrow r_2 = 0.1785$ mm

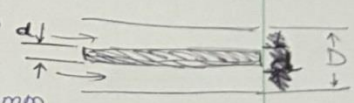

Effective [Hydraulic] diameter, $D_h = \sqrt{D^2 - d^2} = 0.231$ mm

Area of cross section [Effective], $A_h = \frac{\pi}{4} D_h^2 = 4.19 \times 10^{-8}$ m^2

Length of insert, $L = 15$ mm

Velocity [thru' annulus], $V_h = \frac{Q}{A_h} = 3.98 \times 10^{-3}$ m/s

Reynolds #, $Re = \frac{V_h D_h}{\nu} = 0.9194$ [Laminar]

Dynamic viscosity, $\mu = 1.002 \times 10^{-3}$ Pa·s.

Friction factor, $f = \frac{64}{Re} = 69.61$

From modified Poiseuille's law for flow through an annulus,

$$Q = \frac{\pi}{8\mu} \frac{\Delta P}{L} \left[r_2^4 - r_1^4 - \frac{(r_2^2 - r_1^2)^2}{\ln(r_2/r_1)} \right]$$

Re-arranging, we can determine ΔP

$$\Delta P = \frac{8 Q \mu L}{\pi} \left[\frac{1}{r_2^4 - r_1^4 - \frac{(r_2^2 - r_1^2)^2}{\ln(r_2/r_1)}} \right]$$

$\therefore \Delta P = 395.92$ Pa $= 0.0404$ m of water — (VI)

Total Head loss in the Setup [① to ⑤] $= 0.04042$ m of water

Difference in elevation b/w transducer and outlet $= 28 - 5 = 23$ mm

Net loss $= 0.04042 - 23 \times 10^{-3} = 0.01742$ m of water

$= 2.48 \times 10^{-2}$ psi

$= 1.28$ mm Hg

→ The calculated value is close to the value shown in Table 5.3.1.

Appendix K: Experimental Procedure

Goal

The primary purpose of this experiment is to investigate the effect of introducing absorbable suture material inserts into Baerveldt Glaucoma Implant [BGI] tubes.

Criteria for Success/Failure

If the measured pressure lies between 15 to 30 mm of Hg when the flow rate is at 2.5 µl/min, then this experiment is considered a success. If not, the results would direct achievement of the pressure drop using alternate suture and tube sizes.

Background

Glaucoma is a condition that causes damage to the optic nerve due to buildup of pressure inside the eye. The increase in pressure, called intraocular pressure (IOP), damages the optic nerve resulting in poor eyesight and may lead to blindness after a significant period of time. When diagnosed with serious non-medicine treatable glaucoma, implants such as Baerveldt [Fig. K.1] or Ahmed [Fig. K.2] can be surgically inserted into a patient's eyes. Regardless of the type of implant, its aim is to decrease the IOP to a lower limit of 5 mm Hg, by increasing the ease of outflow of fluid from the eye.

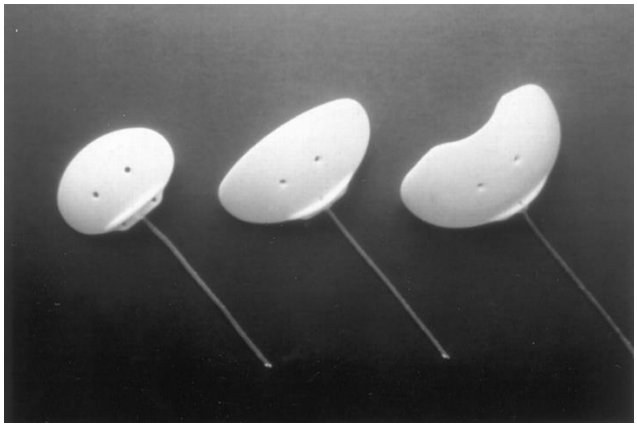

Figure K.1: Baerveldt Implant [reproduced from Ref. 14]

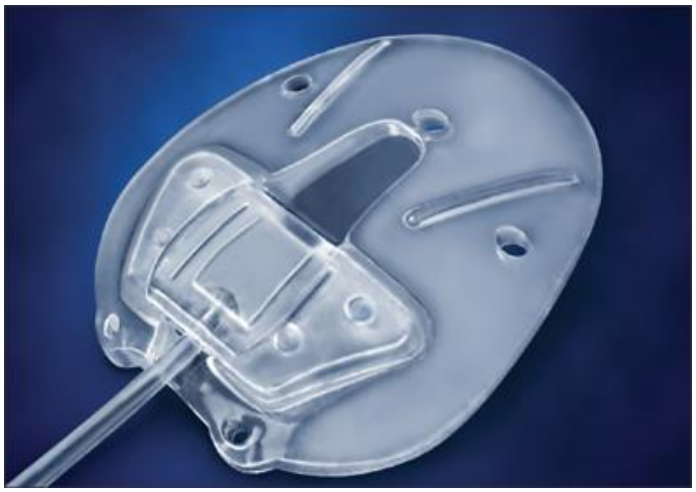

Figure K.2: Ahmed Glaucoma Valve Implant [reproduced from Ref. 5]

There is a possibility of low IOP in the case of BGI, due to low flow resistance immediately after surgery. There also have been instances where implants have failed due to healing and scarring over the surgical opening [bleb]. This will in turn lead to an increase in IOP which could be higher than the pre-surgery levels.

To counter the low flow resistance immediately after surgery, an increase in the IOP could be achieved by creating a temporary blockage in the BGI tubes that would impede the flow until the scar tissue grows over the implant, creating the necessary back pressure to maintain the IOP above 5 mm Hg but below 20 mm Hg. This blockage does not have to be degradable, but biodegradable material was selected so that the normal flow can resume after 4 – 6 weeks.

The pressure drop across the tube with the insert can be determined using modified Poiseuille's equation [Eq. (2) reproduced from main text]

$$Q = \frac{\pi}{8\mu}\frac{\Delta P}{\Delta L}\left[r_2^4 - r_1^4 - \frac{\left(r_2^2 - r_1^2\right)^2}{\ln r_2 / r_1} \right] \qquad \text{(K.1)}$$

where

μ Dynamic viscosity of the fluid, m^2/s

ΔL Length of the tube, m

Q Flow rate, m^3/s

r_2 Inner radius of the tube, m

r_1 Outer radius of the insert, m

ΔP Pressure drop across the tube, Pa

Examples of calculations using Eq. (K.1) [or Eq. (2)] are in Appendices I and J. Alternatively, based on the pressure drop required, the length and/or diameter of the insert required could be calculated, keeping in mind that the insert length should be a maximum 8 mm because the length of the implant tubes used by surgeons while implanting BGIs is 10 mm.

Equipment required for setup

1. Connector tubing (dia. – 6 mm, length – 1 m)
2. Baerveldt implant tubing (1) (dia. – 0.305 mm, length – 10 mm)
3. Airtight container (1) – Dimensions: dia.: 60 mm, height: 120 mm, Volume 500 mL
4. 20 gauge cannula (1)
5. Pressure transducer (1) – Make: Omega; Model: PX429 – 2.5 G series [refer to **App. C**]
6. PneuWave pump (1) – Make: Corsolutions, PneuWave series [refer to **App. E**]
7. Luer locks (1)
8. Absorbable sutures – Size 3-0, 4-0 [Monofilament & Braided – Absorbable & Non-Absorbable] [refer to Table 1 in main text for details]
9. Distilled water – 500 ml
10. Medical grade scissors [6”], tweezers [6”] and super glue [0.34 oz]
11. Microscope (1) – 40X magnification

12. Syringe needles of gauges 25, 27 and 30

Experimental setup

As explained in Chapter 3, the experimental setup is comprised of a PneuWave pump, medical grade connecting tubes, a three-way valve, an Omega pressure transducer, an Omega data logger, a 500 mL glass container, a gauge 20 cannula and a collection trough. Refer to Figure K.3 for a schematic of the experimental setup. Figure K.4 shows the actual benchtop experimental setup.

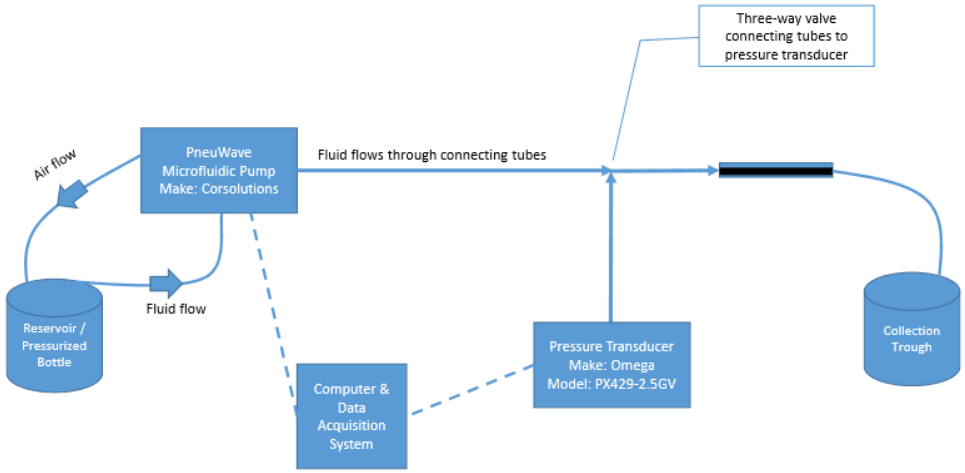

Figure K.3: Schematic of experimental setup [reproduced from main text]

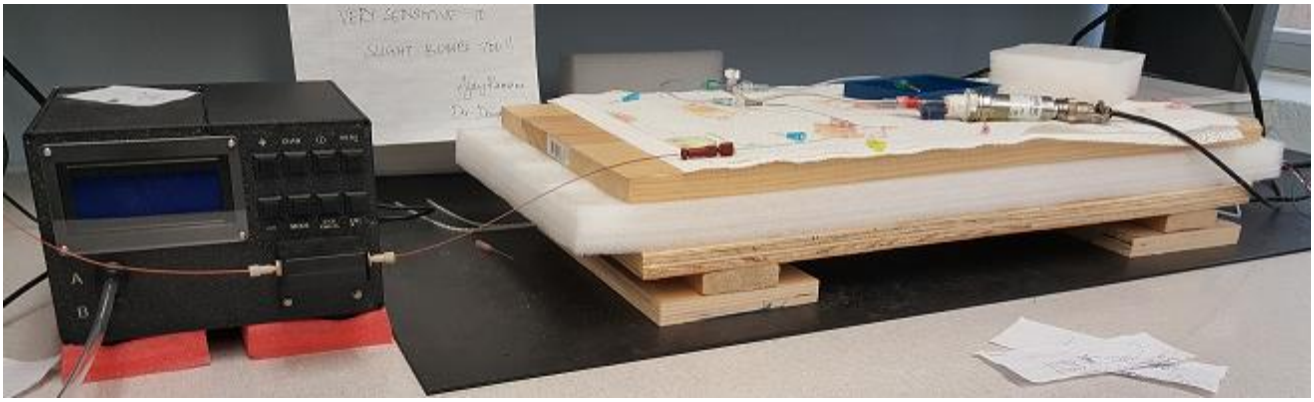

Figure K.4: Benchtop experimental setup [reproduced from main text]

Test procedure

1. Sterilize the airtight container, tubes and other connectors used in the setup.
2. Fill the sterile airtight container with distiller water [DW] and seal the lid. Insert the 10 mm length of implant tubing [without the suture insert] into the 20 gage cannula as shown in Fig. K.5. Secure the implant tubing to the cannula using super glue.

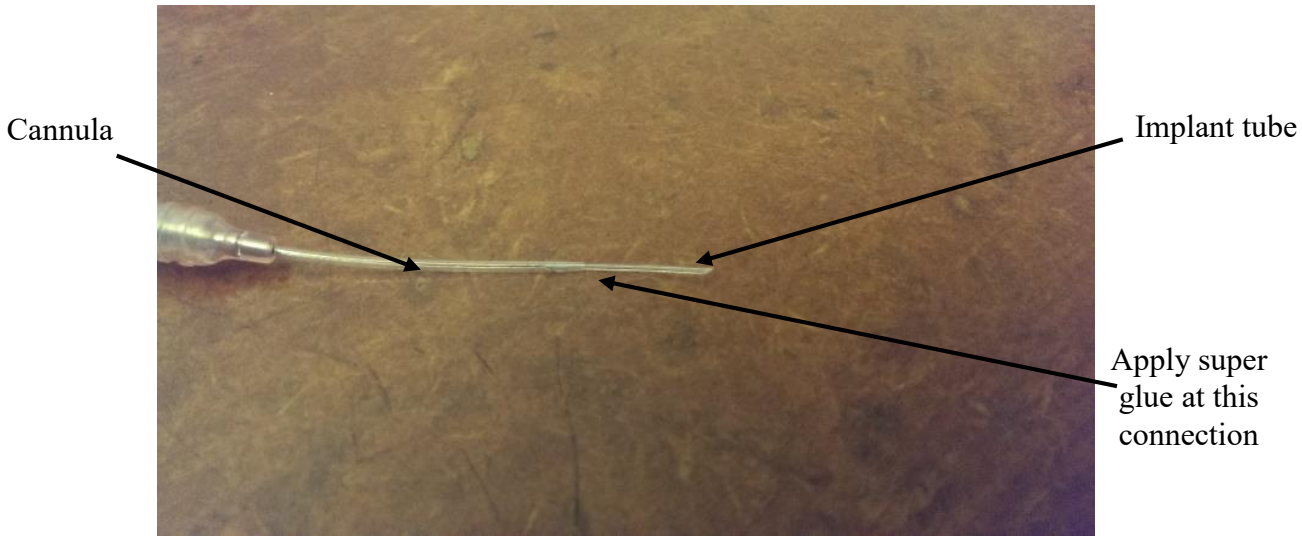

Figure K.5: Implant tube inserted in 20 gauge cannula

3. Make sure that all tube connections and the three-way valve are connected as shown in Fig K.6.

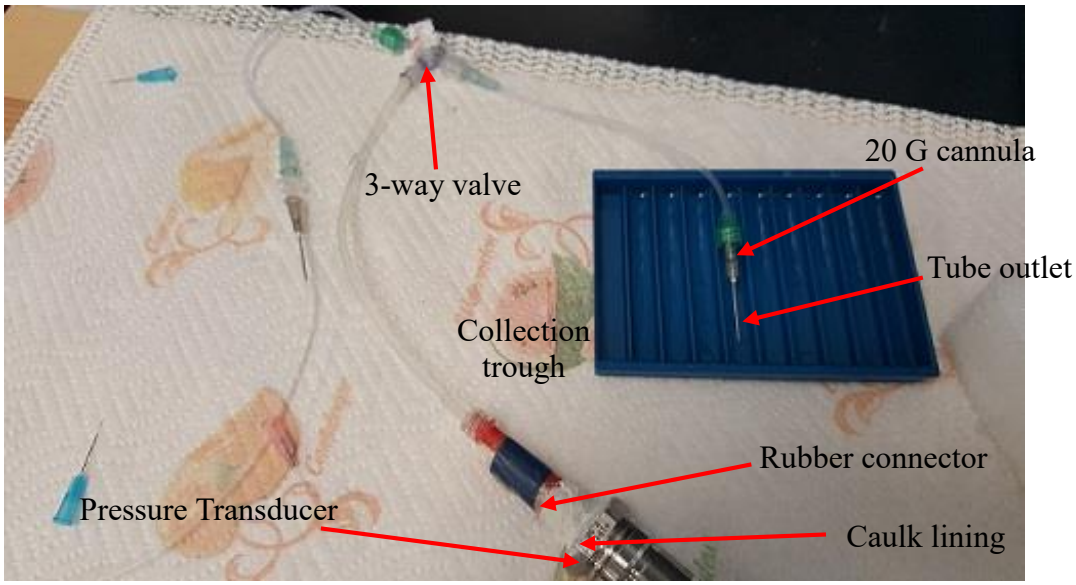

Figure K. 6: Tube connections and three-way valve orientation

4. Prime the tubes with DW, by running the pump at a high flow rate – about 50 µl/min – for about 15 – 20 minutes, to help remove air bubbles from the setup.
5. Perform a baseline trial run without a suture inserted in the implant tubing. A baseline trial is used to check for leaks in the setup and consistency in recorded pressure data at a set flow rate.
6. Set the flow rate at 2.5 µl/min and measure the pressure using the data logger connected to the pressure transducer.
7. Run the trial for a period of 2 – 3 hours and automatically record the variation of pressure both in the pump and transducer. The pump software [refer to **Appendix D**] can be used to record its data, and the data logger's software [refer to **Appendix F**] can be used to record the transducer's data. Normal data logging frequency used is 1 second.
8. Once the experiment is completed, dispose of the tube and check to see if the bottle needs to be refilled [if water level is less than half]. Repeat steps 1 – 7, at least three times, for different samples of 20 gauge cannula in order to check for repeatability.
9. If trials are being conducted without sutures, stop at this point and perform the trials again [steps 2, 3, 4, 6, 7, and 8]. If trials with sutures are being conducted, perform steps 10 – 12.
10. To conduct trials with suture inserts, cut the suture [either absorbable or non-absorbable type] using the medical grade scissors to the required size [between 4 and 8 mm in length] and measure using a scale.
11. Make sure that the cut edge is clean and without any burrs by examining the cut edges under the microscope. If a sample has burrs on the edge, dispose of it and cut another sample until a sample with clean edges is obtained.

12. Insert the suture into the implant tube [10 mm long] and then insert the implant tubing into the 20 gauge cannula. Secure the implant tubing in the cannula by applying superglue in the gap between the cannula and the implant tube [Fig. K. 5].
13. Perform steps 3 and 4 to prime the setup, then begin the experiment [steps 10 – 12]; and record the pump and transducer data in the computer [follow steps shown in **Apps. D and F]**.
14. Conduct at least 3 trials [steps 10 – 12] for each configuration of diameter of the insert, length of the insert and flow rate.
15. Compare the data plots for each configuration to the calculated theoretical pressure range.
16. If trials are conducted for long durations, say 1 to 45 days, repeat steps 3, 4, and 10 – 12. Trials can be extended to longer time periods if the goal is to determine when the pressure drops to the acceptable range [15 – 20 mm Hg] or lower.
17. Ensure that fresh samples of the sutures are used for each trial.

NOTE: Both setups can be used to run similar trials simultaneously; or trials without sutures can be run on one setup, and the other setup can be used to run trials with sutures.

Appendix L: Pump Flow Rate Variation

It was observed that, although the set point specified for pump's flow rate was 2.5 µl/min, the actual flow rate was varying with time owing to the flow control mechanism of the pump software. Hence, in order to determine if the actual flow rate of the pump was within 5% of the set point [**App. C**], the data for Fig. L.1 was taken. Figure L.1 shows the real-time flow rate variation at the pump when 3 trials with 75 micron [inner] diameter tubes were run at 2.5 µl/min in each setup.

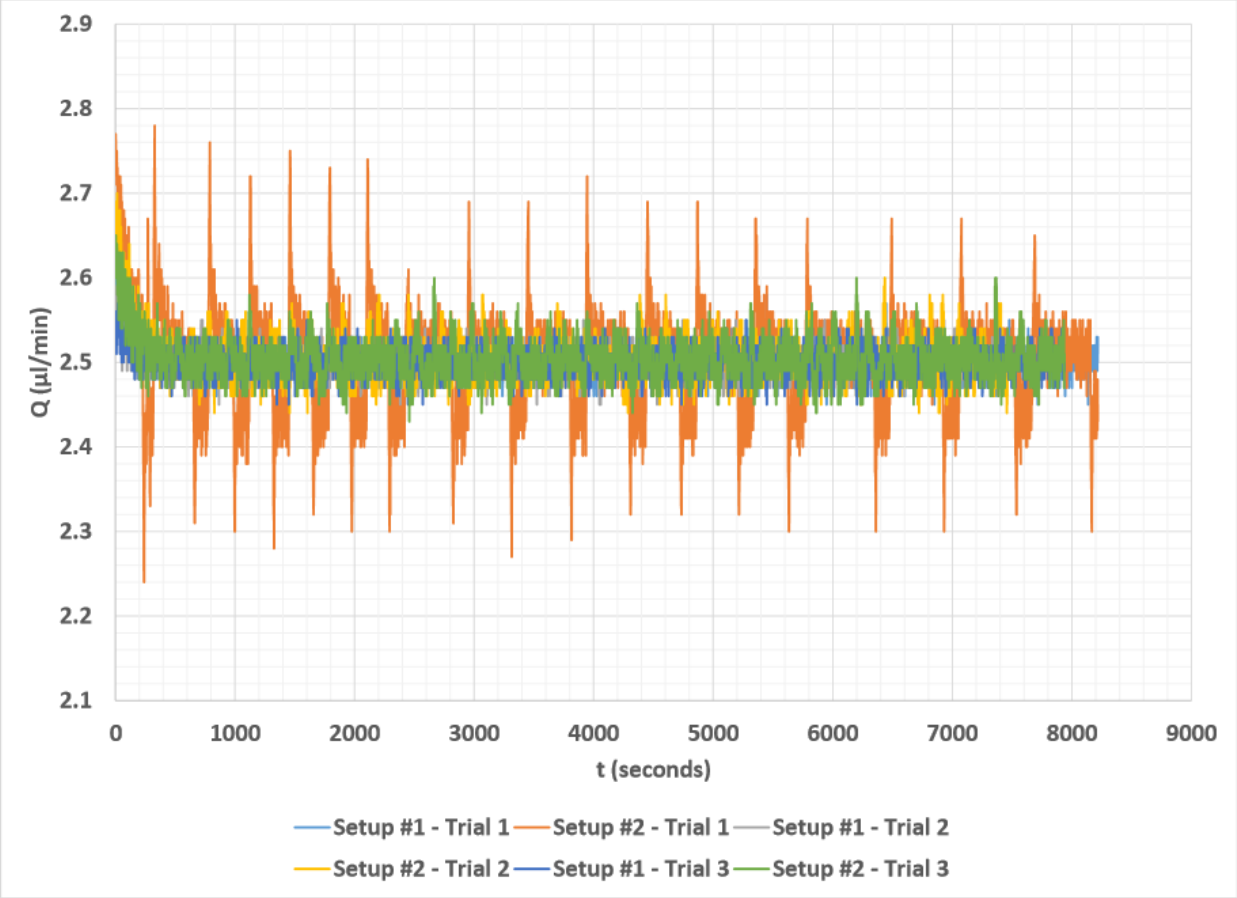

Figure L.1: Flow rate variation vs. time for 75 micron inner diameter tube; set point flow rate of 2.5 µl/min

The average for all trials was close to 2.5 µl/min, but the variance was much higher for trial #1 of Setup #2. There is a slight variance in measured flow rate for all trials because the response time is short between the flow rate measurement sensor and the air compressor in the pump and results in sudden spikes or drops in the actual flow rate. The vendor claimed that this variation would be within 5% of the set point value, which was 2.5 µl/min for these trials. The reason for this variation could not be traced to its source; but some of the factors that might have contributed to this variation were possibly air bubbles in the tubing and/or a constant disturbance from an external source such as bumping into the setup or vibration from the compressor. Table L.1 shows the average flow rate and standard deviation for each trial.

Table L.1: Average flow rate and standard deviation for 75 µm tube data shown in Fig. L.1

Setup #	**Trial #**	**Average Flow Rate [µl/min]**
1	1	2.5 ± 0.02
	2	2.5 ± 0.02
	3	2.5 ± 0.02
2	1	2.51 ± 0.06
	2	2.51 ± 0.03
	3	2.5 ± 0.02

From Table L.1, we can see that the variation in flow rate was between 0.8 – 2.4%, which is less than the 5% accuracy mentioned by the vendor's product catalog [28] [refer to **App. C**].

For the trials with 50 micron tubes, it was observed that the flow rate error varied between 0.6 – 1.2%; and, like the data shown for 75 μm tubes, the flow rate error was less than 5%. Table L.2 lists the average flow rate for each trial, and Fig. L.2 shows the variation in graphical form. It can be seen from Fig. L.2 that the variations were minimal. Therefore, it can be deduced that the vendor's claims that the flow rate error variation is under ± 5% of the set point value is valid.

Table L.2: Average flow rate and standard deviation for 50 micron trials shown in Fig. L.2

Setup #	**Trial #**	**Average Flow Rate [μl/min]**
1	1	2.5 ± 0.02
	2	2.5 ± 0.02
	3	2.5 ± 0.02
2	1	2.52 ± 0.03
	2	2.51 ± 0.03
	3	2.51 ± 0.02

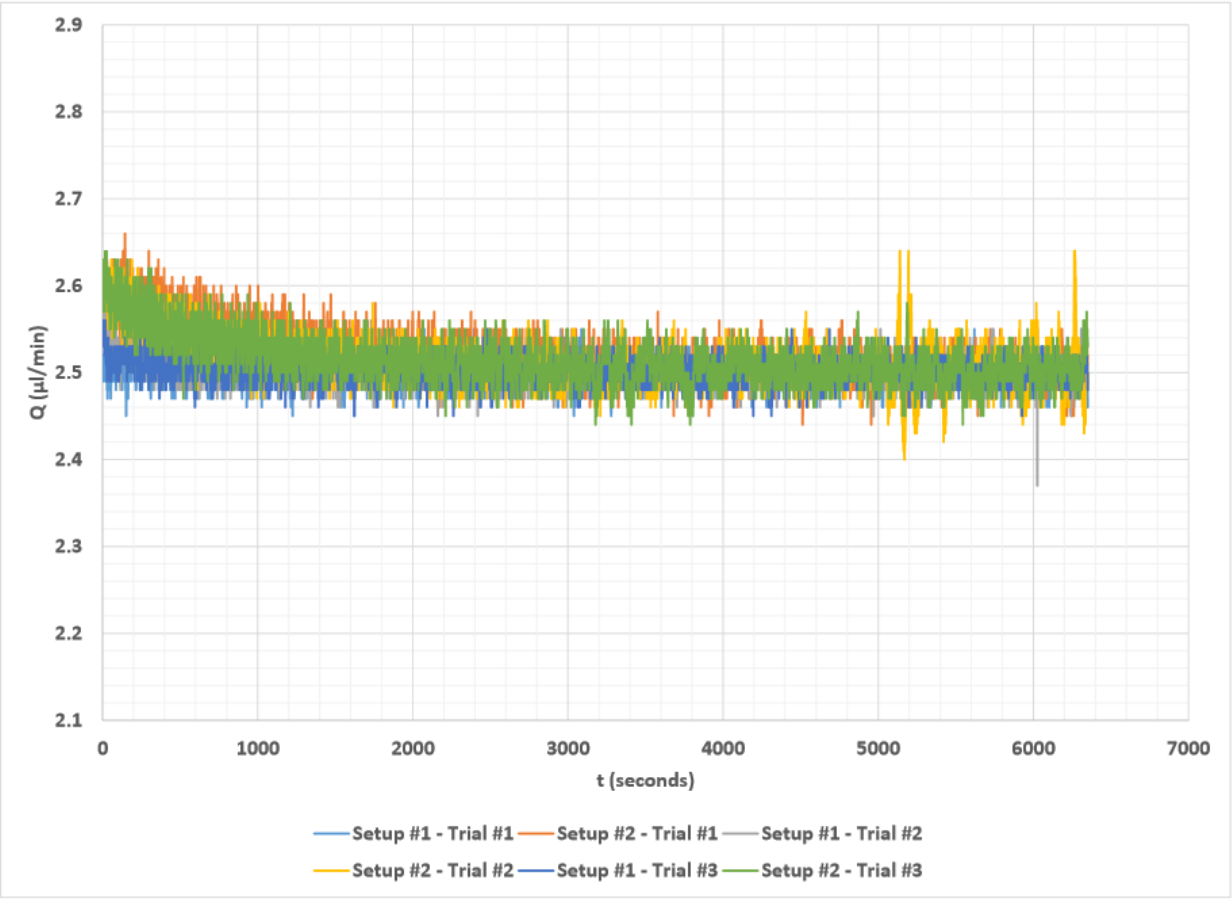

Figure L.2: Flow rate variation vs. time for 50 micron inner diameter tube; set point flow rate of 2.5 µl/min